Brigham Young University
BYU ScholarsArchive

All Theses and Dissertations

2012-08-08

Gas Phase Characterization of Supramolecules Using Cross-Sectional Areas by FTICR and Sustained Off-Resonance Irradiation Collision Induced Dissociation Techniques in a Fourier Transform Ion Cyclotron Resonance Mass Spectrometer

Fan Yang
Brigham Young University - Provo

Follow this and additional works at: https://scholarsarchive.byu.edu/etd

 Part of the Biochemistry Commons, and the Chemistry Commons

BYU ScholarsArchive Citation

Yang, Fan, "Gas Phase Characterization of Supramolecules Using Cross-Sectional Areas by FTICR and Sustained Off-Resonance Irradiation Collision Induced Dissociation Techniques in a Fourier Transform Ion Cyclotron Resonance Mass Spectrometer" (2012). *All Theses and Dissertations*. 3292.
https://scholarsarchive.byu.edu/etd/3292

This Dissertation is brought to you for free and open access by BYU ScholarsArchive. It has been accepted for inclusion in All Theses and Dissertations by an authorized administrator of BYU ScholarsArchive. For more information, please contact scholarsarchive@byu.edu, ellen_amatangelo@byu.edu.

Gas Phase Characterization of Supramolecules Using Cross-Sectional Areas by FTICR and Sustained Off-Resonance Irradiation Collision Induced Dissociation Techniques in a Fourier Transform Ion Cyclotron Resonance Mass Spectrometer

Fan Yang

A dissertation submitted to the faculty of
Brigham Young University
in partial fulfillment of the requirements for the degree of

Doctor of Philosophy

David V. Dearden, Chair
Daniel E. Austin
Jaron C. Hansen
John D. Lamb
Adam T. Woolley

Department of Chemistry and Biochemistry

Brigham Young University

December 2012

Copyright © 2012 Fan Yang

All Rights Reserved

ABSTRACT

Gas Phase Characterization of Supramolecules Using Cross-Sectional Areas by FTICR and Sustained Off-Resonance Irradiation Collision Induced Dissociation Techniques in a Fourier Transform Ion Cyclotron Resonance Mass Spectrometer

Fan Yang
Department of Chemistry and Biochemistry, BYU
Doctor of Philosophy

In my dissertation, I use a Fourier Transform Ion Cyclotron Resonance Mass Spectrometer (FTICR-MS) to investigate supramolecules.

Cross-sectional areas by Fourier transform ICR (CRAFTI), a novel technique for measurements of collision cross sections by FTICR, is demonstrated for the first time. The CRAFTI method measures the total "dephasing cross section" for removal of the ions from the coherent packet in the FTICR cell, including contributions not only from momentum transfer but also from reactive collisions including those leading to collisional dissociation. Experimental CRAFTI collision cross sections correlate linearly with theoretically computed results and with results obtained using ion mobility measurements. Different collision gases, including Xe, N_2, Ar, and SF_6, are all appropriate for the CRAFTI technique when the experiments are done at proper kinetic energies. The CRAFTI technique was applied to characterize the molecular shape of complexes of alkyl mono- and *n*-alkyldiamine with cucurbit[n]uril in the gas phase. The CRAFTI results are consistent with corresponding computational geometries.

The CRAFTI technique was combined with SORI-CID (sustained off-resonance irradiation collision induced dissociation) for characterization of complexes of α,ω-alkyldiammonium with cucurbit[n]urils (n=5, 7 and 8) and cucurbituril derivatives. The results demonstrate that for bigger cucurbiturils, the complexes have the alkyldiamine tails threaded through the cavity of the host; for smaller cucurbiturils, the complexes have the tails of the alklydiamines external to the portal of the host.

Capping molecules for larger CBn to form larger containers were also investigated. Using SORI-CID methods, CB7, a bigger cucurbituril cage, was found to form a more stable complex with Gu^+ (guanidinium). Several neutral guests (benzene, fluorobenzene and toluene) were trapped in CB7 cavity to form inclusion complexes.

Keywords: FTICR-MS, CRAFTI, SORI-CID, Supramolecular Complexes

ACKNOWLEDGEMENTS

First and foremost, I would like to thank my supervisor, Dr. David V. Dearden. He encouraged me, kept me motivated and maintaining great enthusiasm for my projects, and taught me everything at any time with great patience.

I would like to express my gratitude to my Ph.D. committee members, Dr. Daniel E. Austin, Dr. Jaron C. Hansen, Dr. John D. Lamb, and Dr. Adam T. Woolley, for their good advice and guidance through the years of my research.

I would also like to thank all the group members, especially Nannan Fang, for her friendship and suggestions, especially in the early days of my research. I also want to thank all my dear friends, for your friendship and your ongoing words of encouragement and support.

I sincerely thank the Department of Chemistry and Biochemistry at Brigham Young University, for financial support to give me a great opportunity to pursue my Ph.D. degree.

I gratefully acknowledge the financial support of the National Science Foundation under grants CHE-0615964 and CHE-0957757.

Finally, I would like to thank my beloved parents and husband, for their sacrifice, understanding and support throughout my graduate years.

TABLE OF CONTENTS

LIST OF FIGURES

LIST OF TABLES

Chapter 1 Fourier Transform Ion Cyclotron Resonance Mass Spectrometry for Supramolecular Structure Characterization

Introduction

The gas phase provides unique insights for molecular structural characterization that supplement condensed phase studies, and is particularly valuable given the widely-accepted importance of solvent and counterion effects on the chemistry of supramolecular complexes—in the gas phase, both solvent and counterion can be completely eliminated, allowing comparisons with condensed phase work that lays bare the influence of solvents, counterions, or crystal packing.[1,2] Without gas phase work, it is difficult to pin down how these condensed phase factors affect the system. In the gas phase, the intrinsic chemistry of the complex can be examined in detail and compared with predictions from high-level theory. In addition, the gas phase behavior of these systems is of great interest in its own right, and may have spin-off applications in such diverse areas as modifying the behavior of peptide fragmentation to assist in proteomics studies.

Mass spectrometry remains one of the key tools for performing studies on gas-phase species and is increasingly being applied to supramolecular complexes.[3-5] Mass spectrometry has unique advantages for characterization of supramolecules. It requires only miniscule samples (typically a few microliters of solution at micromolar concentrations), and minimal purification (because that can be easily accomplished via the excellent separation capabilities of the mass spectrometer), and does not require crystallization. These can be large advantages, because many systems of interest in supramolecular chemistry are difficult to characterize by any other

method. For instance, many interesting complexes do not form crystals, preventing the use of X-ray techniques, and are not suitable for NMR studies because of solubility issues or the presence of magnetic nuclei or because of insufficient sample.[6]

At the same time, supramolecular systems present unique challenges for mass spectrometry because the conformations of the complexes, and mechanical fit of the molecular components, is of great importance.[6] Hence, while measuring the mass of the complex (which is the usual initial goal in mass spectrometric experiments) yields useful information, that information alone is often not enough to distinguish between a potentially valuable piece of molecular machinery and a non-specific adduct that is a mass spectrometric artifact arising from the process of transferring the system into vacuum. More advanced "tandem" mass spectrometric techniques are often essential for successful gas phase characterization of supramolecules, which can be utilized to distinguish between isomers and probe information about the shape of the complex.

As noted above, mass spectrometry is becoming an increasingly important tool for characterization of supramolecular systems, and has been applied by several groups to the study of cucurbiturils, usually as a means of probing condensed-phase properties such as the existence of complexes and relative binding constants in condensed media.[7-9]

Fourier Transform Ion Cyclotron Resonance Mass Spectrometry (FTICR-MS)

The main experimental techniques used for supramolecular characterization in Dr. Dearden's laboratory employ Fourier transform ion cyclotron resonance mass spectrometry (FTICR-MS).[10] FTICR has been widely installed in laboratories worldwide since its inception by Comisarow and

Marshall in 1974.[11] A schematic of the 4.7 T FTICR mass spectrometer in Dr. Dearden's group is shown in Figure 1.1.

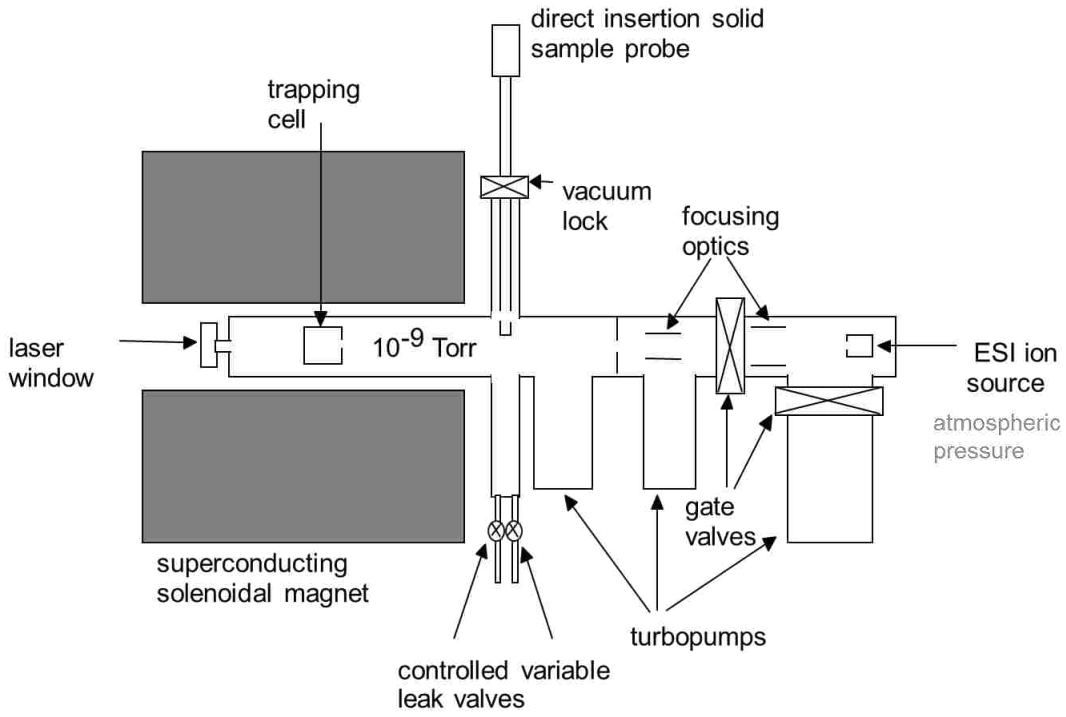

Figure 1.1 Schematic of a 4.7T FTICR mass spectrometer at BYU.

Generally, in a FTICR mass spectrometer, ions are generated by an ion source (usually an EI (electron ionization), ESI (electrospray ionization) or MALDI (matrix-assisted laser desorption/ionization) ion source), transferred through the ion guide focusing optics by applying a series of voltage differences and then trapped into the ICR trapping cell which is located inside a spatially uniform static superconducting solenoidal magnet cooled by liquid helium and liquid nitrogen. Figure 1.2 shows a schematic of a cylindrical trapping cell, where the ions are excited and detected. The trapping cell is composed of trapping plates, excitation plates and detection plates. Once the ions are trapped into this vacuum chamber, they will have three different motions: cyclotron motion, trapping oscillation and magnetron motion.

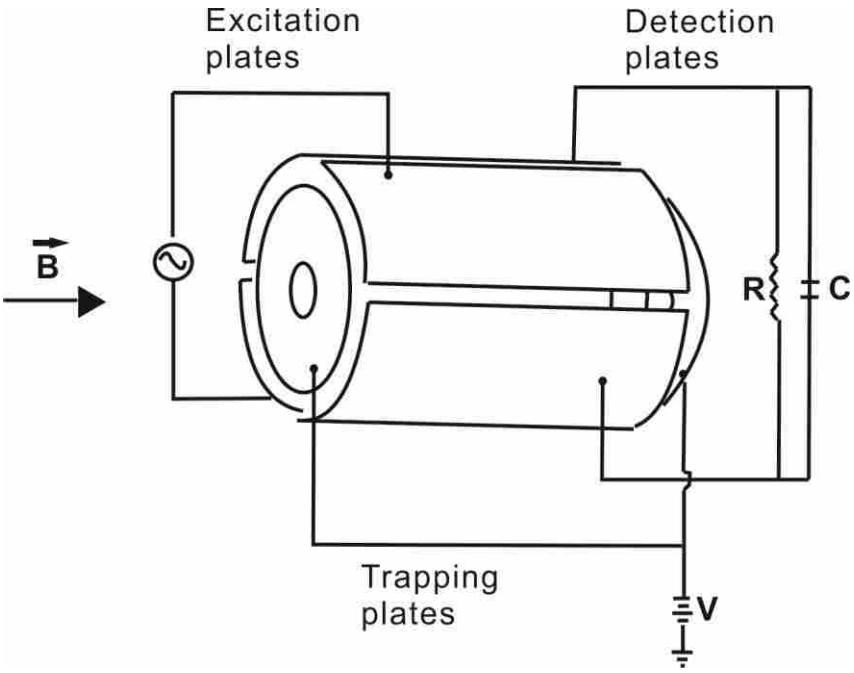

Figure 1.2 Schematic of a cylindrical trapping cell.

Ion cyclotron motion is the primary type. As shown in Figure 1.3, when an ion with charge of q and mass of m, is moving into a spatially homogeneous magnetic field (here, the magnetic field **B** is perpendicular to the plane of the paper, $\mathbf{B}=-B_0\mathrm{k}$, and z-axis is defined to be opposite to the direction of the magnetic field), it is subjected to the Lorenz force F, bent into a cycle with a circular radius r, and moving with a velocity v_{xy}:

$$F = qv_{xy}B_0 = \frac{mv_{xy}^2}{r} \qquad (1\text{-}1)$$

The angular velocity ω, about the z-axis, is defined as:

$$\omega = \frac{v_{xy}}{r} \qquad (1\text{-}2)$$

Combing equation (1-1) and (1-2), we obtain the equation of "unperturbed" ion cyclotron frequency, ω_c:

$$\omega_c = \frac{qB_0}{m} \qquad (1\text{-}3)$$

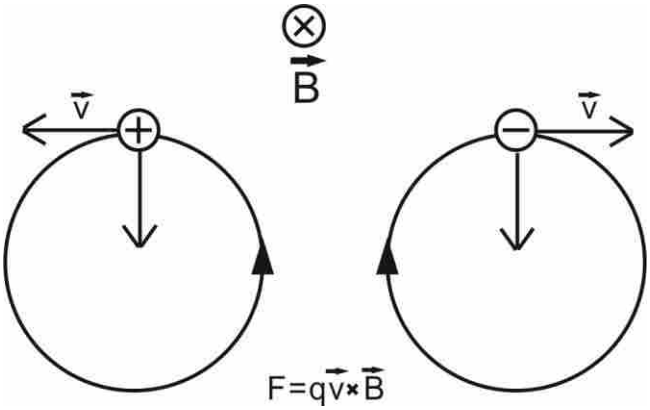

Figure 1.3 Ion cyclotron motion. Positive and negative ions move in opposite directions.

As shown in Figure 1.2, two trapping plates are set to trap the ions in the magnetic field via applying an electric potential, shown in Figure 1.4. However, the existence of this electric potential makes the ions moving in a harmonic oscillation, ω_z, between the two trapping plates and the combination of the radial electric field and the magnetic field results in the magnetron motion, ω-. The "unperturbed" ion cyclotron frequency can be modified to reduced cyclotron frequency, ω_+:

$$\omega_+ = \frac{\omega_c}{2} + \sqrt{\left(\frac{\omega_c}{2}\right)^2 - \frac{\omega_z^2}{2}} \qquad (1\text{-}4)$$

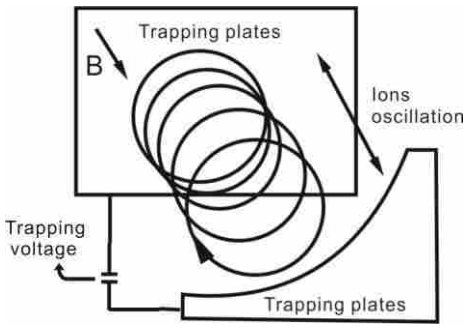

Figure 1.4 Ion trapping oscillation in FTICR-MS.

Applications of FTICR-MS for Molecular Structure Characterization

Ions have a number of fundamental properties that can be exploited for analytical characterization, including mass-to-charge ratio and fragmentation behavior, which are probed using mass spectrometry. Molecular structure is one of the important issues in molecular characterization. Herein, two powerful techniques for determination of ion structures in FTICR will be discussed. They are sustained off-resonance irradiation collision induced dissociation (SORI-CID) and collision cross sectional areas by Fourier transform ion cyclotron resonance (CRAFTI).

Sustained off-resonance irradiation collision induced dissociation (SORI-CID)

Collision-induced dissociation (CID) is a powerful technique for determination of molecular structures in the gas phase. Sustained off-resonance irradiation CID is one of the dissociation techniques in FTICR. In this technique, a neutral gas is introduced into the mass analyzer cell for collisional activation of the target ion. The radiofrequency excitation pulse is set to be slightly off the resonant frequency of the target ion; and the excitation is applied up to hundreds or thousands of milliseconds to make sure multiple collisions occur between the ion and the neutral gas. With multiple collisions, the internal energy of the target ion should slowly increase and the target ion begins to dissociate once its internal energy accumulates to the dissociation threshold. In a word, SORI-CID is a "slow heating" method with multiple low-energy collisions.

In order to use it as a tool to better identify molecular structure, the SORI-CID method is treated quasi-quantitatively in the following chapters. E_{SORI} is the relative energy used for dissociation of parent ions via energy deposition into parent ions by multiple collisions during

the SORI event. Dearden and Zhang[12] derived an expression for the amount of energy deposited in the parent ion during the SORI event based on Laskin and Futrell's papers[13,14]:

$$E_{SORI} = n_n \sigma K_v f_E t_{coll} \frac{\beta^3 q^3}{128\pi^3 d^3 (\Delta f)^3} \left(\frac{M}{M+m} \right) \frac{V_{PP}^3}{m^2} \qquad (1\text{-}5)$$

where n_n is the collision gas number density, σ is the collision cross section of the ion, K_v is the proportionality constant relating v (the ion velocity) to v_{max} (the maximum velocity of the activated ion), f_E is an assumed constant fraction of the maximum energy in the center-of-mass reference frame during SORI that is deposited into the parent ion per collision, t_{coll} is the time during which collisions take place (the SORI excitation event length), β is the trapping cell geometry factor, q is the charge on the parent ion, d is the diameter of the trapping cell, Δf is the frequency offset of the excitation pulse from the resonant frequency of the parent ion, m is the mass of the parent ion, M is the mass of the neutral collision gas, and V_{PP} is the peak-to-peak amplitude of the SORI excitation pulse.

From equation (1-5), we can see the following: E_{SORI} can be changed by changing the SORI excitation amplitude, the SORI event length, or the background pressure of the neutral collision gas. In my experiments, I arbitrarily set the frequency offset to be 1kHz below the resonant frequency of the parent ions (there is some evidence in the literature that 1 kHz off resonance is not the optimum frequency offset[15], but this should not cause significant errors as long as the offset is consistent), choose argon as the neutral gas, keep the background pressure constant and keep the SORI excitation amplitude the same for each series of target ions. As a result, E_{SORI} is proportional to the experimental parameters as shown in equation (1-6):

$$E_{SORI} \propto \sigma\left(\frac{M}{M+m}\right)\frac{t_{coll}}{m^2} \qquad (1\text{-}6)$$

With increasing SORI event length, more energy is deposited to the target ions and the dissociated portion of the parent ions becomes bigger. The collision cross section of the ion is assumed to be in the hard-sphere region and independent of the ion velocity, and can be estimated by computing the solvent accessible surface area of the ion, by measuring the drift time using the ion mobility technique,[16] or by employing the collision cross sectional areas by Fourier transform ion cyclotron resonance (CRAFTI) technique.[17]

Collision cross sectional areas by Fourier transform ion cyclotron resonance (CRAFTI)

Ion conformational studies are becoming increasingly important, for several reasons. First, they provide insights into ion structures. Second, through the structural information they yield, they can be used to probe noncovalent intermolecular interactions within supramolecular complexes. The physical, chemical and biological properties of a molecule are often strongly dependent on the conformation of the molecule. For instance, the physical properties of polymers, which are widely used in construction, coating and many other branches of industry, depend on polymer conformation;[18] the bioactivity of proteins, which is very important in clinical and therapeutic treatments, also depends on their conformation;[19] and the curative effects of a drug are frequently closely related to its conformation.[20] As a result, accurate means of determining molecular conformation are important both intellectually and practically.

Several techniques are currently used for determination of molecular conformation. One is X-ray crystallography.[21] Crystallography provides conformational information based on the

atomic distances within a crystallized compound. However, not all molecules can be crystallized, which means this technique is not always applicable. Nuclear magnetic resonance (NMR) is another powerful technique,[22] which can provide structural information for molecules in solution. However, NMR requires large samples (typically hundreds of milligrams), which limits the application of this technique for samples available in small quantities. Several mass spectrometry-based ion-molecular reaction approaches complement X-ray crystallography and NMR, including H/D exchange[23] and gas-phase proton transfer reactions.[24] They have lower detection limits and do not require special topological features of the molecules. However, these techniques require a suitable reagent, which means they are quite indirect. Further, factors other than conformation definitely influence the measurement results;[25] they give much less detailed information than X-ray or NMR.

Collision cross sections for ions colliding with neutral gases reflect ion size and can provide useful conformational information. The measurements can be carried out using several different approaches.

Measurement of ion mobility is one of the approaches for obtaining collision cross sections, σ. Recently, the structures of macromolecules such as proteins and organic polymers have been elucidated using ion mobility spectrometry (IMS).[16,26] The ions move in a uniform electric field and collide with neutral gas molecules in a drift cell. The collision cross sections can be derived from the drift time, and are dependent on the electric field strength, the pressure and the molecular weight of the neutral collision gas, as shown in equation (1-7)[27,28]:

$$\sigma_{avg} = \frac{(18\pi)^{1/2}}{16} \frac{q}{(k_b T)^{1/2}} \left(\frac{1}{m} + \frac{1}{M} \right)^{1/2} \frac{t_d E}{L} \frac{760}{P} \frac{T}{273.2} \frac{1}{n_n} \qquad (1\text{-}7)$$

Here, k_b is the Boltzmann constant, t_d is the drift time, E is the electric field strength, T is the temperature, P is the pressure of collision gas, L is the drift tube length, and the other notations are the same as mentioned in equation (1-5). Based on this equation, measurements of collision cross sections are easily affected by even small changes in the pressure and temperature in the drift tube, so the instrument should be calibrated with each use. In addition, limited resolution in drift time is also a problem, which impedes the accurate measurement of cross sections. Furthermore, IMS requires a dedicated, specially-designed instrument. And the technique also requires multiple collisions that may influence the structural features .

Another approach for measurements of collision cross sections uses drift ICR. Soon after the introduction of ion cyclotron resonance (ICR) methods for the study of ion-molecule interactions, it was recognized that absorption of power from the irradiating RF field by the ions was in part dependent on the ion-neutral collision rate, which in turn sensitively depends on the ion-neutral collision cross section.[29] Consequently, a number of experiments were performed using ion cyclotron resonance linewidth measurements to measure the mobilities of small ions in various gases.[30-36] These experiments, like the drift ion mobility experiments performed currently, involved drift of ions through a gas cell at pressures typically up to a few millibars, while exciting with an RF field of a few V cm^{-1}. These multiple-collision ICR mobility experiments fell out of practice as trapped ion techniques and Fourier transform methods were developed,

probably because optimum mass resolving power, one of the hallmark benefits of Fourier transform ion cyclotron resonance (FTICR), is obtained at low pressures where collisional contributions to line broadening are minimized.

Consideration of ion motion in the FTICR trap suggests it should be possible to obtain collision cross section information by analyzing the decay of the signal with time. Early in the development of FTICR it was recognized that ion-molecule collision frequencies are related to signal transient decay rates and could be measured by analysis of those rates,[37] but these techniques have never been widely practiced.

Models of ion motion in FTICR[10,38,39] are usually based on earlier models of motion in drift ICR instruments.[29,40-43] These models typically deal with ion-neutral collisions via a frictional damping term in the equation of motion for the ions. The models assume that because in the ICR experiment ion velocity is directly proportional to ion cyclotron radius and because signal is also directly proportional to ion cyclotron radius, it follows that signal is proportional to ion velocity. Thus, descriptions of how velocity changes with time will also describe the evolution of signal with time. The implicit assumption is that ions initially excited to high velocity, producing large signal response because they are close to the detect plates, slow down due to collisions and relax back toward the magnetic field axis, leading to decay of the signal as the orbit radius decreases and the distance to the detect plates increases. If the collision frequency is independent of velocity (as it is for a Langevin ion-induced dipole interaction potential) these models give an exponentially-damped time domain FTICR signal that has a Lorentzian profile in

the frequency domain magnitude spectrum, assuming that signal collisionally damps to background during the time it is being observed.

The assumption of Langevin collision frequencies is problematic, because at the velocities normally employed in modern FTICR excitation and detection, the Langevin collision cross section, which is inversely proportional to velocity, usually is smaller than the hard sphere collision cross section. Frictional damping models that use a hard sphere interaction potential, giving a collision frequency that is directly proportional to ion velocity, have been developed.[39] This kind of model does not yield an analytical expression for the frequency domain signal magnitude, but the expression can be solved numerically and does give a qualitatively accurate description of FTICR line shape.

A frictional damping model for ion motion is clearly applicable to drift ICR experiments, where ion velocities are relatively low and the ions undergo multiple collisions as they traverse the cell. Similarly, such a model is a reasonable description for FTICR experiments such as sustained off-resonance irradiation (SORI) in which the ions are driven through multiple collisions with background gas. It is less clear that a frictional damping model is fully appropriate for FTICR detection, where ions initially excited to a high velocity relative to the neutral background gas are detected while orbiting coherently and undergoing collisions with neutrals. Collisions not only slow the ions down, but they also scatter the ions out of the coherent packet, so that scattered ions no longer contribute to the signal.

I therefore suggest an alternative, kinetic approach for modeling FTICR signal in cases that are collision-limited. I begin by assuming signal is proportional to the number of coherently orbiting ions. I further assume that the ion speed is constant until the ions undergo a collision, at which point the ion is scattered out of the coherent packet and no longer contributes to the signal. Thus, an initial population of $N_I(0)$ coherently orbiting ions, all having the same relative ion-neutral speed, v (assumed to be primarily in the plane perpendicular to the magnetic field, as will be true for ions excited under typical FTICR detection conditions), undergoes collisions with neutrals that depopulate the coherent packet and thereby deplete the time domain signal amplitude. The number of ions collisionally scattered in a given time, dN_I, will be directly proportional to the number of ions N_I and to the reduced collision frequency, which is the collision frequency an ion would have if it lost all its nonrandom velocity in the laboratory frame of reference on each collision.[29] This in turn depends on the mass of the ion, m, the mass of the neutral, M, the collision cross section, σ, the neutral density, n_n, and the relative ion-neutral speed. The negative sign indicates depletion of the coherent packet.

$$dN_I = -\frac{M}{m+M}\sigma N_I n_n v dt \qquad (1\text{-}8)$$

Because the ion speed in the coherent packet is assumed to be constant, this equation is easily integrated to obtain an expression for the evolution of the number of coherent ions with time, $N_I(t)$:

$$N_I(t) = N_I(0)\exp(-\frac{M}{m+M}\sigma n_n v t) \qquad (1\text{-}9)$$

The Fourier transform of equation (1-9) gives the frequency domain magnitude mode signal, *Mag(ω)*, which has Lorentzian shape:

$$Mag(\omega) = \frac{Mag_0}{1 + \left[(\omega - \omega_0) \frac{1}{\frac{M}{m+M} \sigma n_n v} \right]^2} \qquad (1\text{-}10)$$

Here, Mag_0 is the magnitude mode peak amplitude and ω_0 is the ion cyclotron frequency. The Lorentzian lineshape is widely observed in FTICR work, although there is some evidence for deviations,[39] especially under non-ideal conditions. This is similar to the result derived from the collisional damping model for ions undergoing collisions that are dominated by ion-induced dipole (Langevin) interactions with neutrals, but allows for Lorentzian lines without requiring the problematic Langevin collision model for high-velocity ions.

In an FTICR experiment, the masses of the ion and neutral are known, and the ion velocity is easily calculated. The orbit radius of the coherently excited ions, *r*, is given by:[10]

$$r = \frac{\beta V_{pp} t_{exc}}{2 d B_0} = \frac{mv}{qB_0} \qquad (1\text{-}11)$$

Here, β is the cell geometry factor (0.897 for the Bruker Infinity cell[44,45] used here), V_{pp} is the peak-to-peak RF excitation amplitude, t_{exc} is the duration of the RF excitation, *d* is the trapping cell diameter, and B_0 is the component of the magnetic field along the trapping cell axis. Solving for *v*:

$$v = \frac{\beta V_{pp} t_{exc}}{2d\frac{m}{q}} \qquad (1\text{-}12)$$

Neutral number densities can be determined from pressure measurements, but accurate absolute pressure measurements under the conditions of the FTICR experiment are difficult. Therefore, I examine how the line shape changes as pressure is varied, reducing the problem to the more tractable measurement of *relative* pressures and corresponding changes in linewidths. This approach has the added advantage that because the only experimental variable that is changing is the background pressure, other factors that contribute to line broadening[46] (such as resistive coupling between the ions and the detection circuitry, imperfections in the excitation field, axial ejection due to coupling between the excitation and the axial motion, scattering due to inhomogeneities in the magnetic or electric trapping fields, space charge effects, etc.), which are presumably the same in each measurement, do not contribute to the change in linewidth as pressure changes.

In drift ICR experiments, which were clearly carried out under pressure-limited line broadening conditions, common practice[35] was to set the FWHM linewidth of the power absorption spectrum equal to the collision frequency for momentum transfer, ξ, which is given as follows:

$$\xi = \frac{M}{m+M}\sigma n_n v = FWHM \qquad (1\text{-}13)$$

Simple rearrangement and substitution of Equation (1-12) for v gives an expression for the collision cross section:

$$\sigma = \frac{FWHM}{n_n}\frac{(m+M)}{M}\frac{m}{q}\frac{2d}{\beta V_{pp} t_{exc}} \qquad (1\text{-}14)$$

In this expression, $FWHM/n_n$ is the slope of the line in a plot of power spectrum FWHM linewidth vs. neutral number density n_n. Equations (1-13) and (1-14) are also applicable for the FTICR experiments reported,[17] and all the terms are known or easily measured. Thus, calculation of the cross section from the linewidth data is straightforward.

In chapter 3, I present experimental evidence to support the idea that structurally-informative collision cross sections can be measured via analysis of the FTICR signal response as background pressure is varied, resulting in a technique we hope will become complementary to ion mobility methods. This method is called "CRAFTI," an acronym for cross sectional areas by Fourier transform ion cyclotron resonance.

In chapter 4, the influence of collision gas and kinetic energy on the CRAFTI experiment is examined and the results demonstrate that N_2, Ar, and SF_6 all yield useful data under proper conditions.

In chapter 5, the CRAFTI technique is used to characterize the molecular shape of complexes of alkyl mono- and α,ω-*n*-alkyldiamines (containing 2-10 carbon atoms) with cucurbit[n]uril (including cucurbit[5]uril (CB5), decamethylcucurbit[5]uril (mc5) and cucurbit[6]uril (CB6)) in the gas phase. The CRAFTI results are consistent with corresponding computationally modeled supramolecular geometries.

In chapters 6 and 7, α,ω-alkyldiammonium complexes with cucurbit[n]uril (n=5,7 and 8) and cucurbit[n]uril derivatives are investigated using the SORI and CRAFTI techniques. The CRAFTI technique serves as a complementary method to confirm the conformation information deduced from the SORI experiments.

References

(1) Mock, W. L. *Comprehensive Supramolecular Chemistry*; Elsevier: New York, 1996.

(2) Isaacs, L. *Chem. Commun.* **2009**, 619-629.

(3) Baytekin, B.; Baytekin, H. T.; Schalley, C. A. *Org. Biomol. Chem.* **2006**, *4*, 2825-2841.

(4) Schalley, C. A. *Int. J. Mass Spectrom.* **2000**, *194*, 11-39.

(5) Schalley, C. A.; Springer, A. *Mass Spectrometry and Gas-Phase Chemistry of Non-Covalent Complexes*; John Wiley & Sons: Hoboken, New Jersey, 2009.

(6) Steed, J. W.; Atwood, J. L. *Supramolecular Chemistry*; 2nd ed.; Wiley: Chichester (UK), 2009.

(7) Osaka, I.; Kondou, M.; Selvapalam, N.; Samal, S.; Kim, K.; Rekharsky, M. V.; Inoue, Y.; Arakawa, R. *J. Mass Spectrom.* **2006**, *41*, 202-207.

(8) Mitkina, T.; Fedin, V. P.; Llusar, R.; Sorribes, I.; Vicent, C. *J. Am. Soc. Mass Spectrom.* **2007**, *18*, 1863-1872.

(9) Rauwald, U.; Biedermann, F.; Deroo, S.; Robinson, C. V.; Scherman, O. A. *J. Phys. Chem. B* **2010**, *114*, 8606-8615.

(10) Marshall, A. G.; Hendrickson, C. L.; Jackson, G. S. *Mass Spectrom. Rev.* **1998**, *17*, 1-35.

(11) Comisarow, M. B.; Marshall, A. G. *Chem. Phys. Lett.* **1974**, *25*, 282-283.

(12) Zhang, H.; Ferrell, T. A.; Asplund, M. C.; Dearden, D.V. *I. J. Mass Spec.* **2007**, *265*, 187-196.

(13) Lee, S.; Wyttenbach, T.; von Helden, G.; Bowers, M. T. *J. Am. Chem. Soc.* **1995**, *117*, 10159-10160.

(14) Laskin, J.; Futrell, J. *J. Phys. Chem. A* **2000**, *104*, 5484-5494.

(15) Mirgorodskaya, E.; O'Connor, P. B.; Costello, C. E. *J. Am. Soc. Mass Spectrom.* **2002**, *13*, 318-324.

(16) Mukhopadhyay, R. *Anal. Chem.* **2008**, *80*, 7198-7120.

(17) Yang, F.; Voelkel, J. E.; Dearden, D. V. *Anal. Chem.* **2012**, *84*, 4851-4857.

(18) Flory, J. P. *Statistical mechanics of Chain Molecules*; Interscience: New York, 1989.

(19) Nooren, I.; Thornton, J. M. *EMBO J.* **2003**, *22*, 3486-3492.

(20) Alexandrenne, C.; Hanoux, V.; Dkhissi, F. *J. of Neuroimmunol.* **2009**, *209*, 50-56.

(21) Bhattacharya, A. A.; Grune, T.; Curry, S. *J. Mol. Biol.* **2000**, *303*, 721-732.

(22) Choi, J. K.; Curry, S.; Qin, D.; Bittman, R.; Hamilton, J. A. *J. Lipid Res.* **2002**, *43*, 1000-1010.

(23) Freitas, M. A.; Hendrickson, C. L.; Emmett, M. R.; Marshall, A.G. *Int. J. Mass Spectrom.* **1999**, *185/186/187*, 565-575.

(24) Valentine, S. J.; Counterman, A. E.; Clemmer, D. E. *J. Am. Soc. Mass Spectrom.* **1997**, *8*, 954-961.

(25) Robinson, E. W.; Williams, E. R. *J. Am. Soc. Mass Spectrom.* **2005**, *16*, 1427-1437.

(26) Bohrer, B. C.; Merenbloom, S. I.; Koeniger, S. L.; Hilderbrand, A. E.; Clemmer, D. E. *Annu. Rev. Anal. Chem.* **2008**, *1*, 293-327.

(27) Valentine, S. J.; Counterman, A. E.; Clemmer, D. E. *J. Am. Soc. Mass Spectrom.* **1999**, *10*.

(28) Rusyniak, M. J.; Ibrahim, Y. M.; Wright, D. L.; Khanna, S. N.; El-Shall, M. S. *J. Am. Chem. Soc.* **2003**, *125*, 12002-12013.

(29) Wobschall, D.; Graham, J. R.; Malone, D. P. *Phys. Rev.* **1963**, *131*, 1565-1571.

(30) Wobschall, D. C.; Fluegge, R. A.; Graham, J. R., Jr. *J. Chem. Phys.* **1967**, *47*, 4091-4094.

(31) Huntress, W. T., Jr. *J. Chem. Phys.* **1971**, *55*, 2146-2155.

(32) Dymerski, P. P.; Dunbar, R. C. *J. Chem. Phys.* **1972**, *57*, 4049-4050.

(33) Buttrill, S. E., Jr. *J. Chem. Phys.* **1973**, *58*, 656-659.

(34) Ridge, D. P.; Beauchamp, J. L. *Chem. Phys. Lett.* **1976**, *41*, 301-304.

(35) Ridge, D. P.; Beauchamp, J. L. *J. Chem. Phys.* **1976**, *64*, 2735-2746.

(36) Parent, D. C.; Bowers, M. T. *Chem. Phys.* **1981**, *60*, 257-275.

(37) Parisod, G.; Comisarow, M. B. *Chem. Phys. Lett.* **1979**, *62*, 303-305.

(38) Marshall, A. G.; Comisarow, M. B.; Parisod, G. *J. Chem. Phys.* **1979**, *71*, 4434-4444.

(39) Guan, S.; Li, G.-Z.; Marshall, A. G. *Int. J. Mass Spectrom. Ion Proc.* **1997**, *167*, 185-193.

(40) Beauchamp, J. L. *J. Chem. Phys.* **1967**, *46*, 1231-1243.

(41) Beauchamp, J. L. *Ann. Rev. Phys. Chem.* **1971**, *22*, 527-561.

(42) Comisarow, M. B. *J. Chem. Phys.* **1971**, *55*, 205-217.

(43) Viehland, L. A.; Mason, E. A.; Whealton, J. H. *J. Chem. Phys.* **1975**, *62*, 4715-4726.

(44) Sievers, H. L.; Grützmacher, H.-F.; Caravattie, P. *Int. J. Mass Spectrom. Ion Processes* **1996**, *157/158*, 233-247.

(45) Caravatti, P.; Allemann, M. *Org. Mass Spectrom.* **1991**, *26*, 514-518.

(46) Anderson, J. S.; Vartanian, H.; Laude, D. A. *Trends Anal. Chem.* **1994**, *13*, 234-239.

Chapter 2 Gas Phase Cucurbit[n]uril Chemistry[a]

Introduction

Cucurbit[n]urils[1-6] are named after the Latin for the pumpkin family, *Cucurbitacea*, in reference to the pumpkin shape of these molecules. These hollow molecules are cyclic oligomers of glycoluril and related species. As shown in Figure 2.1, carbonyl oxygen atoms line the portals that give access to the hollow interior of the cucurbituril. These electronegative atoms together form ideal binding sites for positive ions, while the molecular interior serves as a cavity in which neutral "prisoner" molecules of the proper size can be incarcerated. Cucurbiturils are gaining increasing attention as prototypical supramolecular hosts and in applications such as drug delivery[7] and sensitive analytical assays.[8] Cucurbiturils composed of n glycoluril units (n=5-10) are named cucurbit[n]urils, CBn hereafter for brevity.

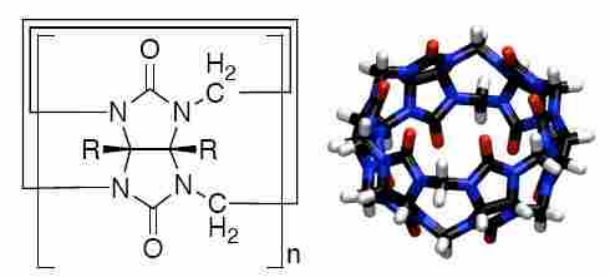

Figure 2.1 Structural formula for cucurbit[n]uril (left) n = 5-10 are known. A model of cucurbit[6]uril, which has R=H and n=6, is shown to the right.

It is widely recognized that the binding of cucurbiturils to guests is sensitive to solvent and counterion effects.[1,6] For example, because cations bind to the cucurbituril rim, the presence of salts can have large effects on binding constants for organic guests. Therefore, mass

[a] A version of this chapter has been published.
"Gas Phase Cucurbit[n]uril Chemistry," Yang, F.; Dearden, D. V. *Isr. J. Chem.* **2011**, *51*, 551-558.

spectrometry is becoming an increasingly important tool for characterization of those supramolecular systems, and has been applied by several groups to the study of cucurbiturils, usually as a means of probing condensed-phase properties such as the existence of complexes and relative binding constants in condensed media.[9-11] The work in Dr. Dearden's group has a somewhat different focus; it is designed to emphasize gas phase properties rather than to use the mass spectra to probe conditions in solution. In this chapter, I will give a brief review about the work that addresses important questions regarding the gas phase chemistry of cucurbit[n]urils, and is based on work carried out in Dr. Dearden's group. Most of the work described in this chapter was done by other members of the group, and I am simply reviewing it. My work about gas phase cucurbiturils is described in detail in Chapters 5-8, utilizing the CRAFTI and SORI techniques. Development of CRAFTI techniques is also related to the cucurbituril chemistry in Chapters 3 and 4.

Fourier transform ion cyclotron resonance mass spectrometry (FTICR-MS) is the main technique we employ.[12] Because it is a trapped-ion technique and neutral reactants can also be introduced into the trapping region of the instrument via controlled variable leak valves, FTICR-MS is particularly useful for probing the kinetics of ion-neutral reactions, which often provide insight into the structures of supramolecular complexes (*vide infra*). When the reactions involved are close to thermoneutral, it is often possible to observe equilibrium, facilitating measurements of equilibrium constants and free energy changes in the absence of solvent species or counterions. The application of these techniques to host-guest chemistry has been reviewed.[13-16]

FTICR-MS also lends itself well to structural studies using tandem-in-time methods. Techniques used for such studies have recently been reviewed.[17] In these experiments, the ion of interest is first isolated in the trapping cell. Next, energy is added to the ion, usually by applying an electric field to accelerate it to super-thermal kinetic energies then allowing the ion to collide with background gas molecules. This converts kinetic to internal energy, which causes the ion to fragment. Supramolecular complexes such as those of cucurbiturils usually fragment by disruption of the noncovalent interactions holding the complex together, so analysis of the fragment ions yields structural information about the complex. Because it is possible to control the amount of energy deposited by controlling the kinetic energies of the ions, these experiments can be carried out in an energy-resolved fashion that allows qualitative, and in some cases quantitative comparisons of the amount of energy required to induce fragmentation. These energy-resolved experiments are the gas phase equivalent of the stability constant measurements made in solution.

The shapes and conformations of supramolecular complexes are often critically important to understanding their function. As it is usually practiced, mass spectrometry yields little information about conformation, but an emerging technique, ion mobility spectrometry,[18-20] can be used to fill this gap. In drift ion mobility studies, a packet of ions is injected into a drift cell where a weak electric field moves them toward a detector. The cell is filled with a collision gas (typically helium) and the ions undergo numerous collisions as they drift through the cell. Ions with large collision cross sections undergo more collisions and take longer to traverse the drift cell than do ions with smaller collision cross sections, so ions traveling through the cell are

separated according to their collision cross sections. Collision cross sections can be determined from the time required to drift through the cell and can be compared with cross sections determined for computed candidate structures, often allowing unambiguous identification of dominant conformers.

The experimental measurements are complemented with computational studies. The computational work provides structural, energetic, and spectroscopic data that are either difficult to obtain experimentally or can be used to increase confidence in the experimental measurements. Computational studies typically begin with extensive conformational searching using computationally-inexpensive methods such as molecular mechanics (typically we use Macromodel (Schrödinger, Inc.; Portland, Oregon) and the Merck Molecular Force Field, MMFF[21-25]) to identify important, low energy conformers. For cucurbiturils, which are quite rigid, typically the number of conformations that need to be considered is only a few thousand starting structures. The lowest-energy structures found in the conformational searches are then refined using electronic structure calculations; typically the NWChem/ECCE computational package[26,27] (Pacific Northwest National Laboratory; Richland, Washington) was used along with the B3LYP density functional method[28] with as large a basis set as available computer resources can accommodate. A number of examples are given below.

Cucurbit[n]uril Molecular Containers

Cucurbit[n]urils are known to form inclusion complexes in condensed media, selectively binding guests of the proper size to fit within their cavities, with cations forming "lids" complexed to the rims to close the cage.[29] These cages are interesting prototypical

supramolecular containers and may even have practical applications in gas phase purification[30] or drug delivery.[31] Therefore, an early goal of the work was to observe and characterize the same types of molecular containers under the purely gas phase conditions available in a mass spectrometer.

Encapsulation of neutral guests by decamethylcucurbit[5]uril(NH_4^+)$_2$ complexes[32]

A few reports demonstrated that decamethylcucurbit[5]uril ($C_{40}H_{50}N_{20}O_{10}$, hereafter referred to by the abbreviation "mc5") worked as an encapsulating agent in condensed media.[33,34] In solution, mc5 has been reported to be a highly selective host for Pb^{2+}.[33] In the gas phase, Dr. Dearden's goup has shown[32] that mc5 mixed with ammonium cation and electrosprayed yields two peaks in its Fourier transform mass spectrum, one corresponding to mc5 with one NH_4^+ attached, mc5(NH_4^+), the other corresponding to mc5 with two NH_4^+ attached, mc5(NH_4^+)$_2$. More interestingly, several neutral guests, including N_2, O_2, methanol, and acetonitrile, can be encapsulated into the cage to form guest@mc5(NH_4^+)$_2$ complexes, where mc5 serves as the walls of the container, the NH_4^+ works as a "lid" to close the container, and the guest molecules are contained as "prisoner" species, as shown in Figure 2.2. The mc5 cavity is size selective; it easily traps methanol, but even when electrosprayed from a 50% ethanol:water solution no ethanol complexes are observed (Figure 2.2). Furthermore, these complexes can be opened by using an ionophore, such as 18-crown-6, to remove the lid species. Typically, when one of the lids is removed, the neutral guest is quickly lost from the remaining singly-charged mc5(NH_4^+) complex. The rate of NH_4^+ removal depends on the size of the trapped guest molecules, which likely influences how strongly the lid is attached. Compared with the corresponding rates for the

empty mc5$(NH_4^+)_2$, the ammonium removal rate enhancement is least for the smaller guests, N_2 and O_2. These preliminary results suggest cucurbit[n]urils might be very useful in gas purification or separation schemes.

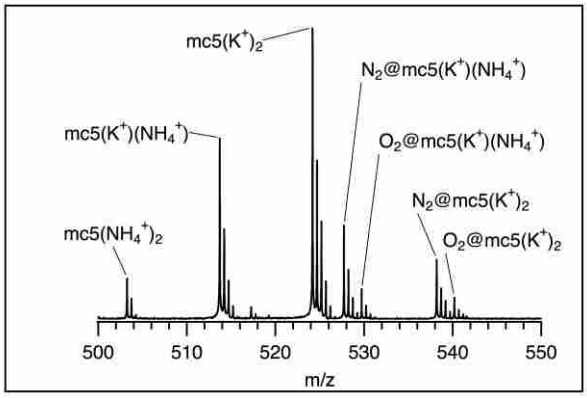

Figure 2.2 Electrospray ionization Fourier transform ion cyclotron resonance mass spectrum of decamethylcucurbit[5]uril (mc5) electrosprayed from an ethanol solution spiked with ammonium acetate. Potassium is present as a contaminant. Complexes with trapped N_2 and O_2 (from air) are evident, but no peaks involving ethanol complexation are observed; mc5 is highly size-selective and will not trap ethanol under these conditions although it has high affinity for methanol.

Guanidinium-capped cucurbit[7]uril molecular cages[35]

Although both mc5 and CB5 have been reported to form supramolecular containers in combination with cations, the small sizes of mc5 and CB5 mean that only a limited range of neutral guests can be trapped inside.[4,30,32] So we further investigated the possibility of constructing larger supramolecular containers based on cucurbit[6]uril or cucurbit[7]uril. Computational modeling suggests that even large ions such as Cs^+ are probably not large enough to close the CB6 cavity and prevent egress of neutrals. We therefore turned to guanidinium (hereafter Gu^+) as a potential capping cation.[35] Molecular mechanics modeling showed that Gu^+

is about the right size to form a lid for a CB6 complex, but also suggests that the portal of CB6, with a diameter of 3.9 Å,[5] is smaller than optimal for binding Gu^+, whereas the 5.4 Å diameter of the CB7 portal[5] is a better fit, as shown in Figure 2.3. Ultra high resolution tandem mass spectrometric techniques demonstrate the hollow pumpkin-shaped host CB7 hydrogen bonded to two guanidinium ions, which form caps to enclose the interior of the cucurbituril. While complexes of the smaller CB6 with two guanidinium ions are also observed when appropriate mixtures are electrosprayed, these exhibit low relative stability (as measured by the relative collision energies required to induce dissociation of the complexes, Figure 2.3) and were not observed to form complexes with neutral guests. The CB7 complex traps benzene, fluorobenzene, or toluene when these neutrals are spiked into the electrospray solution, but similar experiments involving phenol, chlorobenzene, and the xylene isomers did not yield observed inclusion complexes. Relative collision energies required to dissociate the inclusion complexes are in the order benzene ≈ fluorobenzene >> toluene, in qualitative agreement with B3LYP/6-31+G* calculations, which indicate the complexes are not thermodynamically stable in the gas phase (and so are observed likely as a result of formation in solution and kinetic stability in the gas phase).

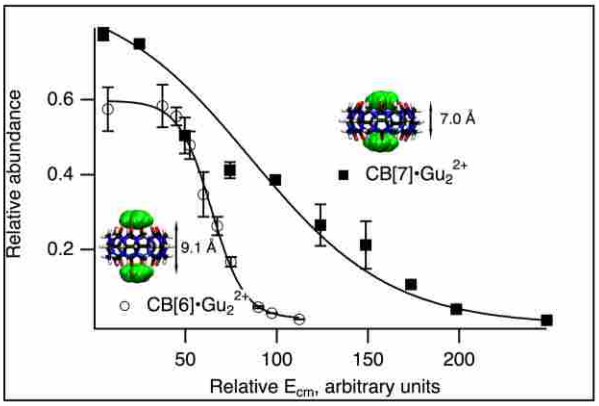

Figure 2.3 Collisional dissociation of guanidinium-capped cucurbit[6]uril (CB6) and cucurbit[7]uril (CB7). Greater center-of-mass collision energies are required to dissociate CB7•Gu_2^{2+} than CB6•Gu_2^{2+}, suggesting greater gas phase stability for the CB7•Gu_2^{2+} complex. B3LYP/6-31+G* calculated structures (insets) indicate the CB6 portal is too small for Gu^+ to reside inside, so the distance between the Gu^+ planes is greater in the CB6 complex than in the more commodious CB7 complex. The hydrogen bonds are also more linear in the latter.

Cucurbit[n]uril Pseudorotaxanes in the Gas Phase

Rotaxane,[36] one of the prototypical supramolecular structures, is the name for a wheel-and-axle architecture with a linear molecule (the "axle") threaded through a cyclic molecule (the "wheel"). CB6 has been reported to form pseudorotaxanes with diammonium cations[37] and other species[38,39] in condensed media. Would these CB6 pseudorotaxanes still survive in the gas phase? A solution of CB6 mixed with 1,4-butanediammonium (DAB) cation was electrosprayed and characterized using FT-ICR.[40] The mass spectra exhibited a doubly charged peak, corresponding to one doubly protonated DAB cation attached to CB6 (1:1 complex). However, the smaller CB5 forms a doubly charged 2:1 complex with DAB cation, corresponding to two singly charged DAB ions attached to CB5. When energy resolved sustained

off-resonance irradiation collision induced dissociation (SORI-CID)[17,41] experiments were carried out on the proposed (DAB+2H)@CB6^{2+} ion, loss of protonated DAB and breakup of the CB6 cage occurred at similar energies, which implies DAB simultaneously binds both rims of CB6. Furthermore, reactivity experiments were also performed to confirm the 1:1 CB6 complex with a pseudorotaxane structure. When the (DAB+2H)@CB6^{2+} ion reacted with neutral tert-butylamine in the gas phase, tert-butylamine slowly adds to the complex. But when similar experiments were performed on non-rotaxane analogs (such as doubly charged 2:1 complexes of either protonated 1,4-butanediamine or protonated ethylenediamine with CB6), collisional activation resulted in loss of the intact amine and reaction with tert-butylamine occurred primarily via rapid displacement of the original amine. From stoichiometry, fragmentation behavior, and reactivity results, the experiments demonstrate the doubly charged 1:1 complex of CB6 with DAB cations is a gas-phase pseudorotaxane.

To further understand the CB6 pseudorotaxanes, Dearden and Zhang explored the collision-induced dissociation behavior of α,ω-alkyldiammonium [$H_3N^+(CH_2)_nNH_3^+$, n=2-10] complexes with the cyclic, hollow ligand CB6 in much greater detail[42] using FT-ICR mass spectrometry with energy resolved SORI-CID. Complementary computational studies were also carried out, beginning with extensive conformational searching using molecular mechanics Monte Carlo techniques employing the Merck Molecular Force Field (MMFF)[21-25] followed by full geometry optimization using HF/6-31G* and B3LYP/6-31G* computational methods. All the lowest-energy structures of the complexes have the diammonium cation threaded through the cavity of CB6. Patterns in the SORI energies required for dissociation and for appearance of

singly protonated diamine product ions and CB6 cage fragments (Figure 2.4), as well as patterns in the computed binding energies suggest that the optimum chain length in the gas phase is n = 4, which is shorter than the solution optimum, n = 6.[1,37] This reflects solvent stabilization of the ammonium groups that is not possible in the gas phase. Further, in the gas phase, the n = 6 complex has an anomalously low dissociation threshold (Figure 2.4), reflecting the compression of the alkyldiammonium chain upon binding by CB6. The shift in threshold, about 20 $kJ \cdot mol^{-1}$, is close to the difference in Coulomb energy expected when the two charged ammonium groups are pulled together from the fully extended conformation to a conformation appropriate for binding CB6. Binding hexanediammonium in CB6 therefore creates a loaded "molecular spring" with a lowered threshold for dissociation, shown in the inset of Figure 2.4. These characterizations provide a fundamental metric for those who are developing syntheses or applications for these supramolecular nanodevices.

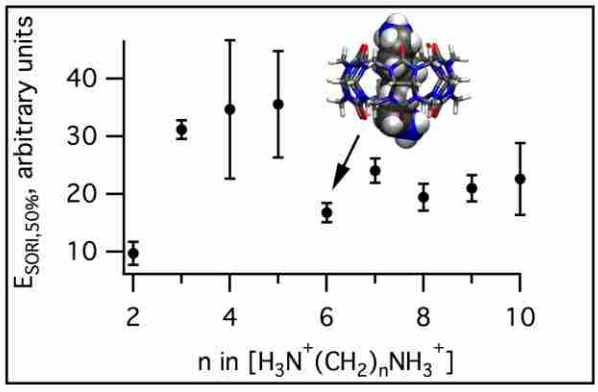

Figure 2.4 Relative SORI energies for 50% loss of $(H_3N^+(CH_2)_nNH_3^+)$@CB6 complexes in the gas phase, m=2-10. Error bars represent standard errors from the linear fitting procedure used to derive the values. The inset gives B3LYP/6-31G* computed structure for the n=6 "molecular spring" complex, showing the "kinking" of the threaded hexanediamine.

Modification of Ion Chemistry via Cucurbit[n]uril Complexation[43]

Cucurbit[n]urils[44-48] and cyclodextrins[49-53] have been suggested as potential drug delivery agents, and cyclodextrins are already in wide use. In order to have wider biological applications for these supramolecules, a fundamental understanding of the interactions between these supramolecular hosts and biomolecular guests is very important. Therefore, experiments were performed to characterize the complexes between amino acids or small peptides with three prototypical "host" molecules: α-cyclodextrin (α-CD), CB5, and CB6, via electrospray FT-ICR mass spectrometry, ion mobility spectrometry and computational methods.[43] Based on previous work on CB6-diammonium complexes,[40,42] lysine was chosen as a guest, because it is structurally similar to the alkyldiammonium species known to complex well with CB6. Ion mobility measurements show lysine forms externally bound, singly charged complexes with either α-CD or CB5, but a doubly charged complex with the lysine side chain threaded through the host cavity of CB6. These structural differences result in distinct dissociation behaviors in SORI-CID experiments: the α-CD complex dissociates via simple loss of intact lysine, whereas the CB5 complex dissociates to yield $[CB5 + H_3O]^+$ and the CB6 complex loses neutral NH_3 and CO, the product ion remaining a doubly-charged complex, probably an intact CB6 with the doubly-charged lysine fragment ion threaded through its interior. These results are consistent with B3LYP/6-31G* binding energies ($kJ \cdot mol^{-1}$) of $D(Lys+H^+–α\text{-}CD) = 281$, $D(Lys+H^+–CB5) = 327$, and $D([Lys+2H]^{2+}–CB6) = 600$. B3LYP/6-31G* geometry optimizations show complexation with α-CD stabilizes the salt bridge form of protonated lysine, whereas complexation with CB6 stabilizes doubly-protonated lysine. Complexation of the larger

polypeptide pentalysine with α-CD forms a non-specific adduct: no modification of the pentalysine charge state distribution is observed on complexation, and dissociation occurs via simple loss of α-CD. Complexation of pentalysine with the cucurbiturils is more specific: the observed charge state distribution shifts higher on complexation, and pentalysine collisionally-activated fragmentation patterns are significantly altered relative to uncomplexed pentalysine. C-terminal fragment ions appear that are consistent with charge stabilization by the cucurbiturils, and the cucurbiturils are retained on the fragment ions. Molecular mechanics calculations suggest CB5 binds to two protonated sites on pentalysine without threading onto the peptide and that CB6 binds two adjacent protonated sites via threading onto the peptide. These observations have interesting and potentially useful implications for techniques that use complexation as a probe of protein or other large molecule conformation and structure.

These results also provide useful information for the influence of the cucurbit[n]urils on the pK_a of bound guests. Because the carbonyl-lined rim of the cucurbituril is electronegative, it stabilizes positive charge and destabilizes negative charge. As noted above, in gas phase studies of $[Lys@CB6+2H]^{2+}$ and $[Lys•\alpha\text{-}CD+H]^{+}$,[43] CB6 strongly favors double protonation of lysine, whereas α-CD stabilizes the salt bridge tautomer. These shifts in pK_a are important for understanding the guest binding behavior of cucurbit[n]urils.

Shape-selective Complexation by Cucurbit[6]uril[54]

Chemical selectivity, usually involving weak, noncovalent interactions, lies at the heart of all methods of chemical separation and purification. Similar weak interactions are in general responsible for controlling assembly of supramolecular complexes, therefore understanding weak

intermolecular interactions is of great current importance.

Cucurbit[6]uril is known to have high shape selectivity in condensed media.[1] Will it exhibit similar shape selectivity in the gas phase? As CB6 is approximately the right size to accommodate a benzene molecule within its interior cavity, *ortho*–, *meta*–, and *para*-phenylenediamines are excellent guests to probe the shape selectivity of CB6 in the gas phase.

Complexes between CB6 and each of *ortho*–, *meta*–, and *para*-phenylenediamines were examined using computational methods, Fourier transform ion cyclotron resonance mass spectrometry, and ion mobility spectrometry.[54] These fundamental gas phase studies showed that the lowest energy binding sites for *ortho*- and *meta*-phenylenediamine are on the exterior of CB6, whereas *para*-phenylenediamine preferentially binds in the interior, in a pseudo-rotaxane fashion. This conclusion is based on the reactivity of each of the complexes with *tert*-butylamine, where the *ortho*- and *meta*-phenylenediamine complexes exchange with *tert*-butylamine, whereas the *para*-phenylenediamine complex undergoes two slow additions without displacement. Further, under sustained off-resonance irradiation conditions, the *ortho*- and *meta*-phenylenediamine complexes fragment easily via losses of neutral phenylenediamine, whereas the *para*-phenylenediamine complex fragments at higher energies primarily via cleavage of covalent bonds in the cucurbituril.

Drift ion mobility techniques were applied to the characterization of these supramolecular isomer complexes. The ion mobility studies show ion populations for the *ortho*- and *meta*-phenylenediamine complexes that primarily have collision cross sections consistent with external complexation, whereas the *para*-phenylenediamine complex has a collision cross

section that is smaller, the same as that of protonated CB6 within experimental error. In agreement with experiment, computational studies indicate that at the HF/6-31G* and B3LYP/6-31G*//HF/6-31G* levels of theory external complexation is favored for *ortho*- and *meta*-phenylenediamine, whereas internal complexation is lower in energy for *para*-phenylenediamine. Thus, shape complementarity between host and guest strongly influences both the collision-induced dissociation and exchange reactivity of the complexes.

Conclusions

The work carried out in Dr. Dearden's group has shown that the marriage between gas phase mass spectrometric methodology and cucurbituril chemistry is a happy one. Gas phase studies have helped elucidate the properties of cucurbiturils, and cucurbituril chemistry has made significant contributions to gas phase technique development.

Many cucurbituril complexes are sufficiently stable that they easily survive the transition from solution to vacuum, where they can be detected with high sensitivity and mass accuracy, making determination of their molecular composition unambiguous. Complexes characterized in this way range from metal- or ammonium-capped cages of cucurbit[5]uril (without and with neutrals trapped inside)[32] through cucurbit[6]uril pseudorotaxanes with threaded diammonium cations,[40,42] guanidinium-capped cucurbit[7]uril supramolecular cages,[35] complexes with amino acids,[43] and even ternary complexes of cucurbit[8]uril.[11] Insights gained about cucurbiturils from gas phase work include that fact that size- and shape-selective binding are intrinsic to these hosts and occur in the absence of solvation (so solvation is not required for selective binding), that cucurbituril-based molecular cages can be opened in highly-controlled fashion (even to the

point of selecting which alkali cation is removed from the container), and that binding of alkyldiammonium ions that mismatch the length of the cucurbituril leads to measurable changes in the energy required to effect dissociation.

While even simple mass spectrometric techniques do a good job of determining molecular weights, it is much more challenging to develop gas phase methods to learn about conformation or about complementarity in size or shape between a host and a guest. Cucurbiturils have been extremely useful in this regard, because they have well-defined sizes and shapes and a high level of symmetry, all of which make them ideal model systems for examining conformation, size, and shape relationships in a mass spectrometer and for developing techniques to probe these things. Using cucurbituril complexes as models, we have learned that ion-molecule reactivity can be indicative of internal vs. external complexation, because externally-bound species generally have more propensity to exchange, and react at higher rates, than comparable but internally-bound species.[54]

Collisional dissociation techniques have also proven to be easily applied methods for higher-order structural characterization, as externally-bound complexes tend to dissociate easily via simple loss of the guest, whereas internally-bound complexes are generally more strongly bound and the energies required to remove the guest are also usually sufficient to fragment the cucurbituril cage itself. Energy-resolved collisional methods[42] allow qualitative comparison of binding strengths, analogous to binding constant measurements in solution, and, with further refinements in data interpretation, show promise as a means of quantitatively measuring bond energies.

It is interesting to note that cucurbituril complexation can significantly influence the chemistry of gas phase ions,[43] changing the distribution of observed charge states and the dissociation behavior. It is therefore possible that cucurbiturils will join crown ethers as reagents used to modify the mass spectra of peptides and proteins,[55] facilitating study of higher-order structure in biomolecules.

The work with ion mobility techniques[43,54] reveals them to be especially promising as a means of learning about higher-order structure in cucurbituril complexes. The significant difference in the mobilities of externally- and internally-bound complexes is easily measured. The application of ion mobility methods to supramolecular characterization is expected to become increasingly common as both instrumentation and techniques improve.

Computational methods work hand-in-hand with gas phase experimental techniques, and again, cucurbituril complexes have been ideal for demonstrating this complementarity because they are large enough to exhibit many interesting characteristics such as size- and shape-selectivity, but are symmetric enough, and rigid enough, that they allow the use of high enough levels of theory (currently B3LYP/6-31+G* for cucurbituril complexes) that accurate answers can be expected. The computational methods are most easily applied to gas phase problems and yield information that is difficult or impossible to obtain from the experiments, such as quantitative bond energetics, detailed structural information, and spectroscopic information. The experimental results are essential for validating the computational findings. In nearly all cases so far the computational and experimental results are in agreement, and this agreement between computational and experimental results increases confidence in both.

The gas phase chemistry of cucurbiturils will be further explored, providing unique information that is not available from condensed phase studies, with renewed emphasis on complementing condensed phase work. The prospect of applying infrared multiphoton dissociation action spectroscopic techniques[56] to cucurbituril systems is especially exciting; it's hoped that this will provide another sensitive structural probe that will help elucidate the properties of these fascinating molecules.

References

(1) Mock, W. L. In *Comprehensive Supramolecular Chemistry*; Vögtle, F., Ed.; Elsevier: New York, 1996; Vol. 2, p 477-493.

(2) Kim, K.; Selvapalam, N.; Ko, Y. H.; Park, K. M.; Kim, D.; Kim, J. *Chem. Soc. Rev.* **2007**, *36*, 267-279.

(3) Freeman, W. A.; Mock, W. L.; Shih, N.-Y. *J. Am. Chem. Soc.* **1981**, *103*, 7367-7368.

(4) Lagona, J.; Mukhopadhyay, P.; Chakrabarti, S.; Isaacs, L. *Angew. Chem. Int. Ed.* **2005**, *44*, 4844-4870.

(5) Lee, J. W.; Samal, S.; Selvapalam, N.; Kim, H.-J.; Kim, K. *Acc. Chem. Res.* **2003**, *36*, 621-630.

(6) Isaacs, L. *Chem. Commun.* **2009**, 619-629.

(7) Wheate, N. J. *J. Inorg. Biochem.* **2008**, *102*, 2060-2066.

(8) Schalley, C. A. *Int. J. Mass Spectrom.* **2000**, *194*, 11-39.

(9) Osaka, I.; Kondou, M.; Selvapalam, N.; Samal, S.; Kim, K.; Rekharsky, M. V.; Inoue, Y.; Arakawa, R. *J. Mass Spectrom.* **2006**, *41*, 202-207.

(10) Mitkina, T.; Fedin, V. P.; Llusar, R.; Sorribes, I.; Vicent, C. *J. Am. Soc. Mass Spectrom.* **2007**, *18*, 1863-1872.

(11) Rauwald, U.; Biedermann, F.; Deroo, S.; Robinson, C. V.; Scherman, O. A. *J. Phys. Chem. B* **2010**, *114*, 8606-8615.

(12) Marshall, A. G.; Hendrickson, C. L.; Jackson, G. S. *Mass Spectrom. Rev.* **1998**, *17*, 1-35.

(13) Dearden, D. V.; Liang, Y.; Nicoll, J. B.; Kellersberger, K. A. *J. Mass Spectrom.* **2001**, *36*,

989-997.

(14) Dearden, D. V. In *The Encyclopedia of Mass Spectrometry*; Armentrout, P. B., Ed.; Elsevier: San Diego, 2003; Vol. 1 (Theory and Ion Chemistry), p 763-770.

(15) Kellersberger, K. A.; Dearden, D. V. In *The Encyclopedia of Mass Spectrometry*; Armentrout, P. B., Ed.; Elsevier: San Diego, 2003; Vol. 1 (Theory and Ion Chemistry), p 338-345.

(16) Schalley, C. A.; Springer, A. *Mass Spectrometry and Gas-Phase Chemistry of Non-Covalent Complexes*; John Wiley & Sons: Hoboken, New Jersey, 2009.

(17) Laskin, J.; Futrell, J. H. *Mass Spectrom. Rev.* **2005**, *24*, 135-167.

(18) Kanu, A. B.; Dwivedi, P.; Tam, M.; Matz, L.; Hill, H. H., Jr. *J. Mass Spectrom.* **2008**, *43*, 1-22.

(19) Bohrer, B. C.; Merenbloom, S. I.; Koeniger, S. L.; Hilderbrand, A. E.; Clemmer, D. E. *Annu. Rev. Anal. Chem.* **2008**, *1*, 293-327.

(20) Creaser, C. S.; Griffiths, J. R.; Bramwell, C. J.; Noreen, S.; Hill, C. A.; Thomas, C. L. P. *Analyst* **2004**, *129*, 984-994.

(21) Halgren, T. A. *J. Comput. Chem.* **1996**, *17*, 616-641.

(22) Halgren, T. A. *J. Comput. Chem.* **1996**, *17*, 587-615.

(23) Halgren, T. A. *J. Comput. Chem.* **1996**, *17*, 553-586.

(24) Halgren, T. A. *J. Comput. Chem.* **1996**, *17*, 520-552.

(25) Halgren, T. A. *J. Comput. Chem.* **1996**, *17*, 490-519.

(26) Papas, B. N.; Schaefer, H. F., III *J. Mol. Struc. THEOCHEM* **2006**, *768*, 175-181.

(27) Bylaska, E. J.; de Jong, W. A.; Kowalski, K.; Straatsma, T. P.; Valiev, M.; Wang, D.; Apra,

E.; Windus, T. L.; Hirata, S.; Hackler, M. T.; Zhao, Y.; Fan, P.-D.; Harrison, R. J.; Dupuis, M.; Smith, D. M. A.; Nieplocha, J.; Tipparaju, V.; Krishnan, M.; Auer, A. A.; Nooijen, M.; Brown, E.; Cisneros, G.; Fann, G. I.; Fruchtl, H.; Garza, J.; Hirao, K.; Kendall, R.; Nichols, J. A.; Tsemekhman, K.; Wolinski, K.; Anchell, J.; Bernholdt, D.; Borowski, P.; Clark, T.; Clerc, D.; Dachsel, H.; Deegan, M.; Dyall, K.; Elwood, D.; Glendening, E.; Gutowski, M.; Hess, A.; Jaffe, J.; Johnson, B.; Ju, J.; Kobayashi, R.; Kutteh, R.; Lin, Z.; Littlefield, R.; Long, X.; Meng, B.; Nakajima, T.; Niu, S.; Pollack, L.; Rosing, M.; Sandrone, G.; Stave, M.; Taylor, H.; Thomas, G.; van Lenthe, J.; Wong, A.; Zhang, Z.; 5.0 ed.; Pacific Northwest National Laboratory: Richland, Washington 99352-0999, USA, 2006.

(28) Zhang, I. Y.; Wu, J.; Xu, X. *Chem. Commun.* **2010**, *46*, 3057-3070.

(29) Jeon, Y.-M.; Kim, J.; Whang, D.; Kim, K. *J. Am. Chem. Soc.* **1996**, *118*, 9790-9791.

(30) Miyahara, Y.; Abe, K.; Inazu, T. *Angew. Chem. Int. Ed.* **2002**, *41*, 3020-3023.

(31) Nau, W. M. *Nature Chemistry* **2010**, *2*, 248-250.

(32) Kellersberger, K. A.; Anderson, J. D.; Ward, S. M.; Krakowiak, K. E.; Dearden, D. V. *J. Am. Chem. Soc.* **2001**, *123*, 11316-11317.

(33) Zhang, X. X.; Krakowiak, K. E.; Xue, G.; Bradshaw, J. S.; Izatt, R. M. *Ind. Eng. Chem. Res.* **2000**, *39*, 3516-3520.

(34) Flinn, A.; Hough, G. C.; Stoddart, J. F.; Williams, D. J. *Angew. Chem. Int. Ed. Engl.* **1992**, *31*, 1475-1477.

(35) Yang, F.; Dearden, D. V. *Supramolecular Chem.* **2011**, *23*, 53-58.

(36) *Molecular Catenanes, Rotaxanes, and Knots*; Sauvage, J.-P.; Dietrich-Buchecker, C., Eds.;

Wiley-VCH: Weinheim, Germany, 1999.

(37) Mock, W. L.; Shih, N.-Y. *J. Org. Chem.* **1986**, *51*, 4440-4446.

(38) Kim, K. *Chem. Soc. Rev.* **2002**, *31*, 96-107.

(39) Buschmann, H.-J.; Wego, A.; Schollmeyer, E.; Döpp, D. *Supramolecular Chem.* **2000**, *11*, 225-231.

(40) Zhang, H.; Paulsen, E. S.; Walker, K. A.; Krakowiak, K. E.; Dearden, D. V. *J. Am. Chem. Soc.* **2003**, *125*, 9284-9285.

(41) Gauthier, J. W.; Trautman, T. R.; Jacobson, D. B. *Anal. Chim. Acta* **1991**, *246*, 211-225.

(42) Zhang, H.; Ferrell, T. A.; Asplund, M. C.; Dearden, D. V. *Int. J. Mass Spectrom.* **2007**, *265*, 187-196.

(43) Zhang, H.; Grabenauer, M.; Bowers, M. T.; Dearden, D. V. *J. Phys. Chem. A* **2009**, *113*, 1508-1517.

(44) Lim, Y.-B.; Kim, T.; Lee Jae, W.; Kim, S.-M.; Kim, H.-J.; Kim, K.; Park, J.-S. *Bioconjug. Chem.* **2002**, *13*, 1181-1185.

(45) Jon, S. Y.; Selvapalam, N.; Oh, D. H.; Kang, J.-K.; Kim, S.-Y.; Jeon, Y. J.; Lee, J. W.; Kim, K. *J. Am. Chem. Soc.* **2003**, *125*, 10186-10187.

(46) Lee, H.-K.; Park, K. M.; Jeon, Y. J.; Kim, D.; Oh, D. H.; Kim, H. S.; Park, C. K.; Kim, K. *J. Am. Chem. Soc.* **2005**, *127*, 5006-5007.

(47) Wheate, N. J.; Buck, D. P.; Day, A. I.; Collins, J. G. *Dalton Trans.* **2006**, 451-458.

(48) Wheate, N. J.; Taleb, R. I.; Krause-Heuer, A. M.; Cook, R. L.; Wang, S.; Higgins, V. J.; Aldrich-Wright, J. R. *Dalton Trans.* **2007**, 5055-5064.

(49) Li, J.; Loh, X. J. *Adv. Drug Delivery Rev.* **2008**, *60*, 1000-1017.

(50) Uekama, K.; Hirayama, F.; Arima, H. *Cyclodextrins Their Complexes* **2008**, 381-422.

(51) Loftsson, T.; Duchene, D. *Int. J. Pharm.* **2007**, *329*, 1-11.

(52) Davis, M. E.; Brewster, M. E. *Nat. Rev. Drug Discovery* **2004**, *3*, 1023-1035.

(53) Szejtli, J. *Pure Appl. Chem.* **2004**, *76*, 1825-1845.

(54) Dearden, D. V.; Ferrell, T. A.; Asplund, M. C.; Zilch, L. W.; Julian, R. R.; Jarrold, M. F. *J. Phys. Chem. A* **2009**, *113*, 989-997.

(55) Ly, T.; Julian, R. R. *J. Am. Soc. Mass Spectrom.* **2006**, *17*, 1209-1215.

(56) Oh, H.-B.; Lin, C.; Hwang, H. Y.; Zhai, H.; Breuker, K.; Zabrouskov, V.; Carpenter, B. K.; McLafferty, F. W. *J. Am. Chem. Soc.* **2005**, *127*, 4076-4083.

Chapter 3 Collision Cross Sectional Areas from Analysis of Fourier Transform Ion Cyclotron Resonance Linewidth: a New Method for Characterizing Molecular Structure[a]

Introduction

Ions have a number of fundamental properties that can be exploited for analytical characterization, including mass-to-charge ratio and fragmentation behavior, which are probed using mass spectrometry. Increasingly, the mobility of ions in a buffer gas and the corresponding collision cross section have been used as another means of separating ions and probing molecular structure.[1,2] These measurements are particularly valuable where clustering to produce multiple species with the same mass-to-charge ratio is possible, or where various isomers or stable conformers are likely to be present. In the field of supramolecular chemistry, where the conformation of a complex is often a key issue, collision cross section measurements can provide important structural information that is difficult to obtain by other methods.[3,4]

While techniques such as drift ion mobility measurements,[5] high-field asymmetric waveform ion mobility spectroscopy (FAIMS),[6] or traveling wave ion mobility (TWIM)[7] have produced a wealth of useful information, these all have the disadvantage that they must be performed on specialized instruments designed for mobility measurements. In addition, because these techniques involve injection of the ions at moderate energies into a high pressure region where the mobility is subsequently measured, it is possible for the ions to experience heating and structural change during injection; indeed, mobility changes that occur as the injection energy is

[a] A version of this chapter has been published. This is the reference:
"Collision Cross Sectional Areas from Analysis of Fourier Transform Ion Cyclotron Resonance Linewidth: a New Method for Characterizing Molecular Structure," Yang, F.; Voelkel, J. E.; Dearden, D. V. *Anal. Chem.* **2012**, *84*, 4851-4857.

varied can be useful in assigning peaks in an arrival time distribution to different structural features.[2,8,9] Similarly, structural changes may occur during the subsequent multiple collisions between ions and neutrals in the high-pressure region of the instrument. Herein I present a complementary approach to the measurement of collision cross section that does not require a dedicated mobility instrument and is in principle a single-collision technique. The basic principles of this technique were discussed in Chapter 1.

In the remainder of this chapter I present experimental evidence to support the idea that structurally-informative collision cross sections can be measured via analysis of the FTICR signal response as background pressure is varied, resulting in a technique we hope will become complementary to ion mobility methods. As described in Chapter 1, the method was referred to as "CRAFTI," an acronym for cross sectional areas by Fourier transform ion cyclotron resonance.

Experimental

Materials

12-crown-4 (12C4), 18-crown-6 (18C6), cucurbit[5]uril (CB5), cucurbit[6]uril (CB6), and α-cyclodextrin (αCD) were purchased from Sigma-Aldrich (St. Louis, MO) and used as supplied. Decamethylcucurbit[5]uril (mc5) was synthesized by Dr. Krzystof Krakowiak using published procedures.[10] Electrospray solutions were 10 μM in ligand and 100 μM in ionic guest. Crown ether complexes were sprayed from 50:50 methanol:water; CB5 and mc5 complexes were sprayed from 50:50 isopropanol:water; and CB6 complexes were sprayed from 48:48:4

methanol:water:formic acid. Damping gases were purchased from Airgas (Radnor, PA) at the following purities: He, 99.995%; Xe, 99.995%.

Instrumentation and pulse sequence

All experiments were performed using a Bruker APEX 47e Fourier transform ion cyclotron resonance mass spectrometer with an Infinity trapping cell[11,12] and a microelectrospray source modified from an Analytica (Branford, MA) design, with a heated metal capillary drying tube based on the design of Eyler.[13] Pressures were adjusted and controlled using a pulsed leak valve based on the design of Freiser.[14] Pressures were measured using a cold cathode tube (Balzers; Fürstentum, Lichtenstein) mounted outside the high field region of the instrument, about 1 m from the trapping cell. All pressures were adjusted for the relative sensitivity of the cold cathode using the method of Bartmess and Georgiadis,[15] wherein the gauge is assumed to be calibrated for N_2 and readings are adjusted according to the relative ease of ionizing the gas.

The instrument was controlled using a MIDAS Predator data system (National High Magnetic Field Laboratory; Tallahassee, FL).[16,17] The excitation clock rate was 5 MHz. All experiments were automated using TCL scripts to vary the duration of the pulsed leak events (and hence, to vary the pressure during the excitation).

A typical pulse sequence for these experiments is shown in detail in Figure 3.1. Experimental sequences began with initialization of voltages on the trapping cell, followed by a quench event to eject all ions from the trap. Newly sprayed ions were accumulated in an external hexapole for 0.6 s, then injected into the trapping cell using the "sidekick" technique.[18] The injection sequence was repeated 1-6 times as needed to accumulate sufficient ion populations for

experiments. To avoid contribution of the isotopic envelope to line broadening, ions of interest were next monoisotopically isolated using SWIFT techniques.[19] At that point the pulsed leak valve was again pressurized with collision gas, with the pressure controlled by the length of time the pulsed valve was opened. After a 2 s rise time to ensure thermalization of the ions and a constant pressure, the detect digitizer was activated and simultaneously the ions were excited using a single-frequency, on-resonance RF pulse. The excitation amplitude was set as needed to achieve the desired kinetic energy in the center-of-mass reference frame; the duration was adjusted to keep the excite event short (typically 300 μs) compared to the expected length of the time domain signal transient. Under conditions typically used in my experiments, this leads to a post-excite cyclotron radius ranging from about 0.5 mm up to about 2 cm, approaching the practical limit in our trapping cell, which has a 3 cm radius. Following signal acquisition (typically 65-130 ms), the pulsed leak valve was evacuated in preparation for beginning a new experimental cycle.

Data analysis

Transient signals were analyzed using the Igor Pro software package (version 6, Wavemetrics; Lake Oswego, OR). Magnitude FFTs were performed on the data beginning 2 s following the end of the excitation event through the return of the transient signal to baseline noise, with zero filling to an appropriate power of 2. The square of the resulting signal yields the power spectrum. The power spectrum peaks were fit to Lorentzians and the FWHM linewidths were extracted from the fits.

Computational modeling of cross sections

Molecular structures were obtained using the Maestro/Macromodel package (Macromodel version 7.1; Schrödinger, Inc.; Portland, OR) for conformational searching using either the MMFF or AMBER* force field provided in the package, with a constant dielectric and no nonbonded cutoffs. The default convergence criteria and the MCMM search method with automatic setup and a minimum of 10,000 starting structures were used. Torsional rotations within fused ring systems were disabled. The 50 lowest-energy conformers found in these searches were used as input to the MOBCAL[20-24] program for calculation of collision cross sections. Parameters for Li^+, K^+ and Cs^+ were estimated from those used in MOBCAL for Na^+ by scaling the Lennard-Jones and hard sphere radii by the ratio of the metal's ionic radius to that for Na^+. Although MOBCAL models collisions in helium, it's assumed that the results for helium are proportional to cross sections that would be obtained using other collision gases. In cases where the conformational search resulted in fewer than 10 conformers (such as the complexes of cucurbit[5]uril with metal cations) the number of trajectories examined was increased to improve the statistics.

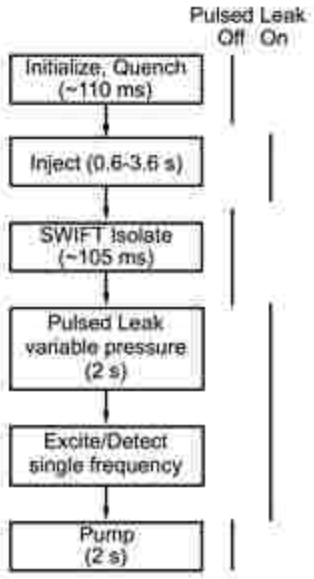

Figure 3.1 Sequence of events in a typical CRAFTI experiment.

Results and Discussion

Variation of FTICR linewidth with collision gas pressure

Figure 3.2 shows how the FTICR signal and resulting linewidth change as the pressure of Xe collision gas is varied. As expected, the rate of transient signal decay increases as Xe pressure increases, resulting in decreasing amplitude and increasing linewidth with increasing pressure. The variation of collision frequency reflected in the linewidth shows excellent linearity with collision gas number density (Figure 3.2c). Deviations from linearity generally occur at very low pressures, where line broadening is likely not pressure limited, at the upper limits of examined pressures, where signal strengths become weak enough they are difficult to observe (and where a significant number of collisions may occur during the excitation), and in cases where the mass of the collision gas is less than about 10% the mass of the ion of interest.

An example of this last case is the doubly-charged complex of two potassium ions with decamethylcucurbit[5]uril colliding with He (see Figure 3.3). At 1048.3 Da, this ion is much more massive than the 4.0 Da He collision gas, and it is likely that single collisions are not sufficient to remove these heavy ions from the coherent packet. In cases such as this, a frictional damping model assuming hard sphere collisions[25] may be a better description of the motion of the excited ions, and a determination of cross section using the method described below is not appropriate.

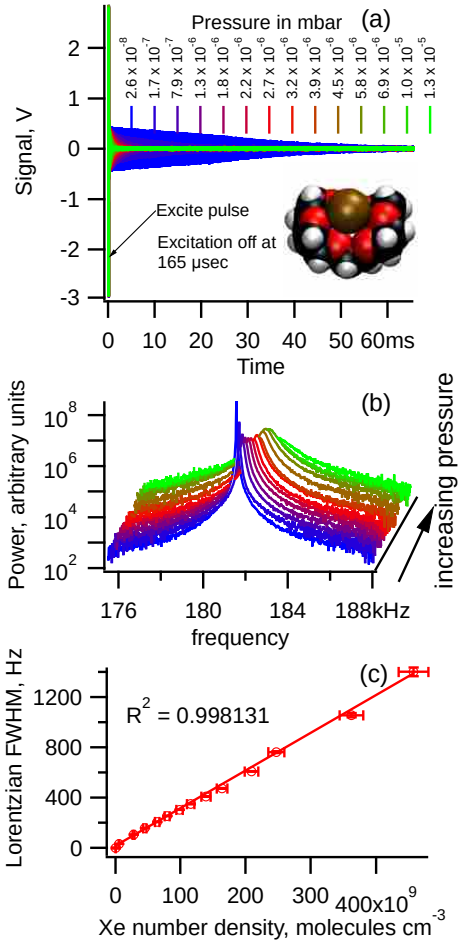

Figure 3.2 Variation of FTICR linewidth for 18-crown-6•Cs^+ complex (inset) as background Xe pressure is varied. (a) Time domain signals over a range of Xe pressures. The excitation pulse, 165 µs long, is

short compared with the signal transients. (b) Power mode frequency domain spectra corresponding to the time domain transients of (a). (c) Full width at half maximum (FWHM) linewidths as a function of Xe number density, showing excellent linearity. Error bars in the y-direction are standard errors from the fitting procedure, and errors in the x-direction are estimated uncertainties in the pressure measurements.

Figure 3.2a suggests some damping of the transient may occur during the excite event, especially at the highest pressures employed. It might be possible to avoid this by pulsing in the collision gas only after the excite event is complete, but the good linearity of the linewidth-vs.-pressure data (Figure 3.2c, for example) suggests that collisions during the excitation did not have large adverse effects on the results.

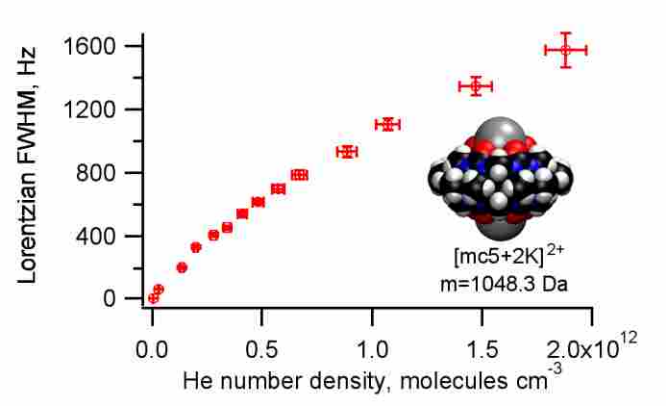

Figure 3.3 The FTICR linewidth for the complex of two K^+ ions with decamethylcucurbit[5]uril ($[mc5+2K]^{2+}$) does not vary linearly as He number density increases. In cases such as this the assumption of single-collision elimination of ions from the coherent packet is not valid.

Extraction of cross sections from linewidth data

In drift ICR experiments, which were clearly carried out under pressure-limited line broadening conditions, common practice[26] was to set the FWHM (full width at half maximum) linewidth of the power absorption spectrum equal to the collision frequency for momentum transfer, ξ, which is given as follows:

$$\xi = \frac{M}{m+M}\sigma n_n v = FWHM \qquad (3\text{-}1)$$

Here, m is the mass of the ion, M is the mass of the neutral, σ is the collision cross section, n_n is the neutral density, and v is the relative ion-neutral speed.

Simple rearrangement and substitution of equation (1-12) in Chapter 1 for v gives an expression for the collision cross section:

$$\sigma = \frac{FWHM}{n_n}\frac{(m+M)}{M}\frac{m}{q}\frac{2d}{\beta V_{pp} t_{exc}} \qquad (3\text{-}2)$$

In this expression, $FWHM/n_n$ is the slope of the line in a plot of power spectrum FWHM linewidth vs. neutral number density n_n (such as Figure 3.2c). Equations (3-1) and (3-2) are also applicable to the FTICR experiments reported here, and all the terms are known or easily measured. Thus, calculation of the cross section from the linewidth data is straightforward.

Kinetic energy dependence

Collision cross sections are known to depend on the kinetic energy involved in the collision. At thermal energies, where ion-induced dipole interactions are dominant, cross sections decrease with increasing energy.[27] Behavior at higher energies is more complex. If dissociation channels are accessed, large changes in cross section may result.[28] As energy increases, the total collision cross section for simple scattering should approach a hard sphere limit, which may

gradually decrease at higher energies due to the fact that molecules are not actually hard spheres and higher energy collisions may penetrate deeper into the repulsive part of the ion-neutral potential.

Our experiments probe the total cross section for removal of ions from the coherent packet generated in the FTICR excite-detect sequence. Thus, they are perhaps best described as "dephasing cross sections." This should include contributions from momentum transfer and from reactive collisions including those leading to dissociation. At energies of tens to hundreds of electron volts in the center-of-mass reference frame, which are typical of ions excited for FTICR detection in a 4.7 Tesla field, we expect in general to be in the hard-sphere collision regime, in which there is little to no dependence of momentum transfer cross section on center-of-mass kinetic energy. I have therefore examined the kinetic energy dependence of the measured CRAFTI cross sections with Xe collision gas for a number of systems, and the results are shown in Figure 3.4.

Examination of Figure 3.4 reveals that for the lower mass complexes (crown ethers bound to alkali cations, up to at least m = 397.1 Da), cross sections are independent of collision energy, suggesting these systems are in the hard-sphere regime and that the assumption that a single collision is sufficient to remove the ion from the coherent packet is valid. For the heavier ions examined (masses around 1000 Da), CRAFTI cross sections rise with increasing kinetic energy until about 200 eV in the center-of-mass frame of reference, and remain constant through 500 eV. Apparently mass is an important contributor to this behavior (rather than m/z), as the shapes of the curves for $[mc5+K]^+$, $[mc5+2K]^{2+}$, and $[MeOH@mc5+2K]^{2+}$, with similar masses of 1009,

1048, and 1080 Da, respectively, are similar despite large differences in m/z. From an analytical standpoint, the data suggest that heavier ions must be accelerated to higher kinetic energies to reach the hard sphere limit.

Several factors may account for the observed increase in cross section with kinetic energy. First, the absolute change in momentum during a collision increases as the total momentum of the collision system increases, so larger momentum changes are expected as kinetic energy increases, increasing the likelihood that collision will result in scattering out of the coherent packet. In addition, the likelihood of collisions transferring sufficient energy to dissociate the ions during the observation period increases with increasing kinetic energy. Clearly, if collision of the ion with background gas results in sufficiently fast dissociation, the ion will be removed from the coherent packet and not contribute to subsequent signal.

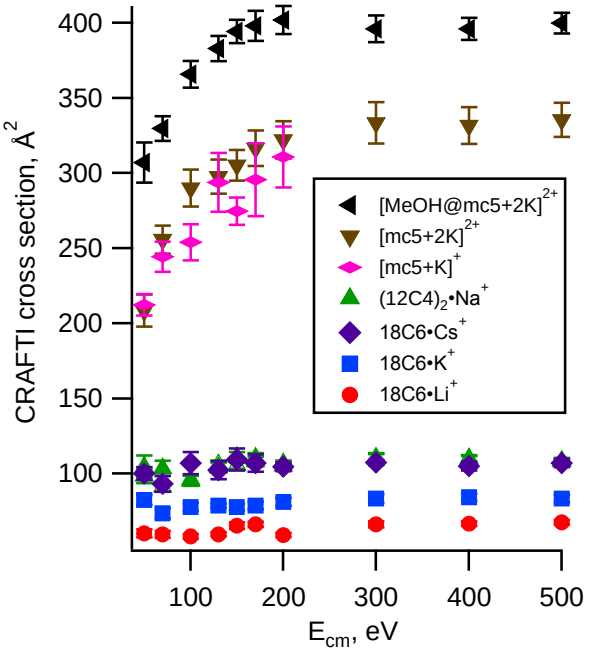

Figure 3.4 Effect of kinetic energy in the center-of-mass reference frame on measured collision cross sections (Xe collision gas). Error bars represent ± 1 standard deviation from the fitting procedure. Measurement at higher kinetic energies for $[mc5+K]^+$ was not possible because ions of this m/z are ejected from the trapping cell under the required conditions.

Absolute values of CRAFTI cross sections

Momentum transfer cross sections have been examined for a wide range of molecular systems using drift mobility measurements in helium.[8] In addition, cross sections for reactive collisions have been measured using guided ion beam techniques by a number of groups.[29-32] Comparison of the CRAFTI results to results obtained using these other well-accepted methods should yield some idea of the reasonability of the CRAFTI results. Cross sections obtained using drift mobility measurements, guided ion beam experiments, and CRAFTI are compared in Table 3.1.

The absolute magnitudes of the CRAFTI cross sections are in reasonable agreement with cross sections determined using more established methods. Except for the largest ions (which involve Lys bound to CB6 or α-CD), the CRAFTI cross sections are generally within a factor of 2 of the results of the drift mobility measurements. In fact, the agreement is perhaps better than should be expected, based on the substantial differences between these experiments. The drift mobility measurements were carried out at close to thermal collision energies, using He as the collision gas, and are designed to probe momentum transfer collision cross sections. Collision energies under drift mobility conditions are generally much too low to cause dissociation. The CRAFTI experiments shown here involve 150 eV collisions with Xe, and reflect all processes that remove ions from the coherent packet in the FTICR cell, including both momentum transfer and dissociation. At these high collision energies, the latter contribution is likely to be substantial, and may account for the CRAFTI cross sections of the Lys complexes being so much larger than what is observed using drift mobility.

Table 3.1 Comparison of cross sections by guided ion beam, drift mobility, and CRAFTI techniques

	Reported Cross Section, Å^2		
Species	Guided Ion Beam[a]	Drift Mobility[b]	CRAFTI[c]
18C6•Li^+		95.0[d]	65 ± 2
18C6•K^+	52[e]	105.0[d]	78 ± 2
18C6•Cs^+	16[e]	104.7[d]	109 ± 7
$[CB6+Lys+2H]^{2+}$		189.1[f]	370 ± 11
$[\alpha\text{-CD}+Lys+H]^+$		220.0[f]	510 ± 20

[a] Collisions with Xe at approximately 15 eV in the center-of-mass frame.

[b] Low energy collisions with He.

[c] At 150 eV in the center-of-mass frame of reference, colliding with Xe.

[d] Reference (33) Lee, S.; Wyttenbach, T.; von Helden, G.; Bowers, M. T. *J. Am. Chem. Soc.* **1995**, *117*, 10159-10160.

[e] Reference (34) More, M. B.; Ray, D.; Armentrout, P. B. Ibid.**1999**, *121*, 417-423.

[f] Reference (3) Zhang, H.; Grabenauer, M.; Bowers, M. T.; Dearden, D. V. *J. Phys. Chem. A* **2009**, *113*, 1508-1517.

The guided ion beam experiments involve collisions with Xe at superthermal energies (up to about 15 eV in the center-of-mass frame of reference), so in some ways these experiments are more similar to CRAFTI, which also involves collisions with Xe at higher-than-thermal energies. However, reference to Table 3.1 indicates that the beam experiments yield absolute cross section values much smaller than those from either drift mobility or CRAFTI. This is not surprising because the beam experiments probe only dissociative collisions and so beam-derived cross sections are expected to be smaller than are observed from techniques that include contributions from non-reactive scattering. The primary objective of the beam experiments is measurement of accurate thermodynamic dissociation thresholds, with absolute cross section measurements being of secondary interest. Finally, the beam measurements are made at much lower collision energies than are required in the CRAFTI experiments (lower kinetic energies do not excite the ions sufficiently to produce good FTICR signal), so again close agreement between the two methods is not expected.

Correlation of CRAFTI cross sections with computed momentum transfer cross sections

Sophisticated methods have been developed to compute collision cross sections for proposed molecular geometries, enabling comparison with experimentally measured cross sections from drift mobility. For example, the MOBCAL[20-24] program is widely used for this purpose. The agreement between computed and experimentally observed cross sections (from drift ion mobility) is generally excellent in the mass range investigated here. Comparison between computed cross sections and CRAFTI measurements therefore offers another means of testing the CRAFTI results, without being limited to the systems that have been experimentally

investigated with drift mobility. While for the reasons noted above I do not expect absolute agreement between computed and CRAFTI cross sections, if the CRAFTI results are structurally informative I do expect a correlation between the two sets of data.

Figure 3.5 shows the correlation between CRAFTI cross sections measured in xenon and momentum transfer cross sections computed for model structures in helium using the trajectory method (TM) in MOBCAL. Qualitatively, the CRAFTI cross sections follow the same trends as the computed cross sections; with few exceptions, ions that are computed to have larger TM cross sections are measured to have larger CRAFTI cross sections, and species that are computed to be similar in cross sections have similar measured CRAFTI cross sections.

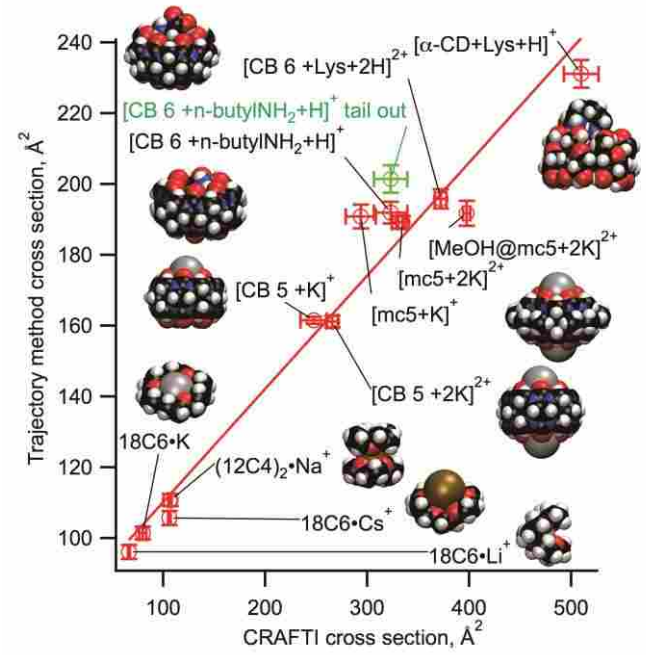

Figure 3.5 Correlation between CRAFTI cross sections in xenon (average value in the hard-sphere collision kinetic energy regime) and momentum transfer cross sections computed for collisions with helium via the trajectory method. The line is a linear least squares fit to the data; error bars represent one standard deviation. The point labeled "[CB6+n-butylNH$_2$+H]$^+$ tail out" (and colored green) was not included in the fit (see text). Each point is an average over a range of center-of-mass kinetic energies.

Both TM and CRAFTI show that the 18-crown-6 complexes with alkali cations have larger cross sections as the size of the metal ion increases. This has also been observed in drift mobility measurements,[33] and is understood to be a result of the fact that as the metal size increases the crown ligand opens up into less folded conformations. For CRAFTI, which includes contributions from dissociation, one might expect cross sections to increase with increasing metal size because the binding energy for the metal decreases as the metal ion gets larger[34] while the number of internal degrees of freedom in the system remains constant.

Therefore, dissociation rates at a given energy increase as the size of the metal increases. If a larger fraction of collisions (perhaps, for example, glancing collisions at larger impact parameters) results in sufficient energy deposition for dissociation to occur, CRAFTI cross sections will increase. However, the general agreement between TM and CRAFTI for the 18-crown-6 complexes suggests such energy effects probably do not play a large role for these molecular systems.

It is interesting to note that the CRAFTI cross section for $(12\text{-crown-4})_2Na^+$ is consistently larger than that for 18-crown-6•Cs^+ (in good agreement with the calculated TM values), even though for the former the molecular weight at 375 Da is smaller than for the latter at 397 Da. Similarly, the CRAFTI cross section for [α-cyclodextrin+Lys+H]$^+$, 1119 Da, is larger than that for [CB6+Lys+2H]$^{2+}$, 1144 Da. This demonstrates that CRAFTI cross sections do not always simply scale with molecular weight.

The cucurbituril-alkali cation complexes offer an opportunity to examine systems that are similar in TM cross section but differ in mass and charge state. [CB5+K]$^+$ and [CB5+2K]$^{2+}$ are computed to have identical momentum transfer cross sections in He, and have similar CRAFTI cross sections, although the doubly-charged ion has a cross section about 7 ± 6% larger than the singly-charged ion by CRAFTI. Similarly, [mc5+K]$^+$ and [mc5+2K]$^{2+}$ have identical TM cross sections, but the doubly-charged ion is found to have a cross section about 13 ± 6% larger than the singly-charged ion by CRAFTI. The similarity in the CRAFTI cross sections, despite the large difference in *m/z*, is encouraging. The fact that the CRAFTI cross sections are larger for the doubly-charged ions likely arises from bond energy effects as described above; it is much

easier to induce loss of K^+ from the doubly-charged complexes[35] (and hence, loss of the ions from the coherent packet) than from the cucurbiturils bound to only one metal cation. In addition, the differences reported here between CRAFTI cross sections for +1 and +2 ions may be exaggerated because of difficulty in reaching hard-sphere limit kinetic energies for the singly-charged ions (achievable kinetic energies in a trap of given size depend inversely on the *m/z* of the ions; ions with larger *m/z* are ejected from the trap at high kinetic energies). Because CRAFTI cross sections rise with increasing kinetic energy until the hard-sphere limit is reached (Figure 3.4), if the singly-charged ions are below the hard-sphere limit their reported cross sections would correspondingly be less.

Another case where the TM calculations suggest similar cross sections whereas CRAFTI indicates large differences is that involving $[mc5+2K]^{2+}$ and the related methanol inclusion complex, $[MeOH@mc5+2K]^{2+}$. On the basis of reactivity and collision-induced dissociation evidence,[36] methanol is believed to reside inside the mc5 cavity, leading to the expectation that the physical sizes of the empty complex and the methanol inclusion complex should be the same. As expected, within computational error, TM calculations find the two systems have the same momentum transfer cross section. However, the CRAFTI measurements place the inclusion complex cross section a surprising 20 ± 2% larger than the identical mc5 complex lacking methanol in its cavity. Very likely this difference in cross sections is the result of much lower energies required to remove methanol from the cavity vs. those needed for dissociation of K^+ from the complex. This assumes that dissociation plays a role comparable to that of momentum transfer in removing these ions from the coherent packet. Indeed, the current results suggest

that under conditions where the FTICR transient length is pressure-limited, collisional dissociation of the ions is an important contributor to loss from the coherent packet, at least for ions similar to those examined here.

One last example illustrates the potential for the CRAFTI technique to distinguish between conformational possibilities. The cavity of CB6 is large enough to allow insertion of an alkyl chain. I have examined the complex of *n*-butylammonium (nBA) ion with CB6, which is primarily held together via hydrogen bonds between the ammonium group of the guest and the carbonyl oxygens of the host. The structural question is whether or not the guest's alkyl tail is inserted into the host's cavity. Insertion would afford energetic stabilization through increased van der Waals contact between host and guest. On the other hand, it is entropically unfavorable to constrain the tail within the host cavity. As is noted in Figure 3.5, the point for $[CB6+n\text{-butyl}NH_2+H]^+$ with the alkyl tail inserted (trajectory method cross section 192 ± 3 $Å^2$) is close to the trend line. The calculated cross section for the tail-out conformer, 206 ± 3 $Å^2$, places that conformer much further from the trendline, suggesting the tail-in conformer is more consistent with the experimental data.

Conclusions

The model for FTICR/MS signal generation based on the rate of ion loss from the coherently orbiting packet of ions presented in Chapter 1 implies that the rate of ion loss from the packet in the high-pressure limit (from either non-reactive scattering or collisional dissociation) is dependent on the ion-neutral collision cross section, suggesting that such dephasing cross sections should be measurable by analysis of the decay of the FTICR/MS signal transient. My

results suggest the role of collisional dissociation in the loss of ions from the coherent ion packet in FTICR/MS has been underappreciated.

The resulting CRAFTI technique adds a new capability to Fourier transform ion cyclotron resonance mass spectrometry. Thus, in one instrument, it is possible to perform ultra high mass resolution, ultra high mass accuracy, tandem-in-time collisional and reactivity studies, and cross section measurements. My data suggest that the CRAFTI technique can be used to obtain structurally informative cross section information for molecules with molecular weights up to the kilodalton range. For characterization of small supramolecules, where conformational relationships are important, I expect this information to enable different conformations to be distinguished, in a manner similar to what is currently successfully practiced using momentum transfer cross sections from drift ion mobility measurements to compare with cross sections computed for candidate structures. For instance, it should be possible to distinguish between conformations where a guest is specifically bound inside a host molecule's cavity, and where the guest is non-specifically attached to the exterior of the host.

Many important challenges remain. At this point it is not possible to distinguish between dephasing resulting from scattering and dephasing resulting from dissociation. The inability to deconvolute binding strength effects from size effects makes interpretation of CRAFTI results more difficult. It is further not clear what will happen when a mixture of isobaric conformers is present; it would be desirable to be able to measure cross sections for each component of the mixture. In addition, CRAFTI may be limited to lower-mass systems in which single collisions

are capable of dephasing the ions; thus, many interesting biomolecular systems may be out of reach of the technique. Nevertheless, I believe the method shows promise.

References

(1) Mukhopadhyay, R. *Anal. Chem.* **2008**, *80*, 7918-7920.

(2) Bohrer, B. C.; Merenbloom, S. I.; Koeniger, S. L.; Hilderbrand, A. E.; Clemmer, D. E. *Annu. Rev. Anal. Chem.* **2008**, *1*, 293-327.

(3) Zhang, H.; Grabenauer, M.; Bowers, M. T.; Dearden, D. V. *J. Phys. Chem. A* **2009**, *113*, 1508-1517.

(4) Dearden, D. V.; Ferrell, T. A.; Asplund, M. C.; Zilch, L. W.; Julian, R. R.; Jarrold, M. F. *J. Phys. Chem. A* **2009**, *113*, 989-997.

(5) Clemmer, D. E.; Jarrold, M. F. *J. Mass Spectrom.* **1997**, *32*, 577-592.

(6) Guevremont, R. *Can. J. Anal. Sci. Spectrosc.* **2004**, *49*, 105-113.

(7) Shvartsburg, A. A.; Smith, R. D. *Anal. Chem.* **2008**, *80*, 9689-9699.

(8) Wyttenbach, T.; Bowers, M. T. *Top. Curr. Chem.* **2003**, *225*, 207-232.

(9) Wyttenbach, T.; Baker, E. S.; Bernstein, S. L.; Ferzoco, A.; Gidden, J.; Liu, D.; Bowers, M. T. *Adv. Mass Spectrom.* **2004**, *16*, 189-200.

(10) Zhang, X. X.; Krakowiak, K. E.; Xue, G.; Bradshaw, J. S.; Izatt, R. M. *Ind. Eng. Chem. Res.* **2000**, *39*, 3516-3520.

(11) Sievers, H. L.; Grützmacher, H.-F.; Caravattie, P. *Int. J. Mass Spectrom. Ion Processes* **1996**, *157/158*, 233-247.

(12) Caravatti, P.; Allemann, M. *Org. Mass Spectrom.* **1991**, *26*, 514-518.

(13) Wigger, M.; Nawrocki, J. P.; Watson, C. H.; Eyler, J. R.; Benner, S. A. *Rapid Commun. Mass Spectrom.* **1997**, *11*, 1749-1752.

(14) Jiao, C. Q.; Ranatunga, D. R. A.; Vaughn, W. E.; Freiser, B. S. *J. Am. Soc. Mass Spectrom.* **1996**, *7*, 118-122.

(15) Bartmess, J. E.; Georgiadis, R. M. *Vacuum* **1983**, *33*, 149-153.

(16) Senko, M. W.; Canterbury, J. D.; Guan, S.; Marshall, A. G. *Rapid Commun. Mass Spectrom.* **1996**, *10*, 1839-1844.

(17) Blakney, G. T.; Hendrickson, C. L.; Marshall, A. G. In *55th ASMS Conference on Mass Spectrometry and Allied Topics* Indianapolis, IN, 2007.

(18) Hofstadler, S. A.; Sannes-Lowery, K. A.; Griffey, R. H. *Rapid Commun. Mass Spectrom.* **2001**, *15*, 945-951.

(19) Chen, L.; Wang, T.-C. L.; Ricca, T. L.; Marshall, A. G. *Anal. Chem.* **1987**, *59*, 449-454.

(20) Mesleh, M. F.; Hunter, J. M.; Shvartsburg, A. A.; Schatz, G. C.; Jarrold, M. F. *J. Phys. Chem.* **1996**, *100*, 16082-16086.

(21) Shvartsburg, A. A.; Jarrold, M. F. *Chem. Phys. Lett.* **1996**, *261*, 86-91.

(22) Shvartsburg, A. A.; Hudgins, R. R.; Dugourd, P.; Jarrold, M. F. *J. Phys. Chem. A* **1997**, *101*, 1684-1688.

(23) Shvartsburg, A. A.; Pederson, L. A.; Hudgins, R. R.; Schatz, G. C.; Jarrold, M. F. *J. Phys. Chem. A* **1998**, *102*, 7919-7923.

(24) Shvartsburg, A. A.; Mashkevich, S. V.; Baker, E. S.; Smith, R. D. *J. Phys. Chem. A* **2007**, *111*, 2002-2010.

(25) Guan, S.; Li, G.-Z.; Marshall, A. G. *Int. J. Mass Spectrom. Ion Proc.* **1997**, *167*, 185-193.

(26) Ridge, D. P.; Beauchamp, J. L. *J. Chem. Phys.* **1976**, *64*, 2735-2746.

(27) Su, T.; Bowers, M. T. In *Gas Phase Ion Chemistry*; Bowers, M. T., Ed.; Academic: New York, 1979; Vol. 1, p 83-118.

(28) Armentrout, P. B. *Int. J. Mass Spectrom.* **2000**, *200*, 219-241.

(29) Rodgers, M. T.; Armentrout, P. B. *Mass Spectrom. Rev.* **2000**, *19*, 215-247.

(30) Ervin, K. M. *Int. Rev. Phys. Chem.* **2001**, *20*, 127-164.

(31) Armentrout, P. B. *Topics in Current Chemistry* **2003**, *225*, 233-262.

(32) Rodgers, M. T.; Armentrout, P. B. *Acc. Chem. Res.* **2004**, *37*, 989-998.

(33) Lee, S.; Wyttenbach, T.; von Helden, G.; Bowers, M. T. *J. Am. Chem. Soc.* **1995**, *117*, 10159-10160.

(34) More, M. B.; Ray, D.; Armentrout, P. B. *J. Am. Chem. Soc.* **1999**, *121*, 417-423.

(35) Mortensen, D. N.; Dearden, D. V. *Chem. Commun.* **2011**, *47*, 6081-6083.

(36) Kellersberger, K. A.; Anderson, J. D.; Ward, S. M.; Krakowiak, K. E.; Dearden, D. V. *J. Am. Chem. Soc.* **2001**, *123*, 11316-11317.

Chapter 4 Kinetic Energy and Collision Gas Effects in Measurement of Collision Cross Sectional Areas by Fourier Transform Ion Cyclotron Resonance (CRAFTI)

Introduction

Fourier transform ion cyclotron mass spectrometry (FTICR-MS) has versatile capabilities. It is capable of high resolving power, high mass accuracy and tandem-in-time experiments. Recently a new cross section measurement technique has been developed: collision cross sectional areas by Fourier transforms ion cyclotron resonance (CRAFTI). This technique provides a promising method to carry out structurally-informative cross section measurements in the same instrument.[1] Now not only fragmentation and reactivity experiments but also cross section measurements can be performed with the same mass spectrometer.

The basic concept of CRAFTI is to observe the collision-limited decay of the FT-ICR transient signal and thus extract a cross section for loss of ions from the coherently-orbiting packet that is produced when ion motion is resonantly excited.[1,2] This is done over a range of collision gas pressures obtained via use of a pulsed leak valve. Therefore, I examine how the FTICR signal and resulting Lorentzian line shape changes as the pressure of the collision gas is varied. I initially assumed that any kind of neutral gas would be appropriate. However, after trying different collision gases (Xe and He) and comparing the experimental cross section results with values computed using the trajectory method,[1] it was found that there are limitations to the choice of collision gas. Helium is too light to provide sufficient momentum transfer to remove the ions from the coherent packet via single collisions at accessible energies. Xenon, on the other hand, is monoatomic and heavy enough to scatter ions up to the kilodalton mass range out of the

coherent packet via single collisions. CRAFTI cross sections determined using Xe correlate well with computational results.

The kinetic energy of the ion-neutral collisions in the center-of-mass frame of reference also plays an important role in these experiments. I examined how the CRAFTI cross sections are dependent on the kinetic energy in Xe at tens to hundreds of electron volts, which are expected to be in the hard-sphere collision regime.[1] Basically, for lower mass ions (crown ethers bound to alkali cations, up to about 400 Da), the cross sections are independent of kinetic energy; for heavier ions, the cross sections increase with kinetic energy until about 200 eV in the center-of-mass reference frame, then remain essentially constant at higher energies. Several factors are thought to account for the increase of cross section with energy, including increasing absolute change in momentum during a collision and the likelihood of collisions transferring sufficient energy to dissociate the ions during the measurement period, both of which increase with energy.

In this chapter, I further examine the influence of collision gas on the CRAFTI experiment, using N_2, Ar, and SF_6 as collision gases at various kinetic energies. I show that each of these gases may be used effectively under proper conditions.

Experimental

Materials

12-crown-4 (12C4) and 18-crown-6 (18C6), as well as cucurbit[5]uril (CB5), cucurbit[6]uril (CB6), α-cyclodextrin (αCD), and L-lysine (Lys) were purchased from Sigma-Aldrich (St. Louis, MO) and used without further purification. Decamethylcucurbit[5]uril (mc5) was

synthesized by Dr. Krzystof Krakowiak using published procedures.[3] All the solvents, including methanol, isopropanol, and water were purchased from Mallinckrodt Baker Inc. (Phillipsburg, NJ). The sample preparation was performed essentially as described.[1] Damping gases were purchased from Airgas (Radnor, PA) at the following purities: N_2, 99.995%; Ar, 99.995%; SF_6, 99.8%.

Instrumentation

All experiments were carried out using a Bruker model APEX 47e Fourier transform ion cyclotron resonance mass spectrometer with an Infinity trapping cell[4,5] and a microelectrospray source modified from an Analytica (Branford, MA) design, with a heated metal capillary drying tube based on the design of Eyler.[6] This instrument has been described in detail in a previous paper,[1] so herein just a brief overview is provided. Pressures were adjusted and controlled using a pulsed leak valve based on the design of Freiser,[2] and measured using a cold cathode tube (Balzers; Fürstentum, Lichtenstein) mounted outside the high field region of the instrument, about 1 m from the trapping cell. The instrument was controlled using a MIDAS Predator data system (National High Magnetic Field Laboratory; Tallahassee, FL).[7,8] The pulse sequence for these experiments was described in detail elsewhere.[1] In general ions were injected into the trapping cell of the instrument, monoisotopically isolated using SWIFT, allowed to collisionally relax, subjected to elevated collision gas pressures using a pulsed leak valve, then coherently excited via a single-frequency RF pulse, after which the image current they generate on the detection plates was monitored.

Data analysis

The CRAFTI experimental results were processed using the Igor Pro software package (version 6, Wavemetrics; Lake Oswego, OR). Details for the analysis process are reported elsewhere.[1] Analysis involved calculation of the power spectrum and measurement of the full width at half maximum linewidth of the frequency domain peak as a function of collision gas pressure, from which CRAFTI cross sections are extracted.

Computational modeling

Molecular structures were obtained using the Maestro/Macromodel package (Macromodel version 7.1; Schrödinger, Inc.; Portland, OR) for conformational searching using either the MMFF or AMBER* force field provided in the package, then the conformers were put into the MOBCAL[9,10,11,12,13] program for calculation of low energy collision cross sections in helium. The modeling was performed using the same recipe as described previously.[1]

Results and Discussion

Choice of collision gas

As mentioned previously,[1] the CRAFTI cross sections were measured by analysis of the power spectrum FWHM linewidth response as the neutral number density of the collision gas is varied. Normally, linewidth varies linearly with number density, and the slope of the resulting line is the critical parameter used in determining the CRAFTI cross section. However, as shown previously,[1] in cases where the ion is several hundred times more massive than the neutral (specifically, $[mc5+2K]^{2+}$, at m/z 1048 Da, colliding with m/z 4 He), the linewidth does not vary linearly with number density. It is likely that the assumption of single collisions leading to dephasing of the ion is violated under these conditions, such that the straightforward extraction

of cross sections via our previously developed methods is not possible. On the other hand, with a heavier collision gas such as Xe, linewidth does depend linearly on number density and the calculation of CRAFTI cross sections is straightforward.

However, Xe is expensive, and the question arises about using other collision gases. I therefore carried out experiments using N_2, Ar, and SF_6. As in the earlier work, I seek to determine whether CRAFTI cross sections measured in a certain gas are structurally informative, based on the correlation between CRAFTI results in the gas of interest and cross sections derived from computational results. As before, I use cross sections calculated from expected molecular structures using the trajectory method as our standard for comparison in these correlations.

Correlation of CRAFTI cross sections with computed momentum transfer cross sections

Figure 4.1 shows the correlation between CRAFTI cross sections measured in (a) N_2, (b) Ar and (c) SF_6, all measured at the same relative center-of-mass kinetic energy (24.27eV), and momentum transfer cross sections computed for model structures in helium using the trajectory method (TM) using the MOBCAL[9-13] program. The CRAFTI cross sections are much larger than TM cross sections. This is not surprising, because the CRAFTI results include contributions from ion dissociation as well as from momentum transfer scattering.[1] Although the CRAFTI cross sections in these three gases are different, the cross sections measured in each gas all follow the same trends as the computed cross sections; with few exceptions, ions that are computed to have larger TM cross sections are observed to have larger CRAFTI cross sections, and species that are computed to be similar in cross sections have similar measured CRAFTI cross sections. Furthermore, the CRAFTI cross sections in the different gases correlate very

strongly with each other. This is strong evidence that I am doing things correctly and may be getting answers that are closer to the "truth" than the MOBCAL values.

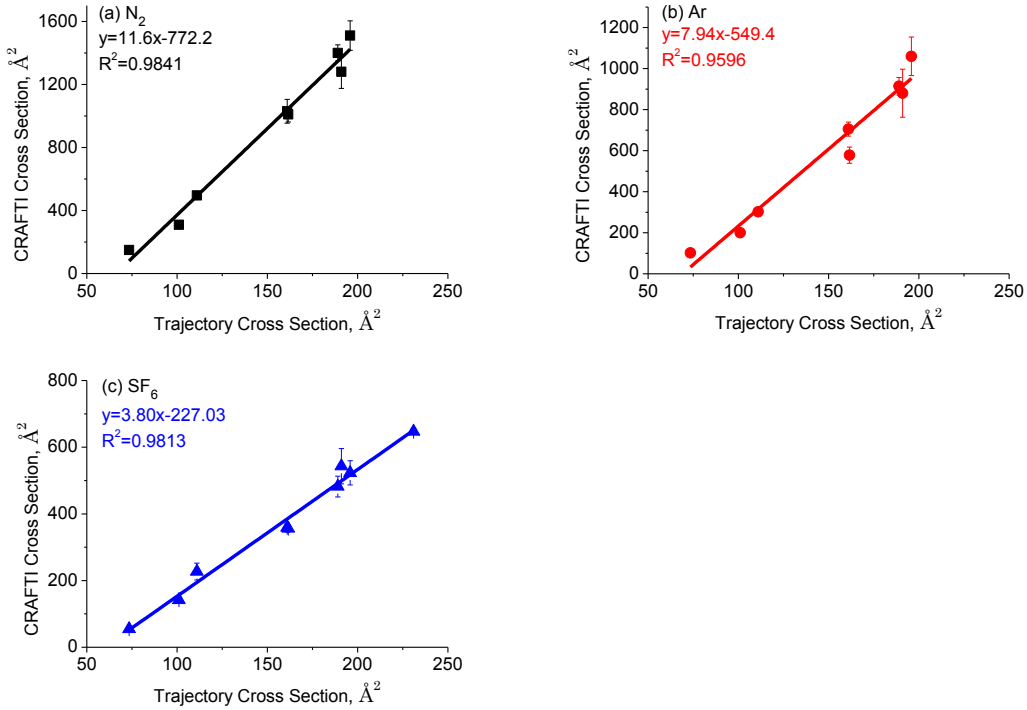

Figure 4.1 Correlation between CRAFTI cross sections in Nitrogen (a), Argon (b), SF_6(c) and momentum transfer cross sections computed for collisions with helium via the trajectory method. The lines are linear least squares fit to the data; error bars represent one standard deviation.

Dependence on Kinetic energy

CRAFTI cross sections are perhaps best described as "dephasing cross sections" since CRAFTI measures the total cross section for removal of the ions from the coherent packet in the FT-ICR excitation-detection sequence, which should include contributions from momentum transfer and from reactive collisions including those leading to dissociation.[1] At energies of tens of electron volts in the center-of-mass reference frame, which are normal for ions excited for detection in a

4.7 Tesla FT-ICR mass spectrometer, I expect generally to be in the hard-sphere collision regime and to have significant contributions from dissociation. Herein, I explored how the CRAFTI cross sections change with variation of the relative center-of-mass kinetic energies (E_{cm}) for a number of systems, and the results in N_2, Ar and SF_6 are shown in Figure 4.2(a), 4.2(b) and 4.2(c), respectively.

It is interesting to note that although the CRAFTI cross sections for the same complexes are different when measured in different gases, the shapes of the curves in N_2, Ar and SF_6 are similar.

For lower mass complexes (three crown ether complexes with alkali metal ions, including $[12C4+Na]^+$, 199 Da, $[(12C4)_2+Na]^+$, 375 Da and $[18C6+K]^+$, 303 Da), the CRAFTI cross sections are independent of kinetic energy in every collision gas, which means these systems are in the hard-sphere regime.

On the other hand, for heavier ions (masses around 1000 Da, including $[CB5+K]^+$, 869 Da, $[CB5+KK]^{2+}$, 908 Da, $[mc5+KK]^{2+}$, 1048 Da, , and $[\alpha CD+Lys+H]^+$, 1119 Da), the CRAFTI cross sections measured in N_2, Ar and SF_6 increase almost linearly with increasing kinetic energies until about 20 eV, then rise slowly at energies higher than 20 eV. This behavior is similar to that reported earlier for CRAFTI cross sections measured in Xe,[1] With increasing kinetic energy, the absolute change in momentum during a collision is larger, and the probability of collisions transferring sufficient energy to dissociate the ions is also bigger, which increases the probability for ions being removed from the coherent packet, and increases the observed linewidth and corresponding CRAFTI cross section.

Above I noted the good linear correlation between CRAFTI cross sections at 24.27 eV (Figure 4.1) and TM cross sections in three collision gases. Since CRAFTI cross sections depend on kinetic energy for the heavier ions, I would like to explore the correlation between CRAFTI cross section and TM cross section at other kinetic energies in these collision gases, shown in Figure 4.3. When the kinetic energies are too low, the heavier ions are not dephased effectively, so the CRAFTI technique is not appropriate and does not provide good correlation with the theoretical cross sections. At a kinetic energy of 14.56 eV, the correlation is better: in N_2 and Ar, the CRAFTI cross sections have a good linear relation with TM cross sections except for the heaviest ion ($[\alpha CD+Lys+H]^+$, 1119.5Da); while in SF_6, the CRAFTI cross sections of all the ions correlate linearly with TM cross sections. When the kinetic energy is high enough ($\geq$ 24.27eV), the linear relationship between CRAFTI cross sections and TM cross sections is excellent.

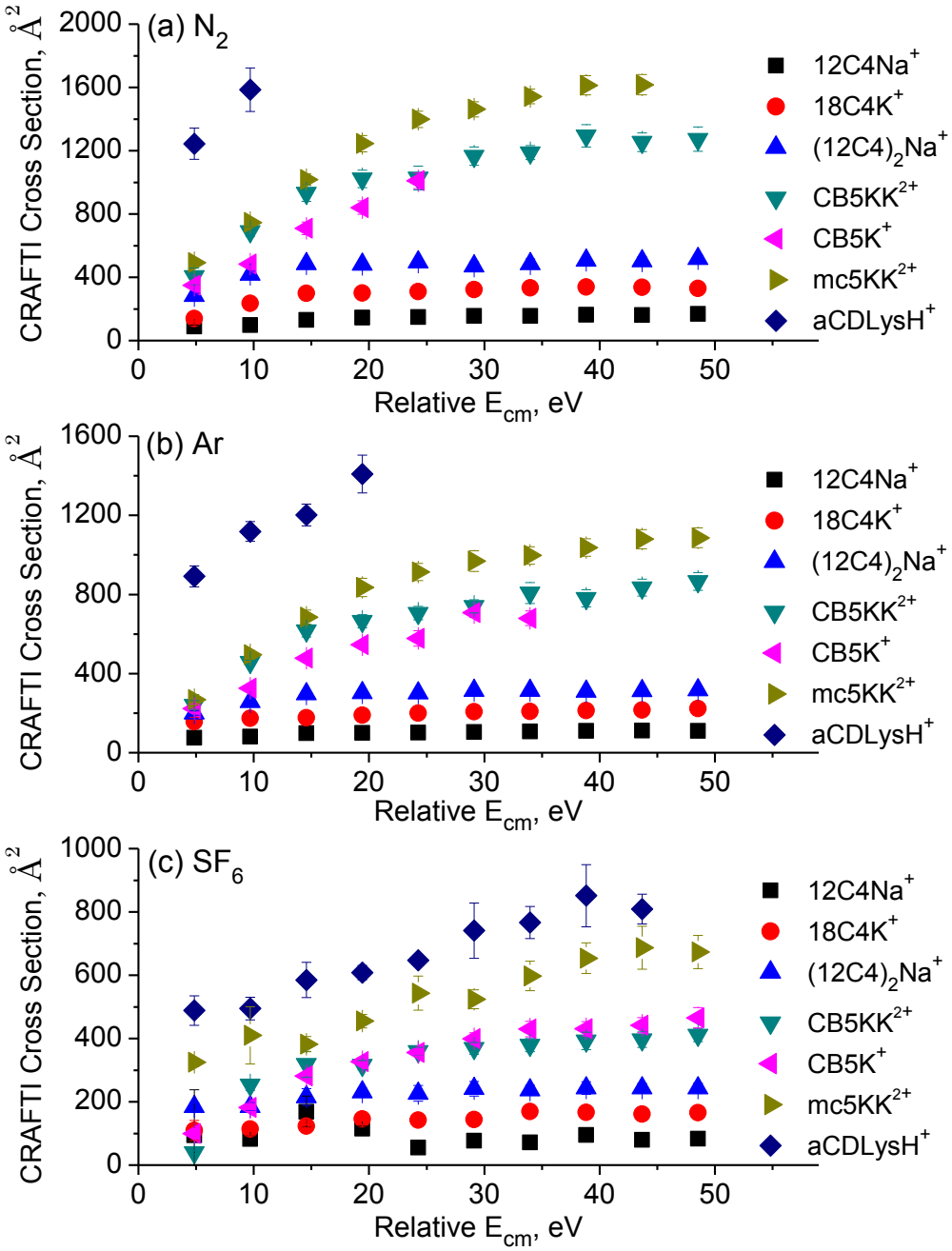

Figure 4.2 Effect of kinetic energy in the center-of-mass reference frame on measured collision cross sections in N_2 (a), Ar (b), SF_6 (c). Error bars represent ± 1 standard deviation from the fitting procedure.

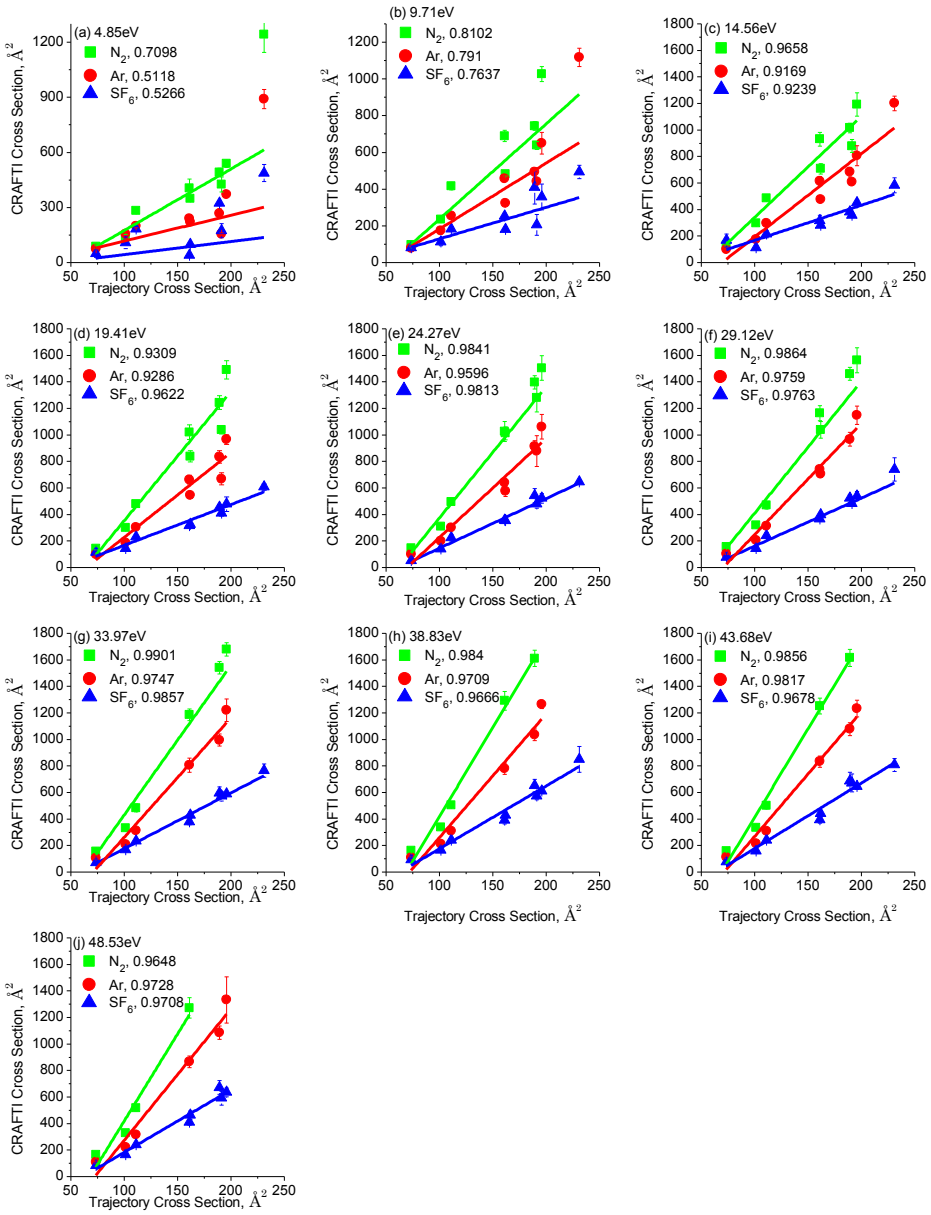

Figure 4.3 Correlation between CRAFTI cross sections at different kinetic energies (in the center-of-mass reference frame) in N_2, Ar, SF_6 and momentum transfer cross sections computed for collisions with helium via the trajectory method. The lines are linear least squares fits to the data; error bars represent one standard deviation. The numbers after the names of the collision gases are r^2 values for each linear fit.

Comparison of CRAFTI cross section in different collision gas

As is evident in Figure 4.2, the same ion measured at the same kinetic energy has different CRAFTI cross sections dependent on the choice of the collision gas. How should the value of the CRAFTI cross section change with variation of the damping gas?

I begin by considering the expression for the collision cross section in CRAFTI:[1,14,15,16]

$$\sigma = \frac{\xi}{n_n}\frac{(m+M)}{M}\frac{m}{q}\frac{2d}{\beta V_{pp} t_{exc}} = \frac{FWHM}{n_n}\frac{(m+M)}{M}\frac{m}{q}\frac{2d}{\beta V_{pp} t_{exc}} \quad (4\text{-}1)$$

In this expression, σ is CRAFTI cross section, ξ/n_n is the reduced collision frequency and is equal to $FWHM/n_n$ (which is the slope of the line in a plot of power absorption spectrum FWHM linewidth vs. neutral number density n_n of collision gas), m is the mass of the ion, q is the charge of the ion, M is the mass of the neutral gas, d is the trapping cell diameter, β is the cell geometry factor (0.897 for the Bruker Infinity cell[4,5] used here), V_{pp} is the peak-to-peak RF excitation amplitude, and t_{exc} is the duration of the RF excitation. Because I am comparing CRAFTI cross sections for the same ion measured at the same kinetic energy in the center-of-mass reference frame (E_{cm}) but in different collision gases, simple rearrangement and substitution of Equation (4-4) (which is derived from substitution of equation (4-2) into equation (4-3)) for V_{pp} into Equation (4-1) gives equation (4-5) for CRAFTI cross sections including E_{cm}.

$$E_{lab} = \left(\frac{\beta q t_{exc} V_{pp}}{d}\right)^2 \frac{1}{8m} \quad [14] \qquad (4\text{-}2)$$

$$E_{cm} = \left(\frac{M}{m+M}\right) E_{lab} \quad [17] \qquad (4\text{-}3)$$

$$E_{cm} = \left(\frac{\beta q t_{exc} V_{PP}}{d} \right)^2 \left(\frac{M}{m+M} \right) \frac{1}{8m} \qquad (4\text{-}4)$$

$$\sigma = \frac{FWHM}{n_n} \sqrt{\frac{m+M}{M} m \frac{1}{2E_{cm}}} \qquad (4\text{-}5)$$

Here, E_{lab} the ion kinetic energy and E_{cm} is kinetic energy in the center-of-mass reference frame. Based on Equation (4-5), when the CRAFTI cross section for the same ion is measured in different collision gases with the same E_{cm}, the cross section should only depend on the magnitude of $FWHM/n_n$ and the mass of neutral gas, M. Therefore, I need to investigate how values of $FWHM/n_n$ vary when changing the damping gas for the same ion at the same kinetic energy, and explore how the type of collision gas influences the CRAFTI cross sections.

Three systems, including $[18C6+K]^+$ (303Da, lower mass ion, singly charged), $[CB5+K]^+$ (869Da, heavier ion, singly charged) and $[CB5+2K]^{2+}$ (908Da, heavier ion, doubly charged), are selected to study this issue, and the results are shown in Figure 4.4.

In Figure 4.4(a), 4.4(b), and 4.4(c), for each complex, CRAFTI cross sections at the same kinetic energy measured in different gases exhibit the following trend: the cross section decreases with increasing neutral gas mass. This is consistent with what we would expect from Equation (4-3).

The results for how $FWHM/n_n$ varies with the damping gas for different ions are shown in Figure 4.4 (d), (e) and (f). It is clear that $FWHM/n_n$ increases with increasing kinetic energy in each collision gas. However, when comparing values for $FWHM/n_n$ measured at the same kinetic

energy but in different collision gases, the values of $FWHM/n_n$ monitored in N_2 are always the largest for any ion, while those measured in Ar and SF_6 are similar to each other and about 20% less than those in N_2. The reduced collision frequency at constant kinetic energy should increase as the collision gas becomes lighter, because the relative velocity must increase to keep the kinetic energy the same as the mass of the collision gas goes down. With higher velocity, the ions should undergo more collisions per unit time. The N_2 results have higher reduced collision frequencies than those in Ar, as predicted.

The relative magnitudes of reduced collision frequencies for Ar and SF_6 are not consistent with this analysis in terms of relative velocity: Ar has generally smaller reduced collision frequencies than SF_6. This requires a different explanation. I note that Ar is monoatomic and SF_6 is a much larger, polyatomic molecule. The physical size of SF_6 must therefore become more important than the difference in velocity. The $[CB5+2K]^{2+}$ results don't exactly fit this interpretation, but perhaps for them, with a very weak binding energy, dissociation effects dominate, making velocity more important than size. The understanding of these effects is incomplete.

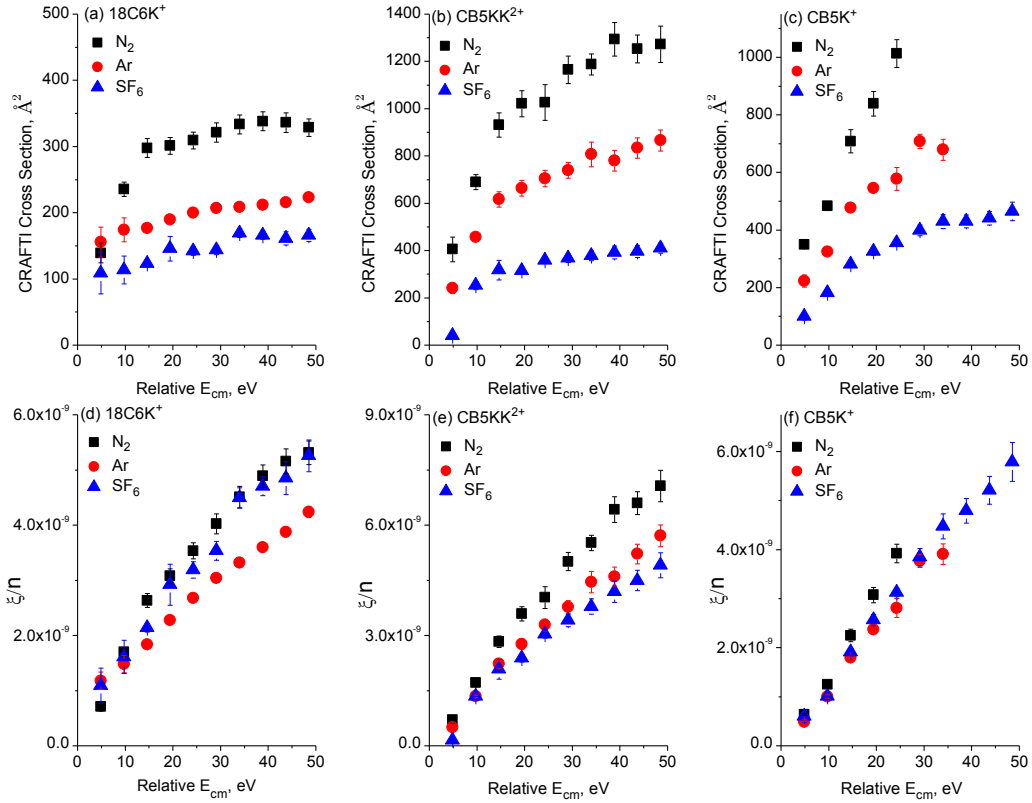

Figure 4.4 CRAFTI cross sections of $[18C6+K]^+$ (a), $[CB5+KK]^{2+}$ (b), $[CB5+K]^+$ (c) measured in N_2, Ar and SF_6 at various kinetic energies in the center-of-mass reference frame; Values of reduced collision frequency ($FWHM/n_n$) for $[18C6+K]^+$ (d), $[CB5+KK]^{2+}$ (e), and $[CB5+K]^+$ (f) in N_2, Ar and SF_6 at various kinetic energies in the center-of-mass reference frame. Error bars represent ± 1 standard deviation from the fitting procedure.

Conclusions

CRAFTI is an encouraging technique for acquisition of structurally informative cross section information for molecules with molecular weights up to the kilodalton range via monitoring the rate of ion loss from the coherently orbiting packet of ions in an FT-ICR mass spectrometer.[1] Helium is too light to provide efficient collisions for damping the motion of heavy ions, whereas

xenon works well but is expensive. So another appropriate choice for a collision gas is desirable. In this paper, N_2, Ar, and SF_6, which are heavier but not expensive, are all shown to yield a good correlation between CRAFTI cross sections measured in each collision gas and computed results from the trajectory method.

As with CRAFTI cross sections measured in xenon, the kinetic energy dependence for CRAFTI results measured in other damping gases also confirm that the CRAFTI method measures the total "dephasing cross section" for removal of the ions from the coherent packet in the FT-ICR cell, including contributions not only from momentum transfer but also from reactive collisions such as those leading to collisional dissociation.

Absolute CRAFTI cross sections are different in different damping gases. Since the reduced collision frequency, ξ/n_n, does not have a large collision gas dependence, the mass of the neutral gas becomes an important factor for determining the absolute values of CRAFTI cross section as the collision gas is varied.

References

(1) Yang, F.; Voelkel, J. E.; Dearden, D. V. *Anal. Chem.* **2012**, *84*, 4851-4857.

(2) Jiao, C. Q.; Ranatunga, D. R. A.; Vaughn, W. E.; Freiser, B. S. *J. Am. Soc. Mass Spectrom.* **1996**, *7*, 118-122.

(3) Zhang, H.; Grabenauer, M.; Bowers, M. T.; Dearden, D. V. *J. Phys. Chem. A* **2009**, *113*, 989-997.

(4) Sievers, H. L.; Grutzmacher, H.-F.; Caravattie, P. *Int. J. Mass Spectrom. Ion Processes* **1996**, *157/158*, 233-247.

(5) Caravatti, P.; Allemann, M. *Org. Mass Spectrom.* **1991**, *26*, 514-518.

(6) Wigger, M.; Nawrocki, J. P.; Watson, C. H.; Eyler, J. R.; Benner, S. A. *Rapid Commun. Mass Spectrom.* **1997**, *11*, 1749-1752.

(7) Senko, M. W.; Canterbury, J. D.; Guan, S.; Marshall, A. G. *Rapid Commun. Mass Spectrom.* **1996**, *10*, 1839-1844.

(8) Blakney, G. T.; Hendrickson, C. L.; Marshall, A. G. In *In 55th ASMS Conference on Mass Spectrometry and Allied Topics;* Indianapolis, IN;, 2007.

(9) Mesleh, M. F.; Hunter, J. M.; Shvartsburg, A. A.; Schatz, G. C.; Jarrold, M. F. *J. Phys. Chem.* **1996**, *100*, 16082-16086.

(10) Shvartsburg, A. A; Jarrold, M. F. *Chem. Phys. Lett.* **1996**, *261*, 86-91.

(11) Shvartsburg, A. A.; Hudgins, R. R.; Dugourd, P.; Jarrold, M. F. *J. Phys. Chem. A* **1997**, *101*, 1684-1688.

(12) Shvartsburg, A. A.; Pederson, L. A.; Hudgins, R. R.; Schatz, G. C.; Jarrold, M. F. *J. Phys. Chem. A* **1998**, *102*, 7919-7923.

(13) Shvartsburg, A. A.; Mashkevich, S. V.; Baker, E. S.; Smith, R. D. *J. Phys. Chem. A* **2007**, *111*, 2002-2010.

(14) Marshall, A. G.; Hendrickson, C. L.; Jackson, G. S. *Mass Spectrom. Rev.* **1998**, *17*, 1-35.

(15) Ridge, D. P.; Beauchamp, J. L. *J. Chem. Phys.* **1976**, *64*, 2735-2746.

(16) Guan, S.; Li, G.-Z.; Marshall, A. G. *Int. J. Mass Spectrom. Ion Proc.* **1997**, *167*, 185-193.

(17) Gross, J. H. *Mass Spectometry*; Springer: New York, 2006.

Chapter 5 Cross Sectional Analysis of Supramolecular Complexes Between Cucurbit[n]urils and Alkylamines Using the FTICR "CRAFTI" Technique

Introduction

In the field of supramolecular chemistry, molecular shape is often the most important factor influencing the strength of complexation between host and guest.[1,2] With the ability to measure momentum transfer collision cross sections, ion mobility techniques have become important for obtaining information about molecular shape using miniscule samples. However, such measurements require specially-designed, dedicated instrumentation.[3,4] I have developed a method for obtaining shape information using a Fourier transform ion cyclotron resonance (FTICR) mass spectrometer (cross sectional areas by Fourier transform ion cyclotron resonance, or "CRAFTI"), and have demonstrated the validity of the CRAFTI technique. [5]

In this chapter, I apply the CRAFTI technique to a series of supramolecular complexes between pumpkin-shaped cucurbit[n]uril (CBn) host molecules and straight-chain alkyl mono- and diamine guests to study the supramolecular complexation of those complexes.

Experimental

Materials

Cucurbit[5]uril (CB5), cucurbit[6]uril (CB6), alkyl monoamines ($H(CH_2)_{n-1}NH_2$, n=3-11, abbreviated $C_{n-1}A$, where n is the number of heavy atoms in the straight chain) and alkyl diamines ($NH_2(CH_2)_{n-2}NH_2$, n=4-12, abbreviated $C_{n-2}DA$, where n is the number of heavy atoms in the straight chain) were purchased from Sigma-Aldrich (St. Louis, MO) and used without further purification. Decamethylcucurbit[5]uril (mc5) was synthesized by Dr. Krzystof

Krakowiak using published procedures.[6] Stock solutions of CBn were prepared at about 200 μM by dissolving the solid samples in 88% formic acid (Mallinckrodt Baker Inc., Phillipsburg, NJ) and then diluting with methanol/water (50:50) or n-propanol/water (50:50). The electrospray solutions were prepared at concentrations of 100 μM in CBn and 200 μM in amines. Argon (99.995%) was purchased from Airgas (Radnor, PA) to be used as collision gas.

Instrumentation

All the CRAFTI experiments were performed on a Bruker model APEX 47e Fourier transform ion cyclotron resonance mass spectrometer. The instrument is equipped with an infinity cell and a 4.7T superconducting magnet. Ions are generated in a microelectrospray source modified from an Analytica (Branford, MA) design, with a heated metal capillary drying tube based on the design of Eyler.[7] The MIDAS Predator data system[8] (National High Magnetic Field Laboratory; Tallahassee, FL) is employed to control the FTMS instrument. All the CRAFTI experiments were carried out via 15eV collisions with Ar over a range of pressures from 10^{-8}-10^{-5} mbar. Detailed sequences for CRAFTI experiments were described in elsewhere.[5]

Data analysis

The CRAFTI experimental results were processed using Igor Pro software package (version 6, Wavemetrics; Lake Oswego, OR). Details for the analysis process have been published.[5]

Computational modeling

The structures of the complexes were modeled using the *MacroModel* package (version 9.2; Schrödinger Inc.; Portland, OR) with the Merck Molecular Force Field (MMFF94s). Typically 10,000 structures examined. The 50 lowest energy conformers were chosen to compute the

theoretical cross section via the MOBCAL program using the exact hard spheres method,[9] and the resulting cross sections were Boltzmann-weighted and averaged (300 K). The lowest-energy structures found in the conformational searches were also used as the starting point for B3LYP/6-31G* or B3LYP/6-31+G* geometry optimizations. These calculations were performed using NWChem (version 5.1; Pacific Northwest National Laboratory; Richland, WA).

Results and Discussion

CRAFTI cross sections of complexes of cucurbit[n]uril with alkylmonoammonium ions

Alkyl monoamines can easily form 1:1 singly-charged complexes with cucurbit[5]uril (CB5), its permethylated analog, decamethylcucurbit[5]uril (mc5), and the larger cucurbit[6]uril (CB6). Herein, I chose to examine CRAFTI cross sections for these 1:1 complexes to gain insight about their conformational structures. As I have discussed in prior chapters, the values of CRAFTI cross sections are strongly dependent on the kinetic energy in the center-of-mass reference frame. I therefore measure cross sections for each of the ions at constant center-of-mass kinetic energy. The experimental results are demonstrated in Figure 5.1.

For CB5 and mc5, CRAFTI cross sections generally increase with increasing chain length of the alkyl monoamines at the rate of 22±4 $Å^2$/methylene and 24±6 $Å^2$/methylene, respectively. For a guest ion with same chain length, the cross section of mc5 complex is larger than that of CB5 complex due to the presence of the equatorial methyl groups.

For CB6 complexes, cross sections are almost independent of chain length from 3 to 6 heavy atoms, and only begin to increase, almost linearly, for chain lengths longer than 6.

For the same alkylmonoamine guest and holding the center-of-mass kinetic energy constant, the CRAFTI cross sections are in the order CB5 < CB6 ≤ mc5. These trends indicate the alkylmonoamines are attached on the exteriors of CB5 and mc5, but thread through the cavity of CB6. This is consistent with the portal sizes of the hosts: CB5 and mc5, with a portal diameter of 2.4 Å, have portals too small to admit the alkyl chain, while CB6, with a portal diameter of 3.9 Å, has a larger portal and can form rotaxanes.

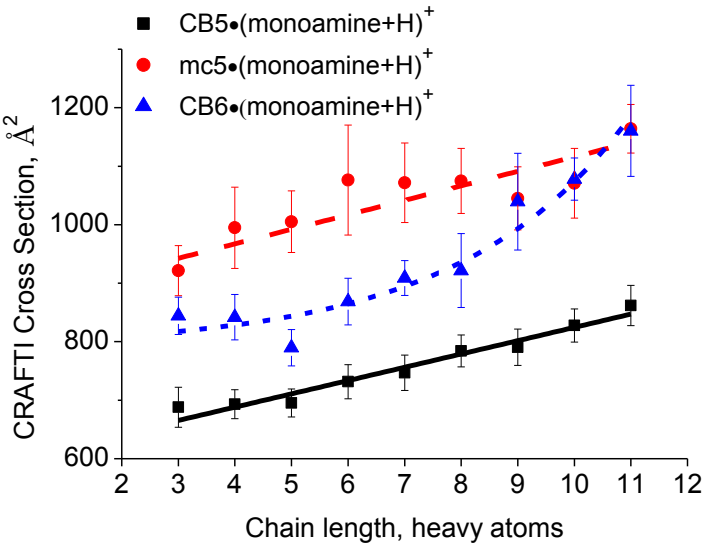

Figure 5.1 CRAFTI cross section of alkylmonoamine (the x-axis is the heavy atom chain length of the alkylmonoamine) complexes of CB5, CB6 and mc5 at constant kinetic energy in the center-of-mass reference frame (Ar as the collision gas). Error bars represent ± 1 standard deviation from the fitting procedure.

CRAFTI cross sections of complexes of cucurbit[n]uril with α,ω-alkyldiammonium ions

Mass spectra were obtained when electrospraying α,ω-alkyldiamines with CB5, mc5 and CB6, respectively. As with the alkylmonoamines, diamines are prone to form 1:1 singly-charged

complexes with CB5 and mc5. However, these diamines form 1:1 complexes with CB6 not only in singly-charged form but also in doubly-charged form.

Herein, I use the CRAFTI technique to measure the cross sections of α,ω-alkyldiamines with CB5, mc5 and CB6 at the same center-of-mass kinetic energies as those used for the alkylmonoamine complexes. All the alkyldiamine complex cross sections are shown in Figure 5.2.

The cross sections of alkyldiamine complexes of CB5 and mc5 show trends similar to those of the monoamine complexes: the cross section rises with increasing alkyldiammonium chain length, at a rate of 29±4 $Å^2$/methylene and 31±6 $Å^2$/methylene, respectively. For the same diammonium guest, the mc5 complex is larger than the CB5 and CB6 complexes, just as was seem for the corresponding monoamine complexes, which implies the CB5 and mc5 complexes with diamines are also external complexes while the CB6 complexes may be inclusion complexes.

The alkyldiamine complexes of CB6 are different from the alkylmonoamine complexes of CB6. Because α,ω-alkyldiammonium has two amine groups, it can easily form not only singly charged complexes, similar to the monoamine complexes, but it can also form doubly charged complexes with CB6, which are strongly-bound rotaxanes.[10] For a given chain length of alkyldiammonium ion, because the doubly-protonated CB6 complex makes strong ionic hydrogen bonds at both ends of the chain, its cross section is smaller than that of the corresponding singly-protonated CB6 complex, as shown in the experimental results in Figure 5.2. However, the doubly-charged complexes and the singly-charged complexes still have

similarity: the cross section for the n=4 complex is bigger than that of its neighbors (n=5 and n=6), which indicates the n=4 complex is different from the other longer chain length complexes. When the chain length is longer than 6, the cross section begins to gradually increase with increases in the chain length. I may speculate that for chain lengths longer than 4, the diamine cations are threaded through the CB6 cavity, while for n=4, the diamine rests on the portal.

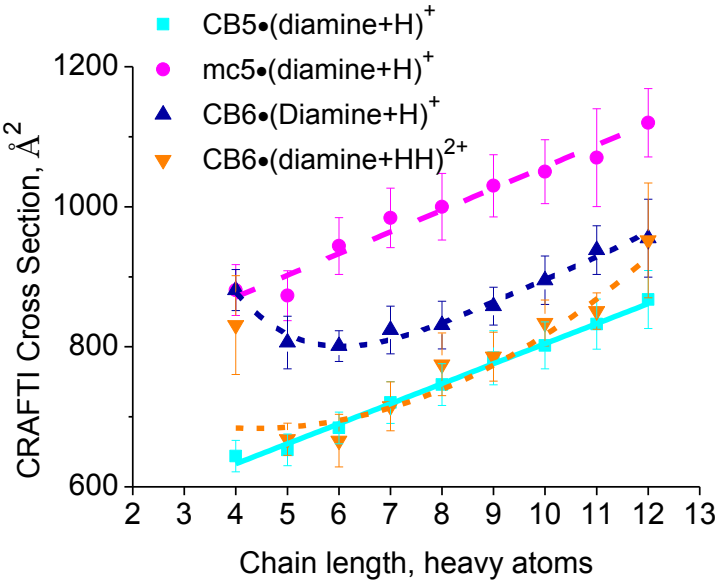

Figure 5.2 CRAFTI cross section of α,ω-alkyldiammonium (the x-axis is the heavy atom chain length) complexes of CB5, CB6 and mc5 at constant kinetic energy in the center-of-mass reference frame (Ar collision gas). Error bars represent ± 1 standard deviation from the fitting procedure.

Comparison between CRAFTI results of complexes of cucurbit[n]uril with alkyl mono- vs. diamines

In order to know better of CRAFTI cross sections for the alkyl mono- and α,ω-diamine complexes with cucurbit[n]uril are presented together in Figure 5.3.

For both monoamines and diamines, for a given chain length and holding the center-of-mass kinetic energy constant, the CRAFTI cross sections are in the order CB5 < CB6 < mc5. This order indicates that for monoamines or diamines, their cations are attached on the exteriors of CB5 and mc5, while they are threaded through the cavity of CB6 to form rotaxanes (except for n=4, the shortest diamine, which is too short to reach through CB6 to the portal on the other side).

Furthermore, for a given chain length of the guest ion, the CRAFTI cross section of the cucurbituril complexes increases in the order: $(monoamine+H)^+$ > $(diamine+H)^+$ > $(diamine+2H)^{2+}$. This trend is perfectly consistent with increasing host-guest interaction as: $-CH_3$ < $-NH_2$ < $-NH_3^+$.

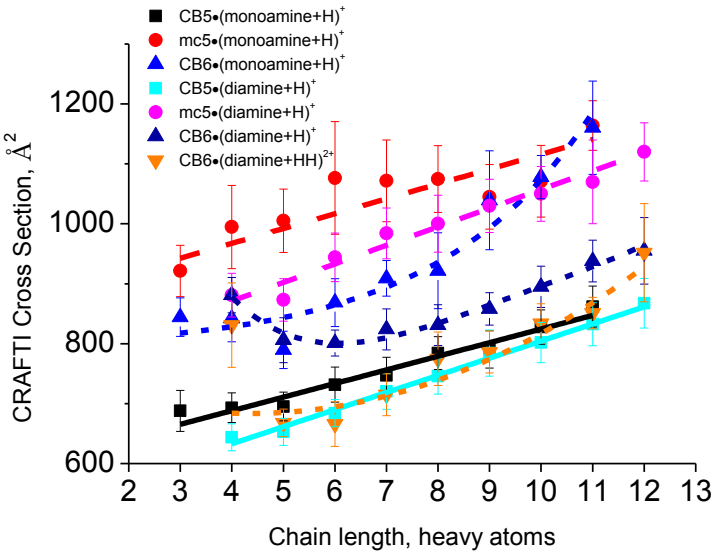

Figure 5.3 CRAFTI cross section of alky monoamine and α,ω-alkyldiamine complexes of CB5, CB6 and mc5 at a constant kinetic energy in center-of-mass reference frame (Ar as the collision gas). Error bars represent ± 1 standard deviation from the fitting procedure.

Comparison of CRAFTI cross sections with computational cross sections

To confirm the structural predictions from the CRAFTI experiments, computational cross sections from Boltzmann-weighted averaging (300 K) exact hard-sphere (EHS) calculations in MOBCAL are compared with experimental results in the following section.

Comparison for Monoamine Complexes

The computational results of monoamine complexes with CBn are shown in Figure 5.4. These calculated results are consistent with the experimental cross sections in Figure 5.1. For a given chain length, the calculated cross sections follow the same trend as the CRAFTI results: CB5 < CB6 < mc5, giving credence to the external structures of the CB5 and mc5 complexes and threaded interior structures of the CB6 complexes. For CB5 and mc5, the computed cross sections increase with the chain length at the rate about 4.4±0.3Å^2/methylene and 3.9±0.3/methylene, respectively, qualitatively similar to the CRAFTI cross sections but much less in absolute value. For CB6, the calculated cross sections are constant for $n \leq 6$, where the alkyl tails are inside the CB6 cavity, then increase with increasing the chain length for $n > 6$, where the threaded alkyl tails protrude from the cavity on the side opposite where the ammonium is bound, as shown in Figure 5.5 for B3LYP/6-31G* structures of alkylmonoammonium@CB6 complexes.

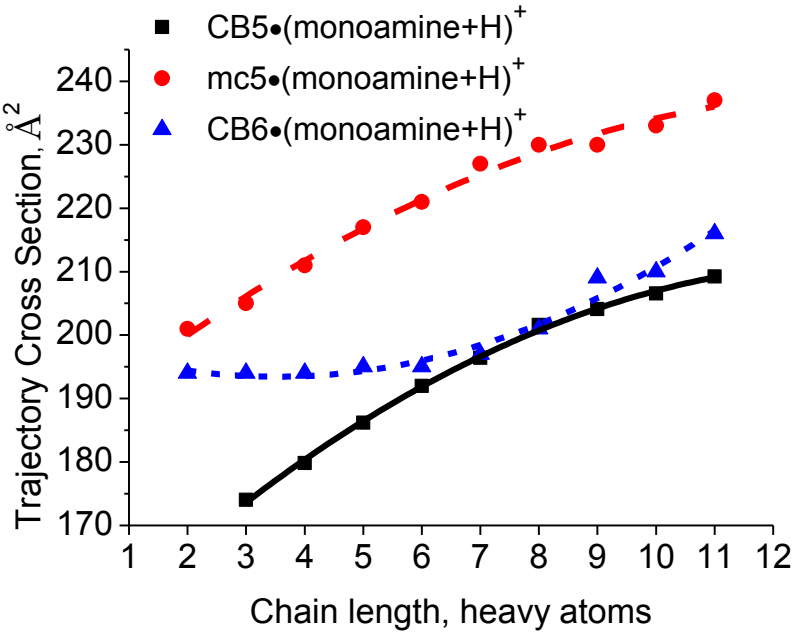

Figure 5.4 Computational EHS cross section of alkyl monoamines complexes of CB5, CB6 and mc5.

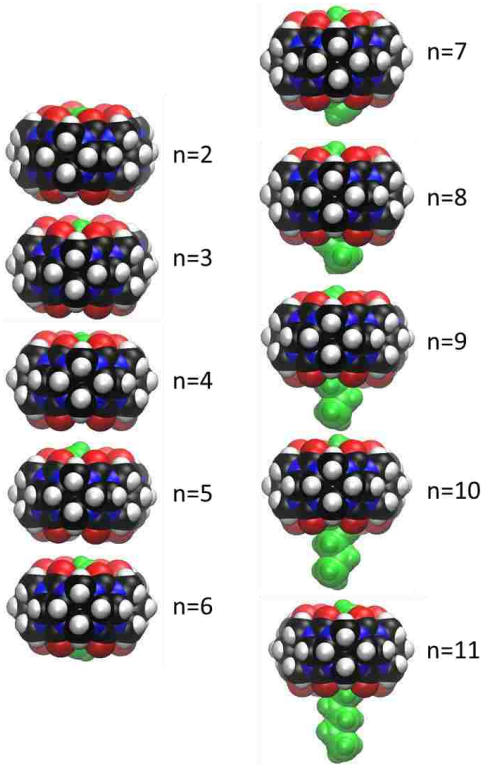

Figure 5.5 B3LYP/6-31G* computed structures for $[H(CH_2)_{n-1}NH_3^+]$@CB6 complexes. Alkylammonium ion (green) and CB6 (colored by atom type) are both represented as space filling models.

Comparison for Diamine Complexes

The computed EHS cross sections of α,ω-alkyldiammonium complexes with CB5, CB6 and mc5 are shown in Figure 5.6. For a given chain length guest ion, the computational cross sections exhibit the same qualitative trends as those for the CRAFTI cross sections: CB5 ≤ doubly charged CB6 <singly charged CB6 < mc5. For the CB5 and mc5 complexes, the computated cross sections increase with the chain length of the diamine cations, at the rate of 3.8±0.2Å^2/methylene and 3.7±0.2Å^2/methylene, again qualitatively similar to the CRAFTI cross sections. Comparing the singly and doubly charged CB6 complexes, the singly charged complexes are bigger than the doubly charged ones. The EHS cross sections both decrease with chain length until n = 4, which suggests that for n = 3, the diamine guest is bound on the CB6 portal face (as shown in Figure 5.7). The cross sections remain approximately constant from n = 4 to n = 6, then increase with increasing chain length for n > 6. This is a little different from the experimental results, which predict the n = 4 diamine attaches on the CB6 portal face.

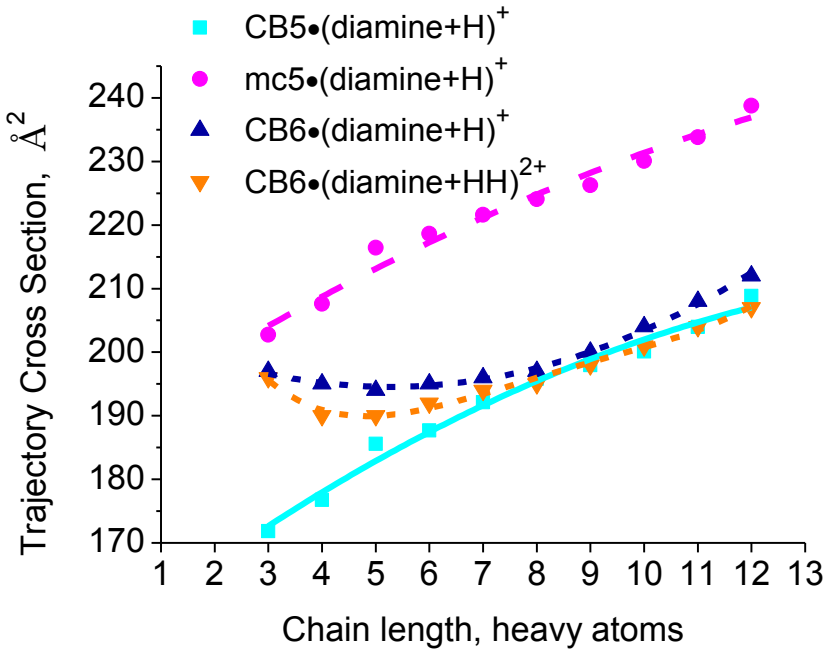

Figure 5.6 Computational EHS cross section of alkyldiamine complexes of CB5, CB6 and mc5.

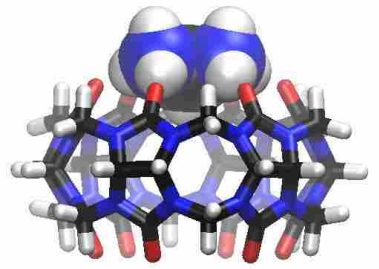

Figure 5.7 B3LYP/6-31G* computed structure for a CB6 complex with the shortest diamine (n = 3) on the CB6 portal face. The diammonium ion is represented with a space filling model, and CB6 is depicted using tubes.

Comparison of Monoamine and Diamine Complexes

The external complexes and internal complexes are shown separately in Figure 5.8(a) and 5.8(b).

Consistent with the experimental CRAFTI cross sections, for a given chain length of the alkylamine, the EHS cross section follows the same order: $(monoamine+H)^+$ > $(diamine+H)^+$ > $(diamine+2H)^{2+}$.

Herein, CB6 complexes were emphasized because of their supramolecular nature. For diamine complexes, the computational calculations suggest when n = 3 the guest is on the CB6 portal face, not inserted as are the diamines with longer chain lengths. However, the CRAFTI technique suggests this occurs for chain length 4. The computational data predicts this effect is larger for the doubly protonated diamine compared with the singly protonated one, consistent with the CRAFTI findings. It is probably not surprising that the quantitative agreement between experiment and computation is not perfect. The CRAFTI technique measures cross sections for dephasing from the coherent ion packet due to medium energy (15eV) collisions with the background gas, Ar; while the theoretical method computes the EHS cross section for momentum transfer due to low energy (< 0.1eV) collisions with He in a drift cell. Therefore, I do not expect quantitative agreement between these two methods.

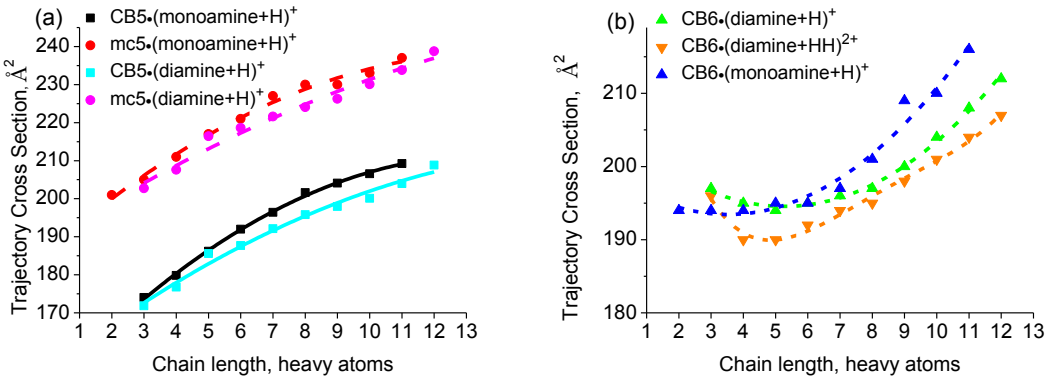

Figure 5.8 Computational EHS cross section of (a) alkylamine complexes of CB5 and mc5; (b) alkylamine complexes of CB6.

Conclusions

The CRAFTI cross sections of cucurbituril-alkylamine complexes demonstrated in this study are qualitatively consistent with computational results: the CB5 and mc5 complexes have the tails of the alklyamines external to the portal of the host, while the CB6 complexes have the alkylamine tails threaded through the cavity of the host, with protrusion of the chain when it is long enough. For a given chain length, the cross sections increase in the order: $(\text{monoamine+H})^+ > (\text{diamine+H})^+ > (\text{diamine+2H})^{2+}$, due to increasing host-guest interactions at the end of the chain. For the CB6 complexes, both CRAFTI and computational results suggest the guest ion is on the face of the host portal when the chain length is very short.

This qualitative agreement between CRAFTI experiments and EHS calculations for molecular structures of this supramolecular system, cucurbit[n]uril with alkyl mono- and α,ω-diammonium complexes, indicates the CRAFTI technique can give structurally-informative cross section measurements for supramolecular systems, without requiring special instrumentation. The good agreement also increases confidence in the computational modeling methods.

References

(1) Dearden, D. V.; Ferrell, T. A.; Asplund, M. C.; Zilch, L. W.; Julian, R. R.; Jarrold, M. F. *J. Phys. Chem. A* **2009**, *113*, 989-997.

(2) Zhang, H.; Grabenauer, M.; Bowers, M. T.; Dearden, D. V. *J. Phys. Chem. A* **2009**, *113*, 989-997.

(3) Mukhopadhyay, R. *Anal. Chem.* **2008**, *80*, 7198-7120.

(4) Bohrer, B. C.; Merenbloom, S. I.; Koeniger, S. L.; Hilderbrand, A. E.; Clemmer, D. E. *Annu. Rev. Anal. Chem.* **2008**, *1*, 293-327.

(5) Yang, F.; Voelkel, J. E.; Dearden, D. V. *Anal. Chem.* **2012**, *in press*.

(6) Zhang, X. X.; Krakowiak, K. E.; Xue, G.; Bradshaw, J. S.; Izatt, R. M. *Ind. Eng. Chem. Res.* **2000**, *39*, 3516-3520.

(7) Wigger, M.; Nawrocki, J. P.; Watson, C. H.; Eyler, J. R.; Benner, S. A. *Rapid Commun. Mass Spectrom.* **1997**, *11*, 1749-1752.

(8) Senko, M. W.; Canterbury, J. D.; Guan, S.; Marshall, A. G. *Rapid Commun. Mass Spectrom.* **1996**, *10*, 1839-1844.

(9) Shvartsburg, A. A.; Jarrold, M. F. *Chem. Phys. Lett.* **1996**, *261*, 86-91.

(10) Zhang, H.; Paulsen, E. S.; Walker, K. A.; Krakowiak, K. E.; Dearden, D. V. *J. Am. Chem. Soc.* **2003**, *125*, 9284-9285.

Chapter 6 Characterization of α,ω-Alkyldiammonium Complexes with Bigger Cucurbit[n]urils (n=7,8) and Cucurbit[6]uril Derivative

Introduction

Host-guest interactions in supramolecules are strongly influenced by solvent and counterion effects in condensed phases. Gas phase studies are ideal for investigating such interactions because the perturbing effects of solvation are not present and subtle yet important differences can be probed.[1]

Cucurbit[n]urils $(CBn)^{2-6}$ are pumpkin-shaped macrocycles that are cyclic polymers of glycoluril. They all have symmetric geometries with two identical openings that are lined with electronegative carbonyl groups that make cucurbiturils ideal for binding with positive ions. The carbonyls are also good hydrogen bond receptors. As a result, the CBn family becomes a good choice for the host component in host-guest systems.

Complexes of the hollow, pumpkin-shaped guest CB6 with α,ω-alkyldiammonium ions have previously been characterized as a function of alkyl chain length using Fourier transform ion cyclotron resonance mass spectrometry using the sustained off-resonance irradiation collision induced dissociation (SORI-CID) technique.[7,8] The experimental results yielding relative dissociation energies combined with HF/6-31G* and B3LYP/6-31G*computational results indicate the diamine complexes with CB6 are internal complexes and n=4 is the optimum chain length for binding CB6 in the gas phase.

In this chapter, I use SORI and CRAFTI[9] techniques to examine other CBn hosts with the same α,ω-alkyldiammonium ($H_3N^+(CH_2)_nNH_3^+$, n=2-10) guests. Cucurbit[7]uril (CB7),

cucurbit[8]uril (CB8) and hexa(cyclohexyl)cucurbit[6]uril (CB*6) are chosen as the hosts because they have the potential to form inclusion complexes as does CB6. This set of hosts offers the opportunity to probe the interactions between alkyldiamines and neutral cucurbiturils, and specifically to examine chain length selectivity.

Experimental

Materials

n-alkyldiamines (n=2-10) were purchased from Sigma-Aldrich (St. Louis, MO) and used without further purification. Hexa(cyclohexyl)cucurbit[6]uril (CB*6), cucurbit[7]uril (CB7) and cucurbit[8]uril (CB8) were synthesized and provided by Dr. Kimoon Kim.[10] Stock solutions of CB[n] were prepared at about 200 μM by dissolving the solid samples in 88% formic acid (Mallinckrodt Baker Inc., Phillipsburg, NJ) and then diluting with methanol/water (50:50). The electrospray solutions were prepared at concentrations of 100 μM in CBn and 200 μM in amines. Argon (99.995%) and SF_6 (99.8%) were purchased from Airgas (Radnor, PA) to be used as collision gases.

Instrumentation

All experiments were performed using a Bruker model APEX 47e Fourier transform ion cyclotron resonance mass spectrometer controlled by a MIDAS data system[11] and equipped with an infinity cell and a 4.7 T superconducting magnet. Ions were generated in a microelectrospray source modified from an Analytica (Branford, MA) design, with a heated metal capillary drying tube based on the design of Eyler.[12]

SORI-CID experiments

The stored waveform inverse Fourier transform (SWIFT) method was used to isolate the ion of interest.[13] Sustained off-resonance irradiation-collision-induced dissociation (SORI-CID) experiments were performed by irradiating 1 kHz below the resonant frequency of the target ion.[14] Argon was introduced as the collision gas using a Freiser-type pulsed leak valve.[15] SORI events included pulsing the Ar background pressure in the trapping cell up to 1.7×10^{-5} mbar, waiting 2 seconds for conditions to fully stabilize, and applying the off-resonance irradiation for a variable amount of time (which allows variation of the total energy deposited in the ions; herein, times ranged from 10 to about 500 ms, with amplitudes kept constant at 11.4 V and durations kept short to minimize radiative cooling between collisions), followed by a 5 second delay to allow the trapping cell to return to baseline pressure (about 10^{-9} mbar) prior to detection. Five scans were averaged for each SORI excitation duration.

CRAFTI experiments

All the CRAFTI experiments were carried out via 200 eV (in the center-of-mass reference frame) collisions with SF_6 over a range of pressures from 10^{-8}-10^{-5} mbar. Detailed sequences for CRAFTI experiments were described in elsewhere.[9]

Data Analysis

Transient signals were analyzed using the Igor Pro software package (version 6, Wavemetrics; Lake Oswego, OR).

For SORI experiments, the Igor program was used to extract peak amplitudes for a set of spectra that differ in one or more experimental parameters and then generate tables of peak intensities as a function of SORI excitation duration. The resulting parent and product ion peak

intensities were normalized and the relative SORI collision energy was scaled to account for differences in mass and excitation amplitude (although most experiments were conducted while maintaining a constant excitation amplitude).[8] Energies obtained from these experiments may be compared qualitatively, but are not quantitative due to uncertainties about the absolute kinetic energies of the colliding ions as well as uncertainties about the efficiency of kinetic-to-internal energy conversion. Calculation of relative SORI energies are based on a previous paper.[8]

For the CRAFTI experiments, data analysis details are given in previous chapters.

Results and Discussion

Electrospray of cucurbit[n]uril with alkyldiamine complexes

Solutions of α,ω-alkyldiammonium (hereafter C_nDA, n equals the number of carbons) with CB[*]6, CB7 and CB8 were electrosprayed separately using FT-ICR. Except for the mass spectra for C_2DA and C_3DA with CB8, all the mass spectra have one point in common: only one main peak was observed in each spectrum, a doubly charged peak corresponding to one doubly protonated diamine cation attached to the cucurbituril (1:1 complex). Considering the similarity between CB6 and the cucurbiturils studied in this chapter, I assume these 1:1 complexes are also pseudorotaxanes (written as $[H_3N^+(CH_2)_nNH_3^+]$@CBn), like the CB6 complexes studied previously.[7,8] It is hard to find any peaks when spraying the solution of C_2DA and C_3DA with CB8. This may result from the bigger cavity and wider portal of CB8, which makes the diamines with shorter chain length not fit either the cavity or the portal of the CB8 host.

Characteristic dissociation channels for SORI-CID of CBn complexes

To better understand the structures of these complexes, SORI-CID experiments were carried out on $[H_3N^+(CH_2)_nNH_3^+]$@CBn ions by varying the SORI duration.

Alkyldiammonium complexes with CB7

The relative signal abundance of the parent ion and product ions are plotted against the relative SORI energies, shown in Figure 6.1. Calculation of relative SORI energies has been discussed in Chapter 1. Collisional activation results in various fragments from $[H_3N^+(CH_2)_nNH_3^+]$@CB7 ions, including protonated CB7 ($CB7H^+$), singly charged α,ω-alkyldiammonium (C_nDAH^+), fragments from the protonated diamine (C_nDAH^+ fragments), doubly protonated CB7 ($CB7HH^{2+}$), singly- and doubly-charged cage fragments, and doubly-charged ions resulting from loss of neutral pieces of the diamines. Details for the product ions of each CB7 complex are illustrated in Table 6.1. Four general fragmentation pathways were observed in dissociation of $[H_3N^+(CH_2)_nNH_3^+]$@CB7 complexes. The first channel is proton transfer dissociation, in which the main products are protonated CB7, singly charged diamine (due to the mass discrimination in the instrument, the relative abundance of C_nDAH^+ is much lower than that of $CB7H^+$) and diamine fragments. The second channel is cage fragmentation; this kind of fragment includes singly-charged cage fragments and doubly-charged cage fragments. The third channel is loss of neutral diamine, resulting in doubly charged CB7. The last channel is loss of pieces of neutral diamines, which results in doubly charged ions of the remaining part of the diamine with CB7.

Proton transfer dissociation and cage fragmentation are observed in dissociation of every diamine complex with CB7. The relative abundance of signals from these two pathways was plotted against the relative SORI energies in Figure 6.2. For proton transfer, the normalized

abundance of $CB7H^+$ was set as the y-axis; for cage fragmentation, the sum of the normalized abundances of singly- and doubly-charged cage fragments was set as the y-axis. The diamine complexes will be discussed in detail in the following paragraphs.

For n=2, the portion of fragments from proton transfer is much larger than that from cage fragmentation. The loss of neutral ethylenediamine is significant because the chain length is too short to reach both ends of the cucurbituril rim. For n=3 and n=4, proton transfer dissociation and cage fragmentation are the only two pathways. Proton transfer dissociation is less prominent for n=4 than for n=3, probably because the longer chain length of n=4 that makes the hydrogen bonding between the terminal ammonium groups and the carbonyl oxygens of the CB7 rim stronger. For n=5, cage fragmentation represents up to 60% of the SORI products, the largest fraction compared with the other diamine complexes. This fact suggests n=5 may be the optimum chain length for the CB7 cage, with the ammonium groups most strongly bound to the CB7 rims. For n=6 and n=7, the relative abundance of cage fragmentation decreases and that of proton transfer dissociation increases, which suggest their chain length are longer than optimal. For n=8-10, the chain lengths are even longer, such that the alkyl chain must be strained to allow both ammonium groups to attach with the carbonyl oxygens. For their complexes, loss of pieces of neutral amines begins to be observed, the cage fragmentations are much weaker than for the other complexes, and proton transfer dissociation is the prominent channel.

To further confirm the optimum diamine chain length for CB7 binding, disappearance curves for the parent ions are shown in Figure 6.3. The falling portions of the curves all have similar slopes except for the n=4 and n=5 data, which require higher energies for complete dissociation.

The n=2 diamine seems to have the weakest binding with CB7. Relative energies for 50% loss of the parent ion, $E_{SORI,\ 50}$, of these C7 complexes were determined by linear fitting of the falling portion of each disappearance curve in Figure 6.3, as shown in Figure 6.4. The complex disappearance energy, $E_{SORI,\ 50}$, which is an indicator of the overall relative stability of the complex, is maximum when n=5, again suggesting that n=5 is the optimal chain length for binding CB7 in the gas phase. Based on computational studies of N-N distances for free and CB6-complexed diammonium ions[8], I assume that for n=5, the N-N distance for the free diamine ion is almost equal to that for the CB7-complexed one; this geometry makes n=5 the most robust complex.

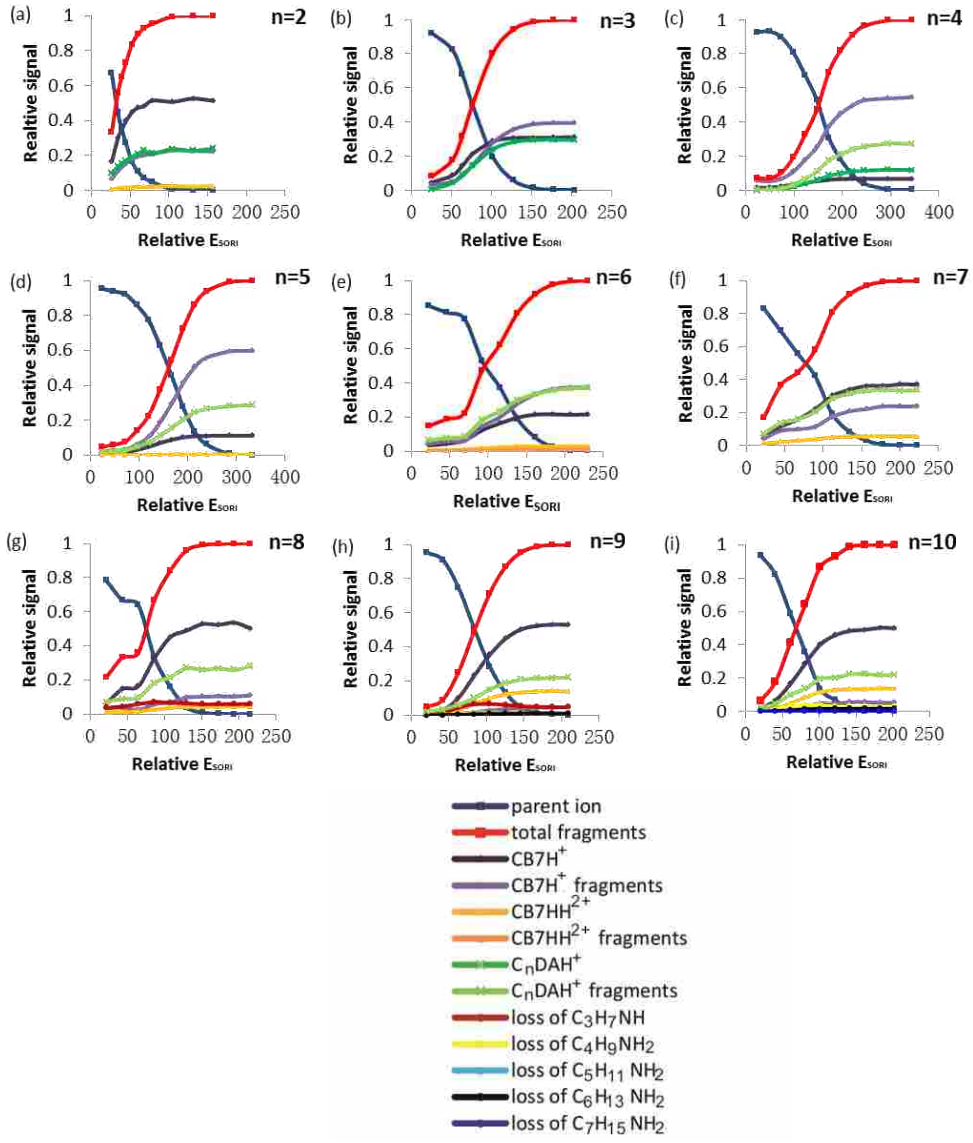

Figure 6.1 SORI ion yield curves for $[H_3N^+(CH_2)_nNH_3^+]$@CB7 complexes, n=2-10.

Table 6.1 SORI-CID fragments for $[H_3N^+(CH_2)_nNH_3^+]$@CB7 complexes, n=2-10.

n in $H_3N^+(CH_2)_nNH_3^+$	Fragments						
	$CB7H^+$	$CB7H^+$ fragments	C_nDAH^+	C_nDAH^+ fragments	$CB7HH^{2+}$	$CB7HH^{2+}$ fragments	Loss of $C_nH_{2n+1}NH_2$
2	×	×	×		×		
3	×	×	×				
4	×	×	×	×			
5	×	×		×	×		
6	×	×		×	×	×	
7	×	×		×	×		
8	×	×		×	×		×
9	×	×		×	×		×
10	×	×		×	×		×

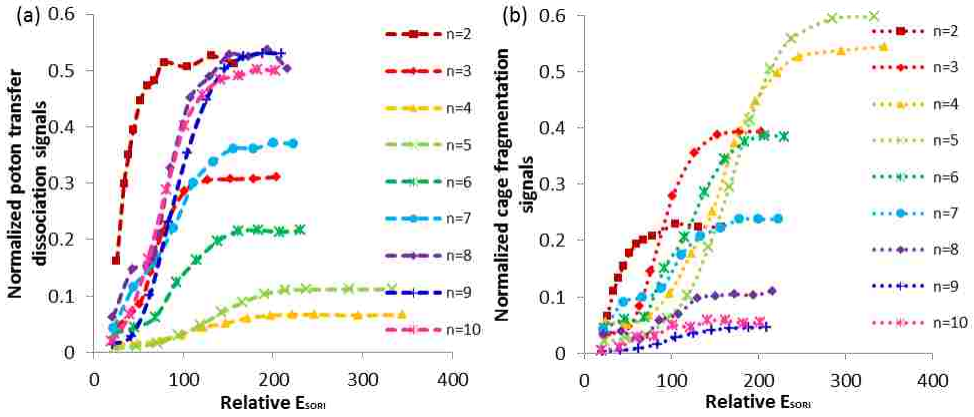

Figure 6.2 SORI ion yield curves for production of proton transfer dissociation channel (a) and cage fragmentation channel (b) for $[H_3N^+(CH_2)_nNH_3^+]$@CB7 complexes, n=2-10.

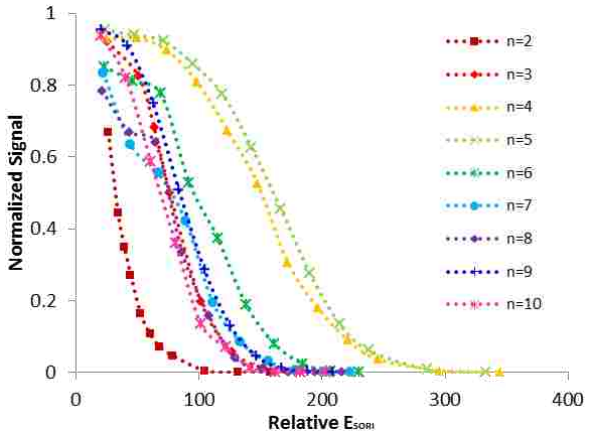

Figure 6.3 SORI parent ion survival yield curves for $[H_3N^+(CH_2)_nNH_3^+]$@CB7 complexes, n=2-10.

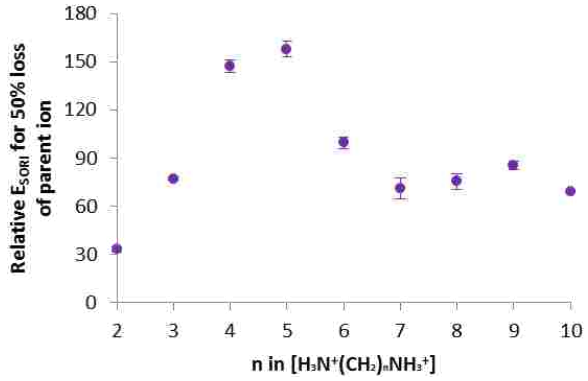

Figure 6.4 Relative SORI energies for 50% survival of $[H_3N^+(CH_2)_nNH_3^+]$@CB7 complexes, n=2-10. Error bars represent standard errors from the linear fitting procedure used to derive the value.

Alkyldiammonium complexes with CB8

SORI-CID experiments similar to those done for the CB7 complexes were performed on the diamine complexes with CB8. The SORI ion yield curves for CB8 complexes are illustrated in Figure 6.5. The observed dissociation fragments of the CB8 complexes are listed in Table 6.2.

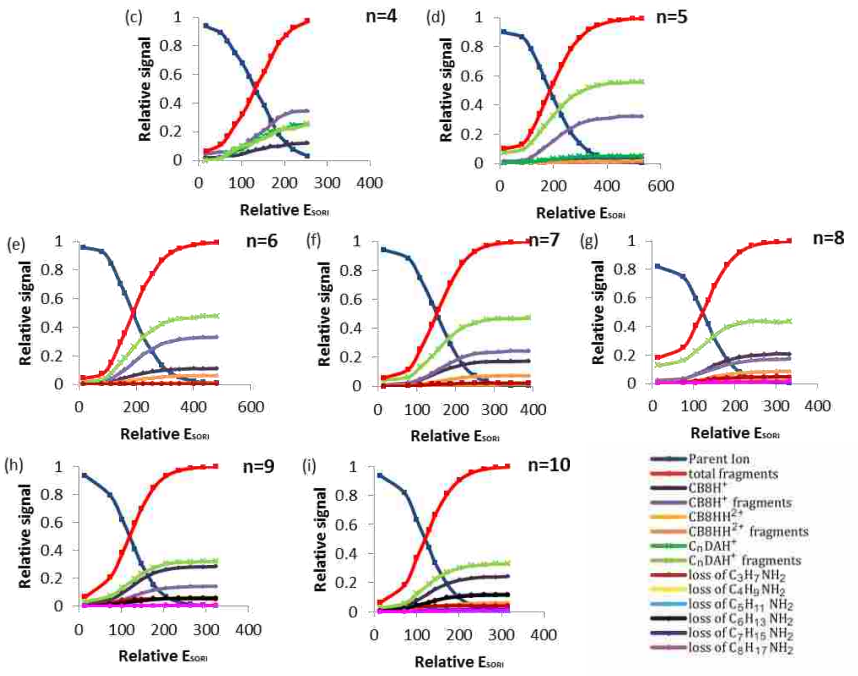

Figure 6.5 SORI ion yield curves for $[H_3N^+(CH_2)_nNH_3^+]$@CB8 complexes, n=4-10.

Table 6.2 SORI-CID fragments for $[H_3N^+(CH_2)_nNH_3^+]$@CB8 complexes, n=4-10.

n in $[H_3N^+(CH_2)_nNH_3^+]$	Fragments						
	$CB8H^+$	$CB8H^+$ fragments	C_nDAH^+	C_nDAH^+ fragments	$CB8HH^{2+}$	$CB8HH^{2+}$ fragments	Loss of $C_nH_{2n+1}NH_2$
4	×	×	×	×			
5	×	×	×	×	×		
6	×	×		×	×	×	×
7	×	×		×	×	×	×
8	×	×		×	×	×	×
9	×	×		×	×	×	×
10	×	×		×	×	×	×

Dissociation of these CB8 complexes also has four pathways, like the CB7 complexes. Among the four channels, proton transfer dissociation and cage fragmentation are dominant for the CB8 complexes. The normalized abundance of signals from these two channels is plotted against the relative SORI energies, shown in Figure 6.6. For n=4, the proton transfer and cage fragmentation channels are the only dissociation pathways; cage fragmentation is the principal one. For n=5, loss of neutral diamine begins to be observed, the portion of proton transfer dissociation decreases, but cage fragmentation is still dominant. For n=6-10, dissociation in all four pathways is observed. Compared with n=6-7, for n=8-10 cage fragmentation is less important, while the fraction of proton transfer increases as does loss of pieces of neutral amines. Proton transfer for n=6 is less abundant than for n=7, while cage fragmentation seems to be the ruling route for these two ions. To sum up, although cage fragmentation is predominant for n=4-7, based on the fraction of proton transfer dissociation, n=5 and n=6 appear to have the highest binding affinity with CB8.

Examining the disappearance curves for parent ions of the CB8 complexes in Figure 6.7, n=5 and n=6 are unique in that their curves are far away from the others. When using linear fitting of the falling portion of each disappearance curve to get the disappearance energy, $E_{SORI,\,50}$ (Figure 6.8), n=5 and n=6, which have the highest $E_{SORI,\,50}$, are again suggested to be the optimal lengths for threading through the CB8 cage.

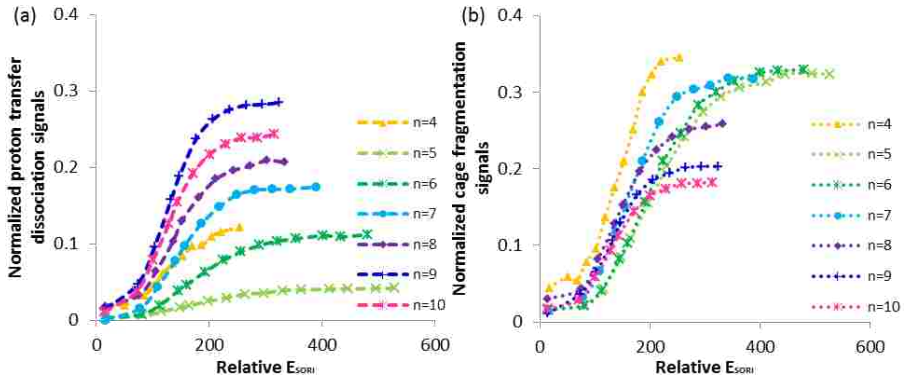

Figure 6.6 SORI ion yield curves for production of proton transfer dissociation channel (a) and cage fragmentation channel (b) for $[H_3N^+(CH_2)_nNH_3^+]$@CB8 complexes, n=2-10.

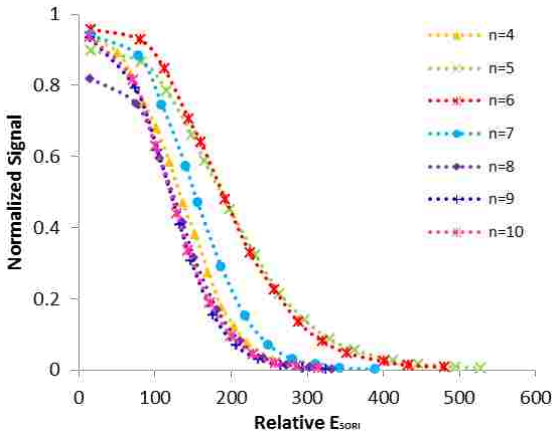

Figure 6.7 SORI parent ion survival yield curves for $[H_3N^+(CH_2)_nNH_3^+]$@CB8 complexes, n=2-10.

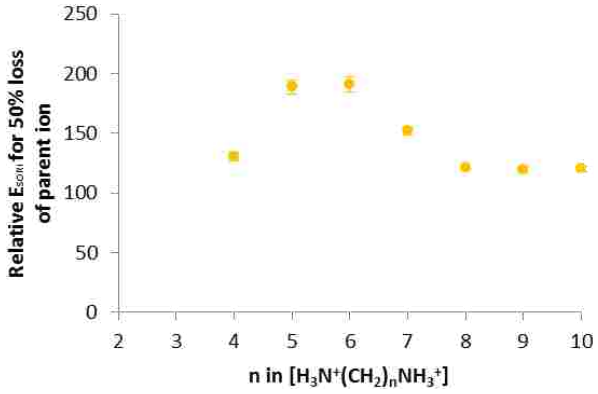

Figure 6.8 Relative SORI energies for 50% survival of $[H_3N^+(CH_2)_nNH_3^+]$@CB8 complexes, n=2-10. Error bars represent standard errors from the linear fitting procedure used to derive the value.

*Alkyldiammonium complexes with CB*6*

For CB^*6 with alkyldiamine complexes, SORI dissociation experiments were carried out in the same way. The observed fragments of the CB^*6 complexes are listed in Table 6.3. The SORI ion yield curves are shown in Figure 6.9.

The same four dissociation channels are observed for the CB*6 complexes: proton transfer dissociation, cage fragmentation, loss of neutral amines and loss of pieces of neutral amines. However, unlike the CB7 and CB8 complexes, there are no same dissociation channels for CB^*6 complexes, and loss of neutral diamine is observed for all the complexes except for n=3.

For n=2, cage fragmentation is the principal channel, proton transfer and loss of neutral amines accounting for less than 1%. For n=3, cage fragmentation is the only dissociation pathway, which implies n=3 may be the optimum chain length for complexion with CB^*6. For n=4, CB^*6HH^{2+} occurs in the fragments, but the sum of singly- and doubly-charged cage fragments is still the most abundant. For n=5, there are three dissociation channels as for n=2, while signals of CB^*6HH^{2+} are more abundant. For n=6, the four channels are all observed, and loss of neutral diamine becomes the predominant channel. For n=7-10, proton transfer is the weakest channel, and loss of pieces of neutral diamine become more abundant with increasing diamine chain length. For n=7, loss of the diamine is still the main channel as for n=6. However, from n=8 and longer, loss of pieces of the neutral diamine becomes the primary pathway because the chain lengths of these diamines are too long to fit into the cucurbituril cage.

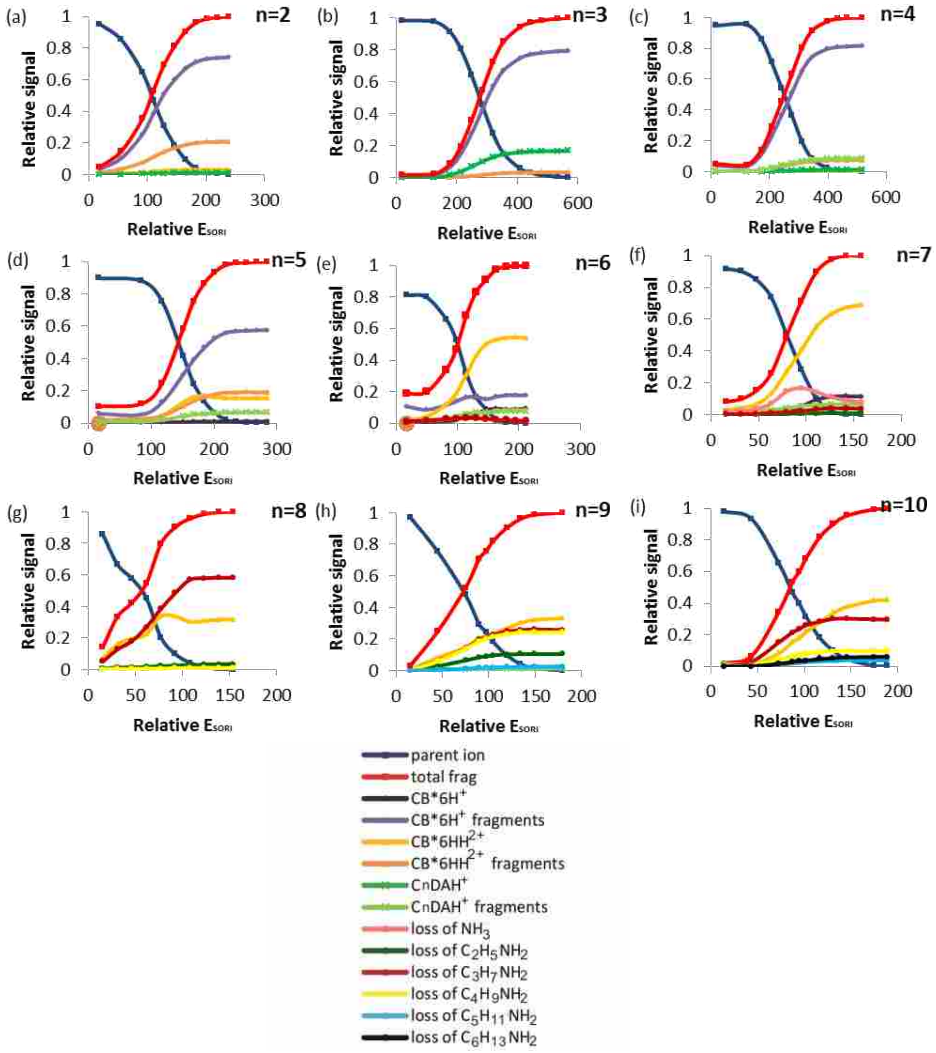

Figure 6.9 SORI ion yield curves for $[H_3N^+(CH_2)_nNH_3^+]$@CB^*6 complexes, n=2-10.

Table 6.3 SORI-CID fragments for $[H_3N^+(CH_2)_nNH_3^+]$@CB^*6 complexes, n=2-10.

n in $[H_3N^+(CH_2)_nNH_3^+]$	Fragments						
	CB^*6H^+	CB^*6H^+ fragments	C_nDAH^+	C_nDAH^+ fragments	CB^*6HH^{2+}	CB^*6HH^{2+} fragments	Loss of $C_nH_{2n+1}NH_2$
2	×	×	×		×	×	
3		×	×			×	
4		×	×	×	×	×	
5	×	×		×	×	×	
6	×	×		×	×	×	×
7	×			×	×		×
8	×			×	×		×
9	×			×	×		×
10	×			×	×		×

The parent ion survival curves of CB*6 complexes are shown in Figure 6.10. The disappearance energies are calculated and plotted against the chain length in Figure 6.11. The results in these two figures are consistent with each other: both indicate n=3 is the most robust of these CB*6 complexes.

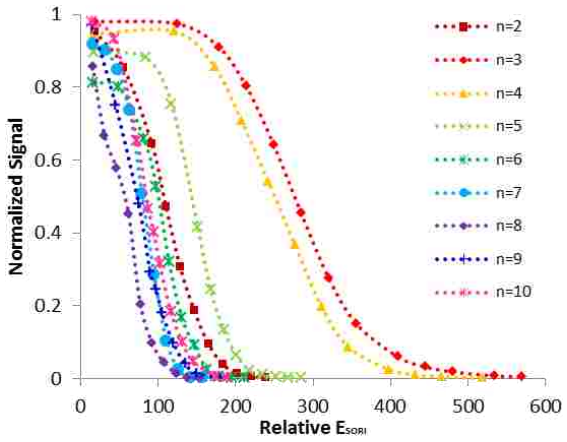

Figure 6.10 SORI parent ion survival yield curves for $[H_3N^+(CH_2)_nNH_3^+]$@CB*6 complexes, n=2-10.

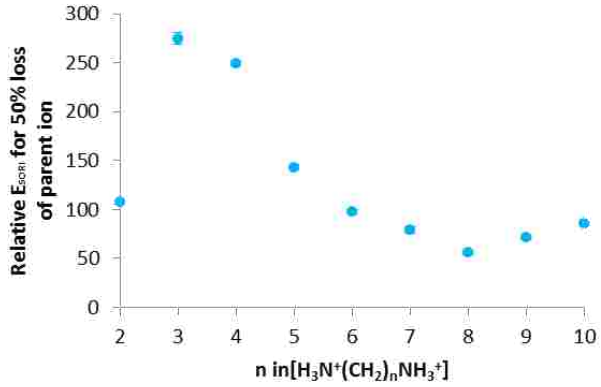

Figure 6.11 Relative SORI energies for 50% survival of $[H_3N^+(CH_2)_nNH_3^+]$@CB*6 complexes, n=2-10. Error bars represent standard errors from the linear fitting procedure used to derive the value.

Cross section measurements of diamine complexes of CB*6, CB7 and CB8 via CRAFTI

The CRAFTI technique[9] is a promising method for additional characterization of supramolecular systems. Further, comparison of SORI dissociation thresholds between different host complexes also benefits from cross section information as mentioned elsewhere.[8] The CRAFTI cross sections of diamine complexes with CB*6, CB7, and CB8 are shown in Figure 6.12.

For a given guest cation, the cross sections follow a reasonable order: CB7 < CB*6 < CB8. Based on the SORI results, I believe all these diamine complexes are interior complexes. This presumption is consistent with that CRAFTI results: because they are inclusion complexes, the cross section of the complex is larger when that of the host molecule is bigger.

For the CB*6 complexes, the shorter diamines, from n=2 to n=4, have cross sections close to each other. The cross sections increase with increasing guest chain length for $n \geq 5$. This is somewhat different from what is expected from the SORI results. Based on the SORI experiments, n=3 requires higher collision energy than any of the other CB*6 complexes, and n=4 has the second highest dissociation threshold. The data suggest n=2-4 are all inclusion (or possibly portal bound, although the CB*6 portal is probably not large enough for that) complexes, with n=3 being the most strongly bound. The cyclohexyl substituents should affect the rigidity of the portal and therefore its effective size and ability to bind a guest, so that might favor n=3 over longer chains.

For the CB7 complexes, the shorter diamines, n=2 and n=3, have larger cross sections than the n=4 complex, which may indicate those diamines binding on the CB7 portal face. n=4 and n=5 are almost the same; for $n \geq 6$, the cross sections increase with increasing chain length which implies the chain begins to protrude from the host cavity when n=6. The best chain length for CB7 is n=5, which agrees with the SORI results.

For the CB8 complexes, n=4 has a bigger cross section than n=5, which may imply the butanediamine attaches outside or on the face of the CB8 cavity; n=5 and n=6 have nearly the same cross sections; for $n \geq 7$, the cross sections begin to increase with increasing chain length,

which suggests the chain protrudes out of the CB8 cavity. This CRAFTI result is consistent with the SORI experimental results: n=6 is the perfect chain length for the CB8 cavity.

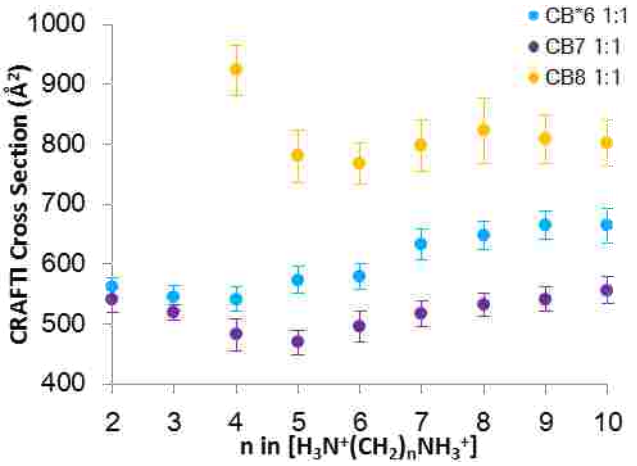

Figure 6.12 CRAFTI cross sections of alkyldiamine ($[H_3N^+(CH_2)_nNH_3^+$, n=2-10) complexes of CB*6, CB7, and CB8 at a constant kinetic energy in the center-of-mass reference frame (SF_6 collision gas). Error bars represent ± 1 standard deviation from the fitting procedure.

Comparison of dissociation behavior of diamine complexes of CB*6, CB7 and CB8

Based on the observation of cage fragmentation and trends in the cross sections for these cucurbituril complexes, I believe most of the alkyldiamine complexes of CB*6, CB7 and CB8 are pseudorotaxanes, with diamine cations threaded through the cucurbituril cage. For diamines with chain length shorter than optimal, there are two situations: for the shortest, the diamines may bind on the cucurbituril portal face as was suggested by the results in Chapter 5; for slightly longer diamines, one of the ammonium groups is probably attached to the carbonyl groups of one cucurbituril rim, whereas the other ammonium group is inside the cucurbituril cage because the chain length is too short to reach the other portal of the cucurbituril. For diamines with chain

lengths longer than optimal, there are two possible classes of geometries. For diamines with one more CH_2 than optimal, the two ammonium groups are attached to the curcurbituril rims, but one ammonium group is bent to foster proximity to the carbonyl groups. For diamines with two or more CH_2 than optimal, the two amine groups may both need to be bent for hydrogen binding with the carbonyl groups at the two rims. This hypothesis is consistent with the experimental results. As an example, consider the CB7 complexes: when n=5 is the optimal chain length for CB7, the n=6 complex needs less dissociation energy than n=5, but needs more energy than the longer chain length ones (n=7-10). The same situation is also seen in the diamine complexes with CB8 and CB^*6.

All the disappearance energies I have examined above include contributions only from the SORI amplitude, SORI duration, and charge of the ions. As mentioned in Equations (1-5) and (1-6) in chapter 1, collision cross section is one of the important factors affecting the relative SORI energy, along with collision duration and collision amplitude. As a result, if I want to do semi-quantitative calibrations to compare the relative SORI energy between different cucurbituril complexes that have significant differences in cross section, I need to take the cross sections into account for calculations of SORI energies. For convenience, I use the CRAFTI cross sections to correct the relative SORI energies (the cross sections are listed in Table 6.4). The uncorrected and corrected SORI energies are shown in Figure 6.13 for all the diamine complexes with CB7, CB8 and CB^*6. Because the difference in cross sections of the diamines with the same cucurbituril are within a 10 % range, the corrected SORI energies as a function of chain length still follow the same trends for the same cucurbituril complexes I have already noted. However,

the difference between different cucurbituril complexes with the same diamine is affected by these corrections. For the same diamine as the cucurbituril host is varied, the SORI energies follow the same trend noted above, CB7 < CB*6 < CB8, except when n=4. This trend can be explained by the extra glycoluril (in CB8) or the six extra cyclohexyl groups (in CB*6), which bring additional vibrational states that increase the density of states, slow down the dissociation, and raise the thresholds.

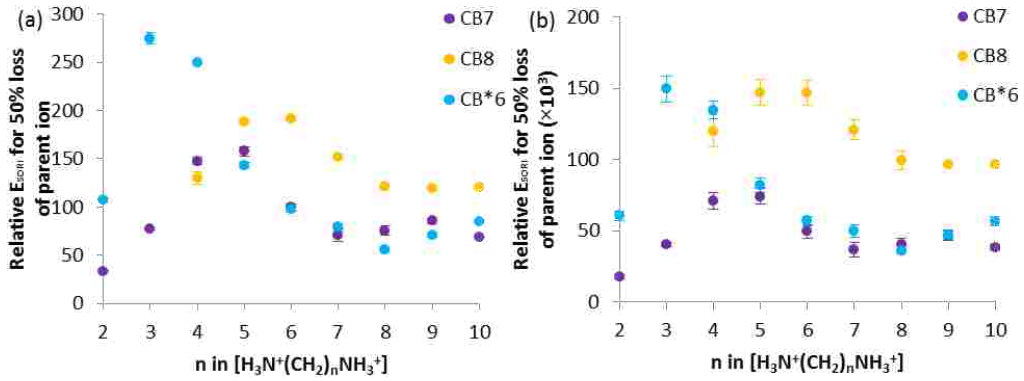

Figure 6.13 Relative SORI energies for 50% survival of $[H_3N^+(CH_2)_nNH_3^+]$@CB*6, $[H_3N^+(CH_2)_nNH_3^+]$@CB7, and $[H_3N^+(CH_2)_nNH_3^+]$@CB8 complexes, n=2-10. (a) $E_{SORI,\ 50}$, not corrected with the cross sections; (b) $E_{SORI,\ 50}$, corrected with cross sections provided by CRAFTI. Error bars represent standard errors from the linear fitting procedure used to derive the value.

Table 6.4 Cross sections for $[H_3N^+(CH_2)_nNH_3^+]$@CB*6, CB7 and CB8, n=2-10.

n in $[H_3N^+(CH_2)_nNH_3^+]$	Cross section (Å^2)		
	CB7	CB8	CB*6
2	540±20		561±15
3	520±12		545±20
4	482±26	924±40	541±20
5	469±20	780±44	573±23
6	496±26	768±33	580±21
7	517±20	798±43	632±25
8	533±19	823±55	647±23
9	541±20	808±40	664±23
10	556±22	802±38	664±29

Conclusions

Complexation of α,ω-alkyl diammonium ions with CB*6, CB7, and CB8 in the gas phase was studied via SORI-CID and CRAFTI techniques. Observation of cage fragmentation indicates most of these complexes are pseudorotaxanes, with the alkyl chain threading through the cucurbituril cavity. With more glycoluril units in the cucurbituril, the distance between carbonyl oxygens axially spanning the cavity increases and the corresponding most suitable alkyl chain length of the diammonium for the cavity should be longer. This geometric expectation agrees with the experimental results: for CB*6, the optimal chain length is n=3; for CB7, the optimal

one is n=5; and for CB8, the suitable one is n=6. The SORI-CID results modified with CRAFTI cross sections also provide the overall dissociation energy trends: CB7<CB*6<CB8. All these data offer basic understanding for future investigation of host-guest interactions in more complicated complexes.

References

(1) Steed, J. W.; Atwood, J. L. *Supramolecular Chemistry*; 2nd ed. ed.; Wiley: Chichester (UK), 2009.

(2) Freeman, W. A.; Mock, W. L.; Shih, N.-Y. *J. Am. Chem. Soc.* **1981**, *103*, 7367-7368.

(3) Lagona, J.; Mukhopadhyay, P.; Chakrabarti, S.; Isaacs, L. *Angew. Chem. Int. Ed.* **2005**, *44*, 4844-4870.

(4) Kim, K.; Selvapalam, N.; Ko, Y. H.; Park, K. M.; Kim, D.; Kim,J. *J. Chem. Soc. Rev.* **2007**, *36*, 267-279.

(5) Isaacs, L. *Chem. Commun.* **2009**, 619-629.

(6) Mock, W. L. *Comprehensive Supramolecular Chemistry*; Elsevier: New York, 1996; Vol. 2.

(7) Zhang, H.; Paulsen, E. S.; Walker, K. A.; Krakowiak, K. E.; Dearden, D. V. *J. Am. Chem. Soc.* **2003**, *125*, 9284-9285.

(8) Zhang, H.; Ferrell, T. A.; Asplund, M. C.; Dearden, D.V. *I. J. Mass Spec.* **2007**, *265*, 187-196.

(9) Yang, F.; Voelkel, J. E.; Dearden, D. V. *Anal. Chem.* **2012**, *84*, 4851-4857.

(10) Zhao, J.; Kim, H. -J.; Oh, J.; Kim, S.-Y.; Lee, J.W.; Sakamoto, S.; Yamaguchi, K.; Kim K. *Angew. Chem., Int. Ed.* **2001**, *40*, 4233-4235.

(11) Senko, M. W.; Canterbury, J. D.; Guan, S.; Marshall, A. G. *Rapid Commun. Mass Spectrom.* **1996**, *10*, 1839-1844.

(12) Wigger, M.; Nawrocki, J. P.; Watson, C. H.; Eyler, J. R.; Benner, S. A. *Rapid Commun. Mass Spectrom.* **1997**, *11*, 1749-1752.

(13) Chen, L.; Wang, T.-C. L.; Ricca, T. L.; Marshall, A. G. *Anal. Chem.* **1987**, *59*, 449-454.

(14) Gauthier, J. W.; Trautman, T. R.; Jacobson, D.B. *Anal. Chim. Acta* **1991**, *246*, 211-225.

(15) Jiao, C. Q.; Ranatunga, D. R. A.; Vaughn, W. E.; Freiser, B. S. *J. Am. Soc. Mass Spectrom.* **1996**, *7*, 118-122.

Chapter 7 Characterization of α,ω-Alkyldiammonium Complexes of Cucurbit[5]uril and Cucurbit[5]uril Derivatives in the Gas Phase

Introduction

Cucurbit[n]urils (CBn)[1-5], named after the Latin for the pumpkin family, are pumpkin-shaped, hollow macrocycles that are cyclic polymers of glycoluril. They all have symmetric geometries with two identical carbonyl-lined portals that make cucurbiturils ideal for binding with positive ions, and an interior cavity that can trap molecules with the right size and shape. The electronegative carbonyl groups are also good hydrogen bond receptors.

1,4-Butanediamine forms complexes with cucurbit[5]uril (CB5) and cucurbit[6]uril (CB6) in the gas phase,[6] and the CB6 complex with butanediamine is a pseudorotaxane. All the other α,ω-alkyldiammonium cations examined also form rotaxanes with CB6.[7] What about smaller cucurbiturils, such as cucurbit[5]uril and cucurbit[5]uril deriviatives? What kind of the structures do those cucurbituril complexes form with α,ω-alkyldiammonium in the gas phase?

In this chapter, I investigate α,ω-alkyldiammonium complexes with cucurbit[5]uril (CB5), decamethylcucurbit[5]uril (mc5) and penta(cyclohexyl)cucurbit[5]uril (CB*5) using Fourier transform ion cyclotron resonance mass spectrometry (FTICR-MS). CRAFTI (cross sectional areas by Fourier transform ion cyclotron resonance)[8] and SORI-CID (sustained off-resonance irradiation collision induced dissociation) techniques are the two methods I employ to explore these complexes.

Experimental

Materials

Cucurbit[5]uril (CB5) and the n-alkyldiamines (n=2-10) were purchased from Sigma-Aldrich (St. Louis, MO) and used without further purification. Decamethylcucurbit[5]uril (mc5) was synthesized by Dr. Krzystof Krakowiak using published procedures.[9] Penta(cyclohexyl)cucurbit[5]uril (CB*5) was synthesized by Dr. Kimoon Kim's group.[10] Stock solutions of CBn were prepared at about 200 μM by dissolving the solid samples in 88% formic acid (Mallinckrodt Baker Inc., Phillipsburg, NJ) and then diluting with n-propanol/water (50:50). The electrospray solutions were prepared at concentrations of 100 μM in CBn and 200 μM in diamines. Argon (99.995%) and SF_6 (99.8%) were purchased from Airgas (Radnor, PA) to be used as collision gases.

Instrumentation

All experiments were conducted using a Bruker model APEX 47e Fourier transform ion cyclotron resonance mass spectrometer controlled by a MIDAS data system[11] and equipped with an infinity cell and a 4.7 T superconducting magnet. Ions are generated in a microelectrospray source modified from an Analytica (Branford, MA) design, with a heated metal capillary drying tube based on the design of Eyler.[12] Sustained off-resonance irradiation-collision-induced dissociation (SORI-CID) experiments were performed by irradiating the target ions 1 kHz off resonance. Argon was introduced as the collision gas using a Freiser-type pulsed leak valve[13] and was maintained at a constant pressure of about 1.7×10^{-5} mbar during the SORI-CID. SORI energies were varied by maintaining constant amplitude at 10.25 V and varying the length of the RF pulse from 10 ms to 500 ms. The details for SORI-CID experiments and threshold data analysis already have been discussed.[7] CRAFTI experiments were carried out at 200 eV collision

energies (in the center-of-mass reference frame) using SF_6 over a range of pressures from 10^{-8}-10^{-5} mbar. Detailed sequences for the CRAFTI experiments were described elsewhere.[8]

Data Analysis

Transient signals were analyzed using the Igor Pro software package (version 6, Wavemetrics; Lake Oswego, OR).

For SORI experiments, the Igor program is used to extract peak amplitudes for a set of spectra that differ in one or more experimental parameters and then generates the tables of peak intensities as a function of SORI excitation duration. The resulting parent and product ion peak intensities were normalized and the relative SORI collision energy was scaled to account for differences in mass and excitation amplitude (although most experiments were conducted while maintaining a constant excitation amplitude).[7] Energies obtained from these experiments may be compared qualitatively, but are not quantitative due to uncertainties about the absolute kinetic energies of the colliding ions as well as uncertainties about the efficiency of kinetic-to-internal energy conversion. Calculation of relative SORI energies has been discussed.[7]

For the CRAFTI experiments, details of cross section data analysis can be obtained elsewhere.[8]

Results and Discussion

Electrospray of cucurbit[n]uril with alkyldiamines

α,ω-Alkyldiammonium ($H_3N^+(CH_2)_nNH_3^+$, n=2-10, C_nDA for abbreviation) complexes with CB5, mc5 and CB^*5 were electrosprayed and Fourier transform ion cyclotron resonance mass spectrometry was performed. 2:1 doubly-charged ions ($[CBn+2C_nDA+2H]^{2+}$) and 1:1 singly charged ions ($[CBn+C_nDA+H]^+$) were observed in the mass spectra for these solutions.

Cross section measurements of diamine complexes of CB5, mc5 and CB*5 via CRAFTI

To get an idea of the conformations of the diamine complexes with CB5, mc5 and CB*5, the CRAFTI technique was utilized to measure their cross sections. The cross sections of 1:1 complexes and 2:1 complexes are shown in Figure 7.1(a) and 7.1(b).

Generally, for both 1:1 and 2:1 complexes, the cross section increases with increasing alkydiammonium chain length for every host molecule. This trend is consistent with the idea that all these complexes are exterior complexes, with guest ions binding outside the cucurbituril cavity. Examining the cross sections listed in Table 7.1, for every host molecule, the 2:1 complex is always bigger than the 1:1 complex for a given guest cation, which results from the additional external diamine.

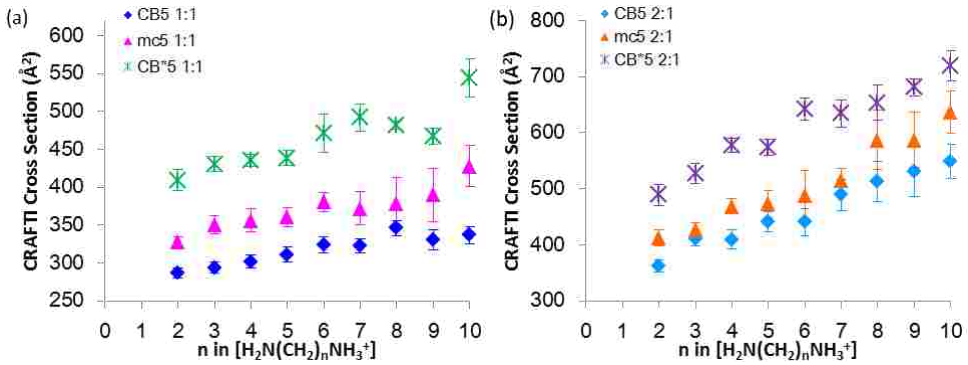

Figure 7.1 CRAFTI cross section of alkyldiamine ($[H_3N^+(CH_2)_nNH_3^+$, n=2-10) complexes of CB5, mc5 and CB*5 at a constant kinetic energy in the center-of-mass reference frame (SF_6 collision gas). (a) 1:1 singly charged complexes; (b) 2:1 doubly charged complexes. Error bars represent ± 1 standard deviation from the fitting procedure.

Table 7.1 Cross sections for $[H_2N(CH_2)_nNH_3^+]$@CB5, mc5 and CB*5, n=2-10.

n in $[H_2N(CH_2)_nNH_3^+]$	Cross Section (Å^2)					
	CB5		mc5		CB*5	
	1:1	2:1	1:1	2:1	1:1	2:1
2	286±6	361±10	328±6	413±14	410±13	489±19
3	293±7	410±11	350±12	426±12	430±9	526±18
4	301±8	410±16	356±15	468±13	435±7	578±12
5	311±9	441±17	360±12	472±25	439±10	573±13
6	323±10	440±24	380±13	487±45	471±25	642±20
7	322±8	488±27	372±22	515±22	492±17	634±23
8	345±9	512±36	378±33	587±23	482±5	653±31
9	330±12	530±43	390±35	587±29	467±11	681±15
10	336±11	548±30	427±27	636±38	544±25	719±33

Dissociation behavior of $[H_2N(CH_2)_nNH_3^+]$•CBn complexes

SORI-CID experiments were performed on the 1:1 complexes, $[CBn+C_nDA+H]^+$. Except for 1,4-butanediamine with CB5, the dissociation fragments for these CB5, mc5 and CB*5 1:1 complexes are all the same type, yielding protonated CBn ($[CBn+H]^+$) and hydronium complexes of CBn ($[CBn+H_3O]^+$). An example showing the dissociation products for n=5 is given in Figure 7.2, where the relative signal abundance of the parent ion and product ions are plotted against the relative SORI dissociation energies. The SORI ion yield curve for $[CB5+C4DA+H]^+$ is shown in Figure 7.3. I observe the only difference for this complex is

having one other product ion, loss of neutral ammonia, $[CB5+C4DA+H-NH_3]^+$. The abundance of this fragment is much less than that of the other two product ions, which implies this n=4 complex experiences dissociation pathways similar to those of the other 1:1 complexes.

According to the observed product ions, there is only one dissociation pathway for these 1:1 complexes, the proton transfer dissociation pathway already discussed in Chapter 6. Due to loss of the neutral diamine, protonated CBn is the product. The hydronium complexes are more difficult to explain. As H_3O^+ has been proposed as a template ion in the formation of CB5,[14] $[CBn+H_3O]^+$ is an unsurprising by-product of the proton transfer dissociation from reaction of the initially-formed protonated CBn with background neutral water. Interestingly, in contrast to the alkyldiamine complexes with CB6,[7] no cage fragmentation is observed for the 1:1 complexes studied in this chapter. This indicates that for these complexes, the guest does not need to break out of the cucurbituril cage during the dissociation. Therefore I conclude that these singly-charged complexes are external complexes, with the protonated ammonium group attached to the carbonyl groups of the CB rim while the remainder of the molecule stays outside the cage.

To further test this conclusion, the disappearance curves of the parent ions are plotted against the relative SORI energies, shown in Figure 7.4. For CB5 and CB*5 1:1 complexes, the falling portions of the curves almost overlap for ions with same host. For the mc5 1:1 complexes, the falling portions of their disappearance curves are parallel to each other. From these data I conclude that for complexes with the same host, roughly the same energy is needed for complete dissociation, independent of the guest. The relative energies for 50% loss of the

parent ion, $E_{SORI,\,50}$, were determined by linear fitting of the falling portion of each disappearance curve in Figure 7.4, with the results shown in Figure 7.5(a) where I take all the factors except the cross sections (including the collision duration, the collision amplitude, the ion charge and the ion mass) related to SORI energies into account (Equations (1-5) and (1-6) in Chapter 1). To compare the same guest ion with different hosts, the cross sections examined via CRAFTI were taken into account to get more accurate disappearance energies because of the significant differences in cross sections between complexes involving different host complexes, shown in Figure 7.5(b). The complex disappearance energies, $E_{SORI,\,50}$, which is an indicator of the overall relative stability of the complex, are very similar for all complexes with the same host; while for the complexes with the same guest cation, they follow this trend: CB5 < mc5 ≤ CB*5. These results further suggest all these 1:1 singly charged complexes have similar dissociation energies, as would be expected if all these complexes are external. Because polarizability plays an important role in determining the strength of ion-neutral interactions and the polarizabilities of the neutral cucurbiturils go up with increasing number and size of substituents, CB*5 and mc5 complexes need more dissociation energy than CB5 complexes.

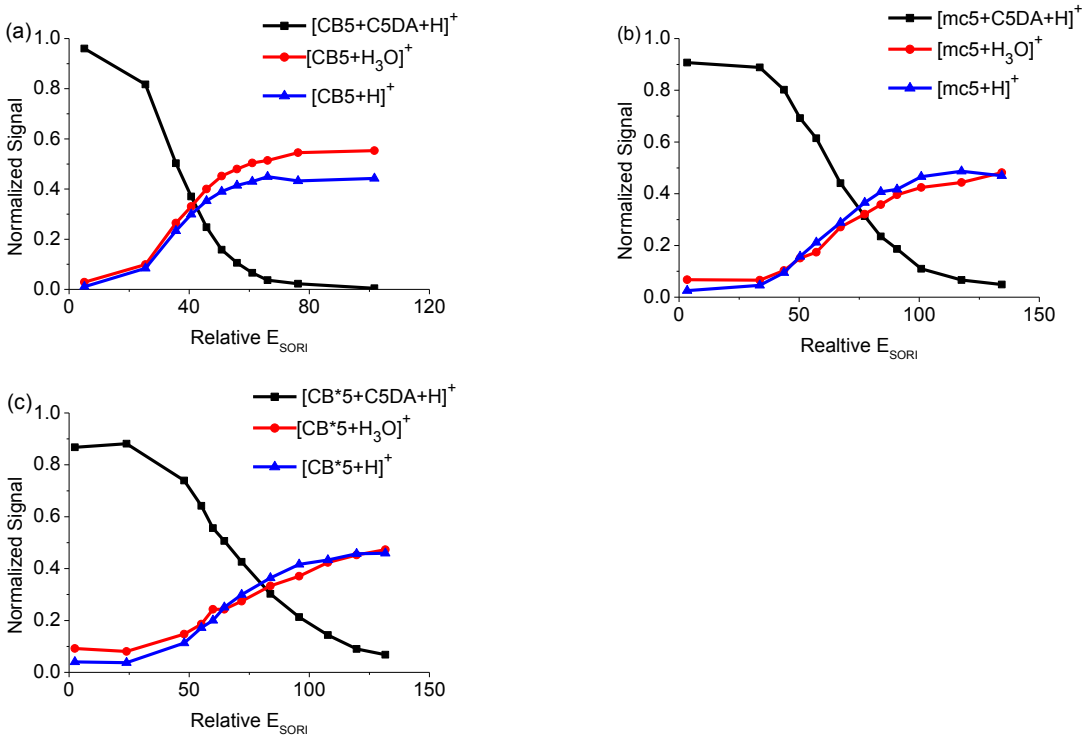

Figure 7.2 SORI ion yield curves for (a) $[H_2N(CH_2)_5NH_3^+]$•CB5, (b)$[H_2N(CH_2)_5NH_3^+]$•mc5, (c)$[H_2N(CH_2)_5NH_3^+]$•CB*5 complexes.

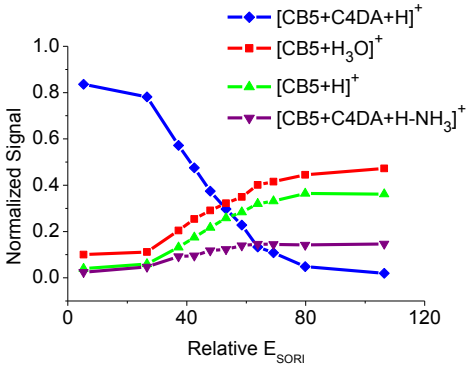

Figure 7.3 SORI ion yield curves for $[H_2N(CH_2)_4NH_3^+]$•CB5.

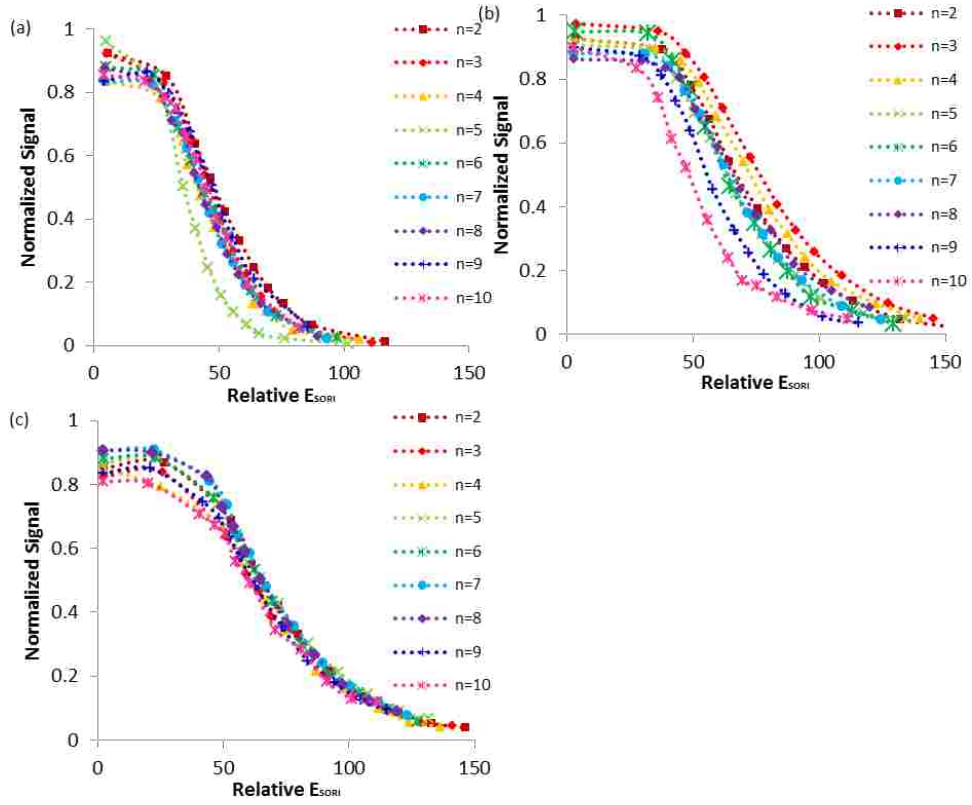

Figure 7.4 SORI parent ion survival curves for (a) $[H_2N(CH_2)_nNH_3^+]$•CB5, (b) $[H_2N(CH_2)_nNH_3^+]$•mc5, (c) $[H_2N(CH_2)_nNH_3^+]$•CB*5 complexes, n=2-10.

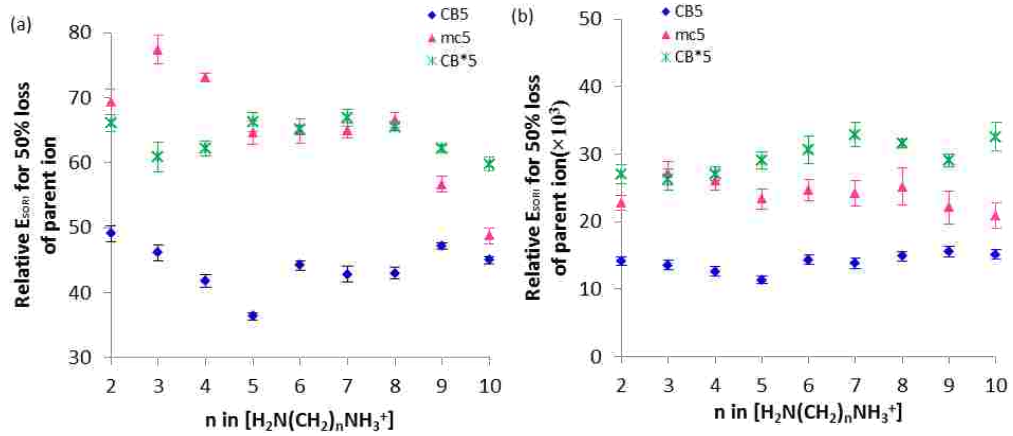

Figure 7.5 Relative SORI energies for 50% survival of $[H_2N(CH_2)_nNH_3^+]$•CB5, $[H_2N(CH_2)_nNH_3^+]$•mc5, and $[H_2N(CH_2)_nNH_3^+]$•CB*5 complexes, n=2-10, (a) uncorrected with cross section, (b) modified with

cross section. Error bars represent standard errors from the linear fitting procedure used to derive the value.

Dissociation Behavior of $[H_2N(CH_2)_nNH_3^+]_2$•CBn Complexes

As for the 1:1 complexes, SORI-CID experiments were carried out on the 2:1 complexes of CB5, mc5 and CB*5 with a constant SORI excitation amplitude. The normalized signal of parent and product ions in the dissociation of $[H_2N(CH_2)_5NH_3^+]_2$•CBn is shown in Figure 7.6. These 2:1 complexes all have the same three types of fragments: singly charged 1:1 fragments ($[CBn+CnDA+H]^+$), protonated hosts ($[CBn+H]^+$) and hydronium complexes of the hosts ($[CBn+H_3O]^+$). As a result, there are two dissociation pathways for the 2:1 complexes: loss of one protonated diamine cation and loss of an additional neutral amine. Just as with the 1:1 complexes, there is no cage fragmentation for the 2:1 complexes, which suggests that the alkyldiammonium is too big to fit into the cage of CB5 and its derivatives. This dissociation behavior provides one more evidence for the external structure of the 1:1 complexes: if the 1:1 complexes are inclusion complexes, dissociation of 2:1 complexes should result in doubly charged 1:1 complexes with the loss of a neutral diamine, not loss of a protonated diamine.[6]

The disappearance curves of $[H_2N(CH_2)_nNH_3^+]_2$•CBn complexes are shown in Figure 7.7. For 2:1 CB5 complexes, the slopes of the falling portions of the curves are the same except when n=2 and n=3. For the 2:1 mc5 complexes, the disappearance curves mostly overlapped except when n=2 and n=10. For the 2:1 CB*5 complexes, the falling portions are parallel. These similarities also give strong support to the hypothesis that these 2:1 complexes are external complexes.

In addition, the disappearance energy, $E_{SORI,\,50}$, was plotted with the chain length number to compare the binding affinity of these 2:1 complexes, as shown in Figure 7.8. Figure 7.8(a) demonstrates the $E_{SORI,50}$ values acquired directly from the disappearance curves; and Figure 7.8(b) exhibits the values of corrected $E_{SORI,\,50}$ obtained by multiplying $E_{SORI,\,50}$ in Figure 7.8(a) with the cross sections from the CRAFTI method (Table 7.1). For complexes with the same hosts, values of the disappearance energies are very close between diamines with different chain length. For complexes with the same diammonium cation, values of disappearance energies follow a consistent trend: CB5 < mc5 < CB*5, the same as for the 1:1 complexes, with the same explanation.

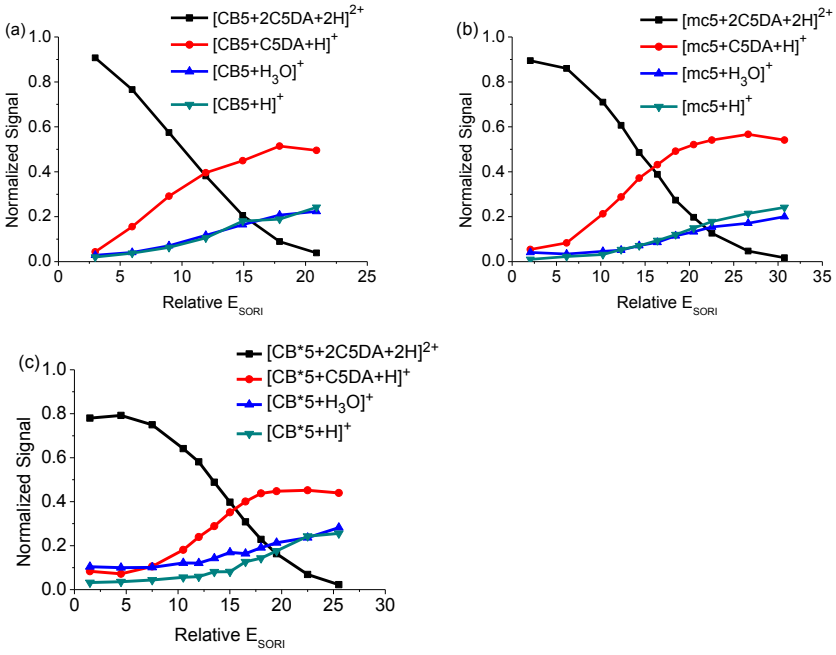

Figure 7.6 SORI ion yield curves for (a) $[H_2N(CH_2)_5NH_3^+]_2$•CB5, (b)$[H_2N(CH_2)_5NH_3^+]_2$•mc5, (c)$[H_2N(CH_2)_5NH_3^+]_2$•CB*5 complexes.

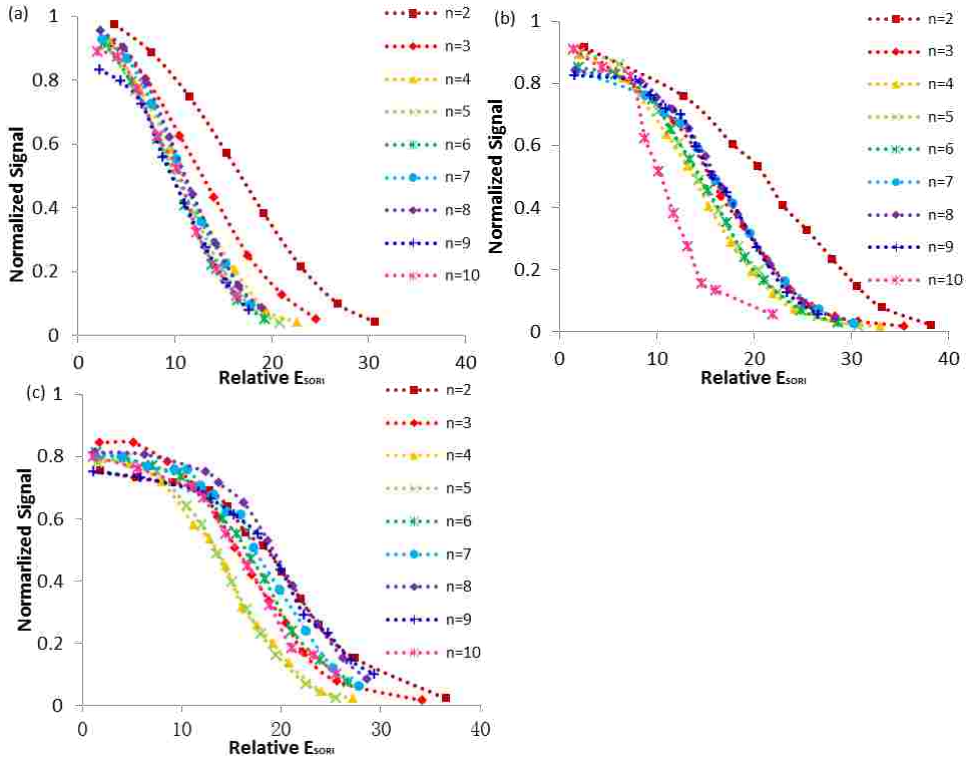

Figure 7.7 SORI parent ion survival yield curves for (a) $[H_2N(CH_2)_nNH_3^+]_2$•CB5, (b) $[H_2N(CH_2)_nNH_3^+]_2$•mc5, (c) $[H_2N(CH_2)_nNH_3^+]_2$•CB*5 complexes, n=2-10.

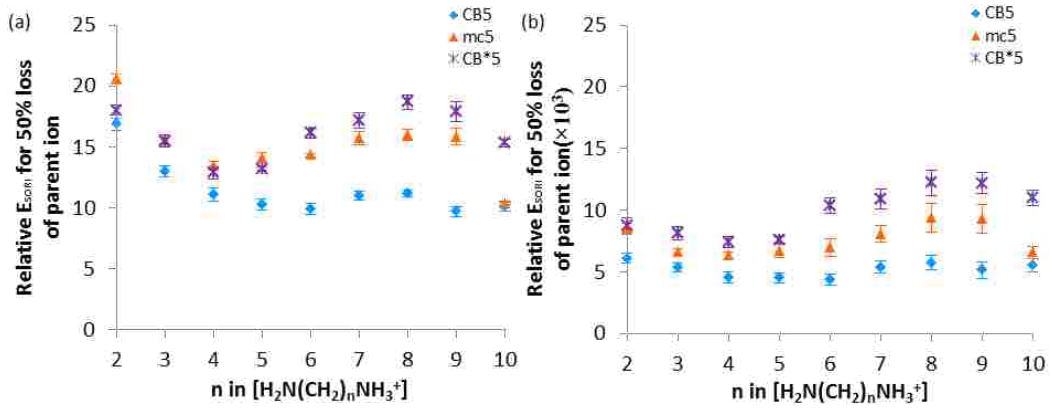

Figure 7.8 Relative SORI energies for 50% survival of $[H_2N(CH_2)_nNH_3^+]_2$•CB5, $[H_2N(CH_2)_nNH_3^+]_2$•mc5 and $[H_2N(CH_2)_nNH_3^+]_2$•CB*5 complexes, n=2-10, (a) uncorrected with cross section, (b) modified with cross section. Error bars represent standard errors from the linear fitting procedure used to derive the value.

Comparisons of 1:1 complexes with 2:1 complexes

As discussed above, because of the similarity of structure among CB5, mc5 and CB*5, all three of these hosts form the same type of complexes with α,ω-alkyldiamines. Because there is no cage fragmentation during the dissociation of either 1:1 or 2:1 complexes, and because of the similar disappearance energies for complexes with the same hosts and the almost linear increasing in cross section with chain length, the evidence is strong that these complexes are external, with the cations staying outside the cucurbituril cages. To compare the 2:1 complexes and 1:1 complexes of diammonium with CB5, mc5 and CB*5, the relative SORI energies for 50% loss of parent ions, $E_{SORI,50}$, were plotted against the chain length of the amine, shown in Figure 7.9. I note three things from the comparison. First, for complexes with the same host and the same charge, the relative energies for 50% loss of parent ions are similar, as expected for externally bound guests. Second, the 2:1 complexes need less energy for dissociation than the corresponding 1:1 complexes, which results from Coulomb repulsion[15]. Third, for either 2:1 complexes or 1:1 complexes, with the same diamine, the disppearence energies follow the same trend: CB5 < mc5 ≤ CB*5, which has been mentioned previously and can be explained by increasing polarizability for the derivatives.

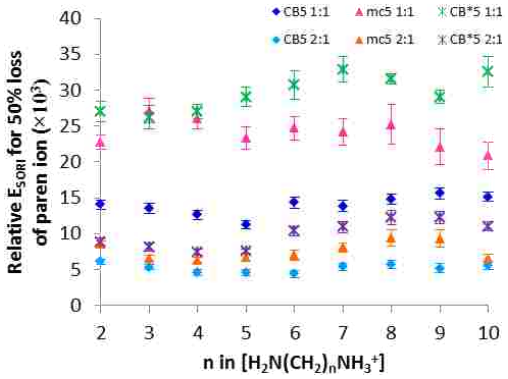

Figure 7.9 Relative SORI energies for 50% survival of $[H_2N(CH_2)_nNH_3^+]$•CB5, $[H_2N(CH_2)_nNH_3^+]$•mc5, $[H_2N(CH_2)_nNH_3^+]$•CB*5, $[H_2N(CH_2)_nNH_3^+]_2$•CB5, $[H_2N(CH_2)_nNH_3^+]_2$•mc5 and $[H_2N(CH_2)_nNH_3^+]_2$•CB*5 complexes, n=2-10. Error bars represent standard errors from the linear fitting procedure used to derive the value.

Conclusions

In contrast to the bigger cucurituril,[6,7] these smaller cucurbiturils mainly form two kinds of complexes with alkyldiamines: singly-charged 1:1 complexes and doubly-charged 2:1 complexes. CRAFTI and SORI-CID experiments were performed on these complexes. The results of cross section trends, dissociation fragments and the similarities of disappearance energies for complexes with the same host all support the conclusion that these are external complexes in the gas phase. Furthermore, cross section and dissociation comparison between complexes with the same guests but different hosts, both exhibit a reasonable trend: CB5 < mc5 ≤ CB*5. These results all demonstrate CRAFTI and SORI-CID are two complementary techniques for characterization of supramolecular systems.

References

(1) Isaacs, L. *Chem. Commun.* **2009**, 619-629.

(2) Kim, K.; Selvapalam, N.; Ko, Y. H.; Park, K. M.; Kim, D.; Kim,J. *J. Chem. Soc. Rev.* **2007**, *36*, 267-279.

(3) Lagona, J.; Mukhopadhyay, P.; Chakrabarti, S.; Isaacs, L. *Angew. Chem. Int. Ed.* **2005**, *44*, 4844-4870.

(4) Freeman, W. A.; Mock, W. L.; Shih, N.-Y. *J. Am. Chem. Soc.* **1981**, *103*, 7367-7368.

(5) Steed, J. W.; Atwood, J. L. *Supramolecular Chemistry*; 2nd ed. ed.; Wiley: Chichester (UK), 2009.

(6) Zhang, H.; Paulsen, E. S.; Walker, K. A.; Krakowiak, K. E.; Dearden, D. V. *J. Am. Chem. Soc.* **2003**, *125*, 9284-9285.

(7) Zhang, H.; Ferrell, T. A.; Asplund, M. C.; Dearden, D.V. *I. J. Mass Spec.* **2007**, *265*, 187-196.

(8) Yang, F.; Voelkel, J. E.; Dearden, D. V. *Anal. Chem.* **2012**, *84*, 4851-4857.

(9) Zhang, X. X.; Krakowiak, K. E.; Xue, G.; Bradshaw, J. S.; Izatt, R. M. *Ind. Eng. Chem. Res.* **2000**, *39*, 3516-3520.

(10) Zhao, J.; Kim, H. -J.; Oh, J.; Kim, S.-Y.; Lee, J.W.; Sakamoto, S.; Yamaguchi, K.; Kim K. *Angew. Chem., Int. Ed.* **2001**, *40*, 4233-4235.

(11) Senko, M. W.; Canterbury, J. D.; Guan, S.; Marshall, A. G. *Rapid Commun. Mass Spectrom.* **1996**, *10*, 1839-1844.

(12) Wigger, M.; Nawrocki, J. P.; Watson, C. H.; Eyler, J. R.; Benner, S. A. *Rapid Commun. Mass Spectrom.* **1997**, *11*, 1749-1752.

(13) Jiao, C. Q.; Ranatunga, D. R. A.; Vaughn, W. E.; Freiser, B. S. *J. Am. Soc. Mass Spectrom.* **1996**, *7*, 118-122.

(14) Oh, K. S.; Yoon, J.; Kim, K. S. *J. Phys. Chem. B* **2001**, *105*, 9726-9731.

(15) Mortensen, D. N.; Dearden, D. V. *Chem. Commun.* **2011**, *47*, 6081-6083.

Chapter 8 Guanidinium-Capped Cucurbit[7]uril Molecular Cages in the Gas Phase[a]

Introduction

Cucurbit[n]urils[1] (Figure 8.1), which are cyclic condensation polymers of formaldehyde and glycoluril and have been made in a variety of sizes ranging from 5 to 10 monomer units, are gaining increasing attention as prototypical supramolecular hosts and in applications such as drug delivery[2-5] and sensitive analytical assays.[6] The carbonyl-lined portals of the n = 5 cucurbit[n]urils are the right size to bind cations such as primary ammonium or alkali metal ions,[1,7] while the interior of the cucurbit[5]uril cage is large enough to accommodate large atoms (such as Kr or Xe) or small molecules (such as methanol).[7,8] Hence, supramolecular cages comprised of cucurbit[5]uril and two cations self-assemble in solution and can trap solvent molecules or gases bubbled through the solvent.[7] Similar metal-capped cage structures involving cucurbit[6]uril[9,10] have been discussed as well. Complexation of metal cations by cucurbit[6]uril[11] or cucurbit[7]uril[12] generally competitively destabilizes the complexes of these ligands with other charged guests. Interesting potential applications of such phenomena in the controlled release of trapped species have been suggested.[13,14]

While these small cages are interesting prototypical supramolecular containers and may even have practical applications in gas purification[8] or drug delivery,[14] the small sizes of cucurbit[5]uril and cucurbit[6]uril means that only a limited range of neutral hosts can be trapped inside. In this chapter I report the formation of larger supramolecular cages based on

[a] A version of this chapter has been published.
"Guanidinium-capped cucurbit[7]uril molecular cages in the gas phase," Yang, F.; Dearden, D. V. *Supramol. Chem.* **2011**, *23*, 53-58.

cucurbit[6]uril (hereafter CB6) and cucurbit[7]uril (CB7). The latter have high stability and trap neutrals as large as toluene. I have characterized these systems both through the methods of computational chemistry and through tandem mass spectrometric techniques.

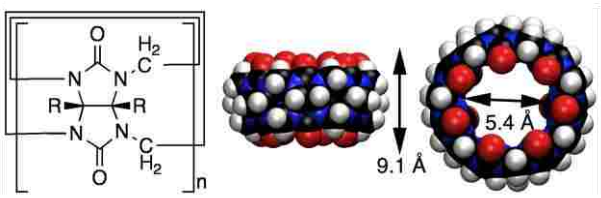

Figure 8.1 Structure and dimensions (from X-ray data in Reference[15]) for cucurbit[7]uril, CB7. R = H for CB7. Dimensions include appropriate van der Waals radii.

Experimental

Materials

CB6 was purchased from Sigma-Aldrich Chemical Co. (St. Louis, MO), and CB7 was provided by Professor Kimoon Kim (POSTECH, Pohang, Korea). Guanidinium hydrochloride, benzene, fluorobenzene, chlorobenzene, toluene, and xylenes were purchased from Sigma-Aldrich. All were used without further purification.

Sample preparation

Stock solutions of CB6 and CB7 were prepared at about 1 mg/mL concentration by dissolving solid samples in 88% formic acid (Fisher Scientific, Fair Lawn, NJ). Guanidinium hydrochloride stock solution was prepared by dissolving the salt in HPLC grade water (Mallinckrodt Baker Inc., Phillipsburg, NJ). Solutions for electrospray were prepared by mixing and diluting the stock solutions with 50:50 methanol:water so that the final concentration

of CBn complex was about 100 μM. Neutral guests of interest were dissolved in methanol at 10-20 mM concentration and added to the electrospray solutions so that the final concentration of neutral guest was approximately 200 μM.

ESI mass spectrometry

Instrumentation

Mass spectrometric measurements were carried out on one of two instruments. Most experiments used a 4.7 Tesla Bruker Daltonics (Billerica, MA) model APEX 47e FT-ICR mass spectrometer controlled by a MIDAS Predator data system[16,17] and equipped with a microelectrospray source modified from an Analytica design, with a heated metal capillary drying tube based on the design of Eyler.[18] The source was typically operated at a flow rate of 30 μL hr^{-1}.

Ultra-high resolution and accurate mass measurements were made on a 9.4 Tesla Bruker Daltonics APEX II FT-ICR mass spectrometer that employed the Bruker Daltonics Apollo electrospray ionization source, typically operated at a flow rate of 150 μL hr^{-1}. All masses determined with either instrument are within 1 ppm of masses calculated for the proposed formulas.

Sustained off-resonance irradiation collision-induced dissociation (SORI-CID) experiments

In sustained off-resonance irradiation collision-induced dissociation (SORI-CID)[19] experiments, parent and product ion abundances are monitored as the parent ions are driven through collisions with an inert neutral gas over a range of kinetic energies. Stored waveform inverse Fourier transform (SWIFT)[20] techniques were used to isolate target peaks. The ions

were excited to superthermal kinetic energies by irradiating 1 kHz below the resonant frequency of the ion of interest. Collision gas (Ar) was introduced using a Freiser-type pulsed leak valve.[21] SORI events involved pulsing the background pressure in the trapping cell up to 10^{-5} mbar, waiting 2 seconds for conditions to fully stabilize, and applying the off-resonance irradiation for a variable amount of time (which allows variation of the total energy deposited in the ions; typically, times ranged from 1 to about 500 ms, with amplitudes kept high and durations kept short to minimize radiative cooling between collisions), followed by a 5 second delay to allow the trapping cell to return to baseline pressure (about 10^{-8} mbar) prior to detection. Typically a series of experiments with differing SORI durations was carried out to examine the energy dependence of the dissociation process. The resulting parent and product ion peaks were normalized and the relative SORI collision energy was scaled to account for differences in mass and excitation amplitude[22] (although most experiments were conducted while maintaining a constant excitation amplitude). Energies obtained from these experiments may be compared qualitatively, but are not quantitative due to uncertainties about the absolute kinetic energies of the colliding ions as well as uncertainties about the efficiency of kinetic-to-internal energy conversion.

Electronic structure calculations

Structures were sketched using the *Maestro/Macromodel* modelling package (*Macromodel* version 7.1; Schrödinger, Inc.; Portland, OR). Conformational searches were performed using the MMFF94s[23] force field with no nonbonded cutoffs and with conjugate gradient minimization using the MCMM search method with automatic setup and 10,000 starting structures; under

these conditions the lowest-energy structures are typically found hundreds of times. Torsional rotations within the cucurbituril ring were disabled. The lowest-energy structures found in the conformational searches were used as the starting point for DFT geometry optimizations (usually at B3LYP/6-31G* or B3LYP/6-31+G* levels of theory, but occasionally using other functionals). These calculations were performed using *NWChem* (version 5.1; Pacific Northwest National Laboratory; Richland, WA)[24] and used *NWChem* default convergence criteria. No atoms were constrained in the geometry optimizations. Computed structures were visualized using the *VMD* software package (version 1.8.7; University of Illinois; Urbana-Champaign, IL)[25] Reported energy differences are at 0 K, uncorrected for zero point energy; vibrational calculations were not carried out because for systems of the size studied here they require greater computational resources than were available to us. Because our conclusions rely on relative energies for the various complexes, and because zero point energies and basis set superposition errors are expected to be similar for complexes of similar size, we do not expect large errors arising from the lack of zero point or counterpoise corrections.

Results and discussion

Cucurbiturils are particularly interesting as molecular containers because they exhibit excellent size selectivity. For instance, decamethylcucurbit[5]uril electrosprayed from methanolic solutions gives intense signal corresponding to inclusion of methanol in the cucurbituril cavity, but when similar experiments are carried out using ethanol as the solvent, empty cages and cages containing O_2 or N_2 scavenged from the environment are dominant, with no ethanol-containing

complexes observed, because ethanol is too large to be easily accommodated inside the cucurbituril.[7]

Complexes of cucurbit[6]uril with guanidinium cation

Attempts to observe similar complexes of CB6 capped by metal ions and containing trapped neutral molecules result in metallated CB6 ions but we have never observed inclusion of neutrals in these systems. Modelling suggests that even large ions such as Cs^+ are probably not large enough to close the CB6 cavity and prevent egress of neutrals. We therefore turned to guanidinium (hereafter Gu^+) as a potential capping cation. Modelling of CB6•Gu_2^{2+} using molecular mechanics suggests Gu^+ is about the right size to form a "lid" on CB6 complexes. In addition, the 3-fold symmetry of the Gu^+ cation is an appealing match to the 6-fold symmetry of CB6. B3LYP/6-31G* geometry optimized calculations indicate that Gu^+ binds to CB6 with an energy of 336 kJ mol^{-1}; binding of a second Gu^+ is weaker (137 kJ mol^{-1}) due to Coulombic repulsion from the first charged group. Other DFT methods (M05-2X/6-31G* and M06-2X/6-31G*)[26,27] suggest binding energies about 10-15% higher, consistent with reports[28] that the B3LYP functional underestimates noncovalent binding energies.

Electrospray of solutions of CB6 mixed with guanidinium hydrochloride does yield a peak corresponding to CB6•Gu_2^{2+} (Figure 8.2), albeit with weak signal. Collisional dissociation of this complex results in loss of Gu^+, confirming the identity of the ion. However, attempts to trap solvent or other neutral species in this cage yielded only the "empty" complex. Hence, although the cage was observed, it does not appear to be effective at trapping larger neutral species, probably due to low intrinsic stability.

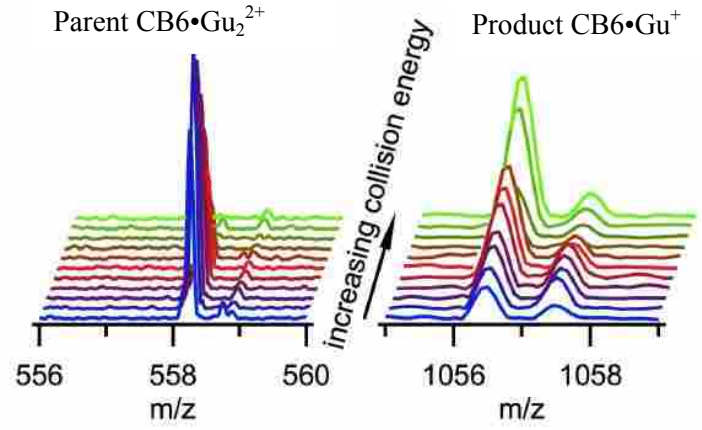

Figure 8.2 Collision-induced dissociation of the CB6•Gu_2^{2+} parent ion (left) results in loss of Gu^+, producing CB6•Gu^+ (right). The all-^{12}C isotope peak of the parent ion was isolated for these experiments, so the ^{13}C isotope peaks are missing.

Inclusion complexes of cucurbit[7]uril with guanidinium cation

Despite the symmetry mismatch between Gu^+ and the 7-fold symmetry of CB7, computational modelling predicts stronger complexes for this cation-host combination than for Gu^+ with CB6. Close examination of the CB6 complexes reveals that all the hydrogen bonds between Gu^+ and CB6 are bent through approximately 45°, whereas those in the CB7-Gu^+ complexes are all within a few degrees of linear (Figure 8.3). Further, the computed distance between the central C atoms of the 2 Gu^+ groups in the CB6 complex is 9.05 Å, whereas that in the CB7 complex is about 2 Å shorter, at 7.03 Å (Figure 8.3). In fact, the distance between the Gu^+ cations in the CB6 complex is the same as the height of the cucurbituril accounting for van der Waals radii, suggesting the Gu^+ cations lie on top of the portal rather than in it. The computed 12 closest H—O distances between the guanidinium hydrogen atoms and CB7 carbonyl oxygen atoms are 2.17 ± 0.13 Å, well within the range expected for hydrogen bonded systems involving

guanidinium. For example, H—O distances in guanidinium nitrate[29] are 2.18, 2.39, and 2.23 Å; in guanindinium benzoate,[30] 1.90, 2.17, and 2.08 Å; and in guanidinium 4-aminobenzoate,[31] 1.87, 2.11, and 2.10 Å. Despite the fact that in these example systems there is no organic framework constraining the bond lengths to be longer, the H—O distances in the CB7 complex are similar, suggesting large hydrogen bonding character in the Gu^+—CB7 interaction.

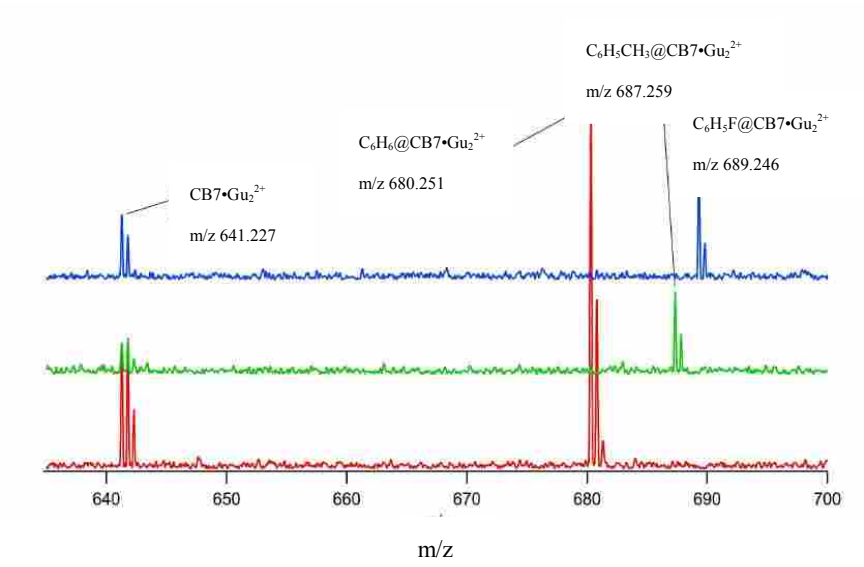

Figure 8.3 Electrospray ionization Fourier transform ion cyclotron resonance mass spectra of solution of cucurbit[7]uril and guanidinium hydrochloride spiked with benzene (bottom trace), toluene (middle trace), or fluorobenzene (top trace).

Despite the closer distance and corresponding increase in Coulombic repulsion in the CB7 complex, the computed binding energy for the 2nd Gu^+ group to CB7•Gu^+ is 2 kJ mol^{-1} stronger, at 138 kJ mol^{-1}, than that computed for the CB6 complex. All these observations suggest that the portal of CB6, with a diameter of 3.9 Å,[15] is smaller than optimal for binding Gu^+, whereas the 5.4 Å diameter of the CB7 portal[15] is a better fit. These theoretical predictions are also in

accord with earlier indirect evidence suggesting preferential binding of CB7 with guanidinium in arginine-containing peptides.[32]

Electrospray of solutions containing CB7 and guanidinium hydrochloride gives intense signal at m/z 641.227, corresponding to CB7•Gu_2^{2+} (Figure 8.3). SORI-CID of this ion results in loss of Gu^+, confirming the assignment of the signal as CB7•Gu_2^{2+}. Comparison of the energy dependence of this dissociation to that for loss of Gu^+ from CB6•Gu_2^{2+} confirms that the CB7 complex is more stable than that of CB6, because dissociation of the CB7 complex requires higher collision energies (Figure 8.5).

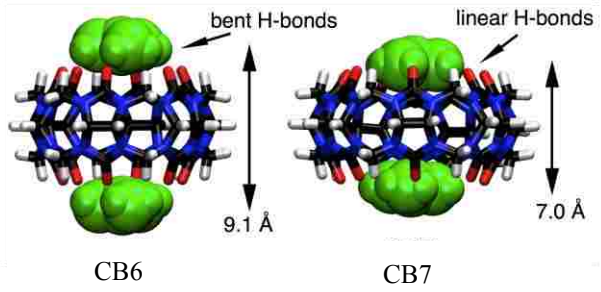

Figure 8.4 B3LYP/6-31+G* structures of CB6•Gu_2^{2+} (left) and CB7•Gu_2^{2+} (right) showing differences in hydrogen bond configurations and in Gu^+–Gu^+ distances for the two hosts.

Spiking the CB7-guanidinium hydrochloride solutions with benzene, fluorobenzene, or toluene, followed by electrospray, results in observation of the corresponding neutral@CB7•Gu_2^{2+} complexes (Figure 8.3). Attempts to spike with phenol, chlorobenzene, *o-, m-, or p*-xylene resulted in only "empty" complexes, suggesting strong size selectivity akin to that exhibited in the CB5-based supramolecular systems. The failure to observe chlorobenzene complexes

deserves further mention, as space-filling models suggest chlorobenzene is similar in size to toluene, which was observed. Perhaps the much greater polarity of chlorobenzene (1.90 debye) makes this guest less likely to enter the non-polar CB7 cavity than toluene (0.39 debye).

Further evidence for size selectivity in the binding of neutrals by the CB7•Gu_2^{2+} complex is found in their SORI-CID behaviour. Collisional excitation of benzene, fluorobenzene, or toluene inclusion complexes of CB7•Gu_2^{2+} results in loss of the neutral from the complex; interestingly, this does *not* involve loss of Gu^+, but apparently involves excitation of a vibrational mode that opens the portal sufficiently to allow the neutral to escape. When the neutral is benzene or fluorobenzene, the relative energy required to do this (Figure 8.6) is about the same as that required to remove Gu^+ from the complex. Loss of benzene or fluorobenzene is achieved at similar energies. Loss of toluene, on the other hand, occurs at much lower energies than are required to liberate the smaller aromatic species, suggesting that toluene is near the upper size limit for the CB7 cavity in at least one dimension.

The trends in the experimental observations of dissociation energies are consistent with the results of computed binding energies. The relative stabilities of the complexes at the B3LYP/6-31+G* level of theory are in the order $C_6H_5F \approx C_6H_6 >> C_6H_5CH_3$ (0, +4, and +22 kJ mol^{-1}, for the three neutrals, respectively), consistent with the relative energies observed in the SORI-CID experiments. Interestingly, all three neutral inclusion complexes observed in the mass spectra are found computationally to be unstable in the gas phase (i.e. the energies of neutral + CB7•Gu_2^{2+} are more favourable than those of neutral@CB7•Gu_2^{2+} at the B3LYP/6-31+G* level of theory). If the computed binding energies are accurate, this suggests

that the cage complexes form in solution and survive the electrospray process retaining solution-like structure, and are kinetically stable in the gas phase even though they are thermodynamically prone to dissociate when solvent is removed. An energetic barrier to dissociation allows them to be observed, but collisional activation results in facile loss of the neutral.

Although the amount of material we have on hand and the achievable concentrations prevent us from directly observing the complexes in solution (and thus proving they have formed in solution) via techniques such as NMR, it is difficult to envision how such complexes could have formed anywhere but in solution prior to electrospray. The low concentrations and Coulombic repulsion between the capping cations in the gas phase environment certainly are not conducive to this type of complex formation, leaving the evaporating electrospray droplets as the only viable alternative; it is conceivable that as the solvent evaporates the increasing concentrations of the involatile materials that make up the complex might promote complexation during the electrospray process, but again it is difficult to understand why the neutral would preferentially move into the CB7 cavity rather than simply evaporating. In solution, on the other hand, hydrophobic effects would promote inclusion of the neutral guest in the CB7 cavity.

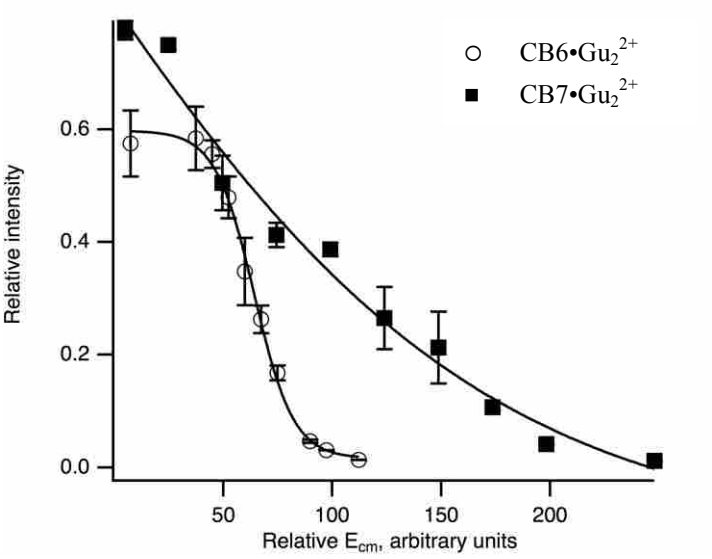

Figure 8.5 Relative surviving parent ion populations for CBn•Gu_2^{2+} as a function of average collision energy in the center-of-mass reference frame. Error bars represent ± 1 standard deviation for replicate runs. Lines are sigmoidal fits to the experimental data, simply to guide the eye.

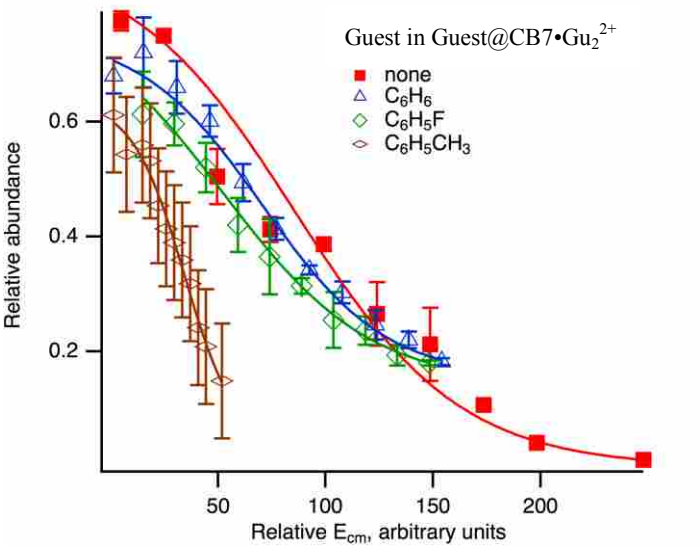

Figure 8.6 Relative surviving parent ion populations for Guest@CB7•Gu_2^{2+} as a function of average collision energy in the center-of-mass reference frame. Error bars represent ± 1 standard deviation for replicate runs. Lines are sigmoidal fits to the experimental data, simply to guide the eye.

Conclusions

Gas phase experiments and electronic structure calculations can be used synergistically to predict and observe the existence of supramolecular cage complexes, while using only miniscule amounts of material. Significant structural information can be obtained without the need for crystallizing the complexes, although at a much lower level of detail than is afforded by X-ray crystallography.

Extending previous characterization of metal cation-cucurbit[5]uril based supramolecular cages suitable for trapping large atoms or small molecules, guanidinium is an appropriate cap for closing the cavity of cucurbit[7]uril, enabling molecules as large as toluene to be trapped and transferred into the gas phase. This suggests that other, larger molecular "lid" species might be used to close the cavities of cucurbit[8]uril or similar, larger container molecules.

References

(1) Lagona, J.; Mukhopadhyay, P.; Chakrabarti, S.; Isaacs, L. *Angew. Chem. Int. Ed.* **2005**, *44*, 4844-4870.

(2) Uzunova, V. D.; Cullinane, C.; Brix, K.; Nau, W. M.; Day, A. I. *Org. Biomol. Chem.* **2010**, *8*, 1977-2268.

(3) Wheate, N. J. *J. Inorg. Biochem.* **2008**, *102*, 2060-2066.

(4) Saleh, N. i.; Koner, A. L.; Nau, W. M. *Angew. Chem., Int. Ed.* **2008**, *47*, 5398-5401.

(5) Wheate, N. J.; Taleb, R. I.; Krause-Heuer, A. M.; Cook, R. L.; Wang, S.; Higgins, V. J.; Aldrich-Wright, J. R. *Dalton Trans.* **2007**, 5055-5064.

(6) Praetorius, A.; Bailey, D. M.; Schwarzlose, T.; Nau, W. M. *Org. Lett.* **2008**, *10*, 4089-4092.

(7) Kellersberger, K. A.; Anderson, J. D.; Ward, S. M.; Krakowiak, K. E.; Dearden, D. V. *J. Am. Chem. Soc.* **2001**, *123*, 11316-11317.

(8) Miyahara, Y.; Abe, K.; Inazu, T. *Angew. Chem. Int. Ed.* **2002**, *41*, 3020-3023.

(9) Jeon, Y.-M.; Kim, J.; Whang, D.; Kim, K. *J. Am. Chem. Soc.* **1996**, *118*, 9790-9791.

(10) Whang, D.; Heo, J.; Park, J. H.; Kim, K. *Angew. Chem. Int. Ed.* **1998**, *37*, 78-80.

(11) Márquez, C.; Hudgins, R. R.; Nau, W. M. *J. Am. Chem. Soc.* **2004**, *126*, 5806-5816.

(12) Megyesi, M.; Biczók, L.; Jablonkai, I. *J. Phys. Chem. C* **2008**, *112*, 3410-3416.

(13) Choudhury, S. D.; Mohanty, J.; Pal, H.; Bhasikuttan, A. C. *J. Am. Chem. Soc.* **2010**, *132*, 1395-1401.

(14) Nau, W. M. *Nature Chemistry* **2010**, *2*, 248-250.

(15) Lee, J. W.; Samal, S.; Selvapalam, N.; Kim, H.-J.; Kim, K. *Acc. Chem. Res.* **2003**, *36*, 621-630.

(16) Senko, M. W.; Canterbury, J. D.; Guan, S.; Marshall, A. G. *Rapid Commun. Mass Spectrom.* **1996**, *10*, 1839-1844.

(17) Blakney, G. T.; Hendrickson, C. L.; Quinn, J. P.; Marshall, A. G. In *56th ASMS Conference on Mass Spectrometry and Allied Topics* Denver, CO, 2008.

(18) Wigger, M.; Nawrocki, J. P.; Watson, C. H.; Eyler, J. R.; Benner, S. A. *Rapid Commun. Mass Spectrom.* **1997**, *11*, 1749-1752.

(19) Gauthier, J. W.; Trautman, T. R.; Jacobson, D. B. *Anal. Chim. Acta* **1991**, *246*, 211-225.

(20) Chen, L.; Wang, T.-C. L.; Ricca, T. L.; Marshall, A. G. *Anal. Chem.* **1987**, *59*, 449-454.

(21) Jiao, C. Q.; Ranatunga, D. R. A.; Vaughn, W. E.; Freiser, B. S. *J. Am. Soc. Mass Spectrom.* **1996**, *7*, 118-122.

(22) Zhang, H.; Ferrell, T. A.; Asplund, M. C.; Dearden, D. V. *Int. J. Mass Spectrom.* **2007**, *265*, 187-196.

(23) Halgren, T. A. *J. Comput. Chem.* **1996**, *17*, 490-519.

(24) Apra, E.; Windus, T. L.; Straatsma, T. P.; Bylaska, E. J.; de Jong, W.; Hirata, S.; Valiev, M.; Hackler, M. T.; Pollack, L.; Kowalski, K.; Harrison, R. J.; Dupuis, M.; Smith, D. M. A.; Nieplocha, J.; Tipparaju, V.; Krishnan, M.; Auer, A. A.; Brown, E.; Cisneros, G.; Fann, G. I.; Fruchtl, H.; Garza, J.; Hirao, K.; Kendall, R.; Nichols, J. A.; Tsemekhman, K.; Wolinski, K.; Anchell, J.; Bernholdt, D.; Borowski, P.; Clark, T.; Clerc, D.; Dachsel, H.; Deegan, M.; Dyall, K.; Elwood, D.; Glendening, E.; Gutowski, M.; Hess, A.; Jaffe, J.; Johnson, B.; Ju, J.; Kobayashi, R.;

Kutteh, R.; Lin, Z.; Littlefield, R.; Long, X.; Meng, B.; Nakajima, T.; Niu, S.; Rosing, M.; Sandrone, G.; Stave, M.; Taylor, H.; Thomas, G.; van Lenthe, J.; Wong, A.; Zhang, Z.; 4.7 ed.; Pacific Northwest National Laboratory: Richland, Washington 99352-0999, USA, 2005.

(25) Humphrey, W.; Dalke, A.; Schulten, K. *J. Molec. Graphics* **1996**, *14*, 33-38.

(26) Dahlke, E. E.; Olson, R. M.; Leverentz, H. R.; Truhlar, D. G. *J. Phys. Chem. A* **2008**, *112*, 3976-3984.

(27) Zhao, Y.; Truhlar, D. G. *Acc. Chem. Res.* **2008**, *41*, 157-167.

(28) Zhang, I. Y.; Wu, J.; Xu, X. *Chem. Commun.* **2010**, *46*, 3057-3070.

(29) Katrusiak, A.; Szafranski, M. *Acta Crystallographica, Section C: Crystal Structure Communications* **1994**, *C50*, 1161-1163.

(30) Pereira Silva, P. S.; Ramos Silva, M.; Paixao, J. A.; Matos Beja, A. *Acta Crystallogr., Sect. E Struct. Rep. Online* **2007**, *E63*, o2783.

(31) Pereira Silva, P. S.; Ramos Silva, M.; Paixao, J. A.; Matos Beja, A. *Acta Crystallogr., Sect. E Struct. Rep. Online* **2010**, *E66*, o524.

(32) Hennig, A.; Ghale, G.; Nau, W. M. *Chem. Commun.* **2007**, 1614-1616.

Chapter 9 Summary and Perspective

Measurement of collision cross sections is one of the most useful techniques for supramolecular chemistry studies, because it yields conformational information that is difficult to obtain by any other method. In my dissertation, a novel technique for measurements of collision cross sections by FTICR (Fourier transform ion cyclotron resonance), which is termed CRAFTI (cross-sectional areas by Fourier transform ICR), is proposed for the first time. The CRAFTI method measures the total "dephasing cross section" for removal of the ions from the coherent packet in the FTICR cell, including contributions not only from momentum transfer but also from reactive collisions including those leading to collisional dissociation[1]. It provides the collision cross sections and accurate mass-to-charge values at the same time, which means now only one instrument is needed to obtain the shape, size and mass of a molecule. The validity of CRAFTI was confirmed by the fact that the experimental collision cross sections correlate linearly with the theoretically computed results obtained from the MOBCAL computational package. Different collision gases, including Xe and He, were investigated in chapter 3. The results showed that the collision gases with higher molecular weight, such as Xe, are more appropriate for CRAFTI, while the collision gases with lower molecular weight, such as He, are not appropriate because they are too light to provide efficient collisions for damping the motion of heavy ions.

I continued by investigating different collision gases for the CRAFTI technique, including N_2, Ar, and SF_6, which are sufficiently heavy but not expensive. Those three types of neutral gases are all appropriate when the experiments are done at proper kinetic energies. The dependence of

CRAFTI cross sections on the center-of-mass kinetic energy (E_{cm}) in these three collision gases was also examined. The results are similar to the results in Xe[1]. For lower mass complexes (masses up to 375 Da), the CRAFTI cross sections are independent of kinetic energy in every collision gas, which means these systems are in the hard-sphere regime. On the other hand, for heavier ions (masses around 1000 Da), the CRAFTI cross sections increase almost linearly with increasing kinetic energies until about 20 eV, then rise slowly at energies higher than 20 eV. With increasing kinetic energy, the absolute change in momentum during a collision is larger, and the probability of collisions transferring sufficient energy to dissociate the ions is also bigger, which increases the probability for ions being removed from the coherent packet, and increases the observed linewidth and corresponding CRAFTI cross section. CRAFTI cross section measurements at higher kinetic energies by using stronger magnetic fields are anticipated. CRAFTI cross sections are collision gas dependent and the mass of the neutral gas is an important factor for determining the absolute values of CRAFTI cross section as the collision gas is varied.

The CRAFTI technique was applied to a series of supramolecular complexes between pumpkin-shaped cucurbit[n]uril host molecules and straight-chain alkyl mono- and diamine guests. The CRAFTI results qualitatively agree with computational results: the CB5 and mc5 complexes with alkylamines are externally bound, while the CB6 complexes with alkylamines are internal complexes. For a given chain length, the cross sections decrease in the order: $(\text{monoamine+H})^+ > (\text{diamine+H})^+ > (\text{diamine+2H})^{2+}$, due to increasing host-guest interactions at the end of the chain. Other applications of the CRAFTI technique are expected for determination

of molecular conformations. One is to examine the conformations of supramolecular complexes with different isomers, such as complexes of phenylenediamine isomers with CB6[2] (for which cross sections have already been measured via ion mobility). Another is conformational studies of biological molecules using CRAFTI, such as examination of the degree of unfolding in biomolecules.

CRAFTI techniques were combined with SORI-CID (sustained off-resonance irradiation collision induced dissociation) for characterization of complexes of α,ω-alkyldiammonium with cucurbit[n]urils (n=5, 7 and 8) and cucurbituril derivatives (mc5, CB*5 and CB*6) in chapters 6 and 7. The results demonstrate that for bigger cucurbiturils, including CB*6, CB7 and CB8, the complexes have the alkyldiamine tails threaded through the cavity of the host, with protrusion of the chain when it is long enough, as in the CB6 complexes;[3] for smaller cucurbiturils, including CB5, mc5 and CB*5, the complexes have the tails of the alklydiamines external to the portal of the host. All these data offer basic understanding for future investigation of host-guest interactions in more complicated complexes. The agreement between CRAFTI cross section trends and dissociation results from SORI suggest CRAFTI will be also a complimentary method to ion-neutral reactions or IRMPD (infrared multiphoton dissociation) for characterization of supramolecules.

As reported, both CB5 and mc5 can be used in combination with alkali metal cations to form supramolecular containers.[4] In chapter 8, I describe capping molecules for larger CBn to form larger containers. Guanidinium (Gu^+) was chosen as a potential capping cation. Modeling of CB6•Gu_2^{2+} using molecular mechanics suggests Gu^+ is about the right size to form a "lid" on

CB6 complexes. Using SORI-CID methods, CB7, a bigger cucurbituril cage, was found to form a more stable complex with Gu^+. Several neutral guests were trapped in the CB7•Gu_2^{2+} complexes. Benzene, fluorobenzene and toluene were all found to have the ability to form inclusion complexes. These results suggest that other, larger molecular "lids" might be used to close the cavities of CB8 or similar, larger container molecules.

In conclusion, the CRAFTI technique is promising for measurements of collisional cross sections and further investigation of CRAFTI is still needed. I hope CRAFTI will prove a viable method for probing the conformational structures of ions, complementary to existing ion mobility techniques.

References

(1) Yang, F.; Voelkel, J. E.; Dearden, D. V. *Anal. Chem.* **2012**, *84*, 4851-4857.

(2) Dearden, D. V.; Ferrell, T. A.; Asplund, M. C.; Zilch, L. W.; Julian, R. R.; Jarrold, M. F. *J. Phys. Chem. A* **2009**, *113*, 989-997.

(3) Zhang, H.; Ferrell, T. A.; Asplund, M. C.; Dearden, D.V. *I. J. Mass Spec.* **2007**, *265*, 187-196.

(4) Kellersberger, K. A.; Anderon, J. D.; Ward, S. M.; Krakowiak, K. E.; Dearden, D. V. *J. Am. Chem. Soc.* **2001**, *123*, 11316-11317.